St18 specifies MGE lineage parvalbumin expressing prototypic neurons of the globus pallidus pars externa

Luke Frazier Nunnelly

Submitted in partial fulfillment of the
requirements for the degree of
Doctor of Philosophy
under the Executive Committee
of the Graduate School of Arts and Sciences

COLUMBIA UNIVERSITY

2021

Abstract

St18 specifies MGE lineage paravalbumin expressing prototypic neurons of the globus pallidus pars externa

Luke Frazier Nunnelly

The medial ganglionic eminence (MGE) is a progenitor domain in the subpallium that produces both locally-projecting interneurons which undergo tangential migration in structures such as the cortex as well as long-range projection neurons that occupy subcortical nuclei. Very little is known about the transcriptional mechanisms specifying the migratory behavior and axonal projection patterns of these two broad classes of MGE-derived neurons. In this study, I identify St18 as a novel transcriptional determinant specifying projection neuron fate in the MGE lineage. St18 is transiently expressed in the MGE subventricular zone (SVZ) and mantle, and I assessed its function using an ES cell-based model of MGE development. Induction of St18 is sufficient to direct ES-derived MGE neurons to adopt a projection neuron-like identity as defined by migration and morphology. Through gene expression analysis I identified a downstream effector of St18, Cbx7, which is a component of Polycomb repressor complex 1. I find that Cbx7 is essential for projection neuron-like migration and is not involved in St18-mediated projection neuron-like morphology. Using genetic loss-of-function in mice, I find that St18 is required for the production of globus pallidus pars externa (GPe) prototypic projection neurons. Single cell RNA sequencing revealed that St18 regulates MGE output of specific neuronal populations: in the absence of St18, I observe a large expansion of cortical interneurons at the expense of putative GPe neurons. I also find that, following St18 genetic loss of function, mouse walk cycles are disrupted downstream of a loss of a critical neuronal projection from the GPe to the sub thalamic nucleus (STN). These results characterize a novel transcriptional determinant that directs GPe prototypic projection neuron identity within the MGE lineage. Further, I have identified a downstream target of St18, Cbx7, which regulates only the migratory behavior of long-range projection neurons, suggesting that specific features of MGE projection neuron identity may be governed in a compartmentalized fashion by distinct transcriptional modules downstream of

St18. I’ve also demonstrated the role of the GPe PV+ prototypic neurons in the production and maintenance of mouse locomotor gait.

Acknowledgements

I would like the thank all of the people that made this work possible. Without this support, I would not have been able to complete my studies. First, I'd like to thank my mentor, Edmund Au, who's guidance and support throughout have been indispensable throughout my PhD journey. I'd like to also thank the Neurobiology and Behavior Doctoral Program for giving me the opportunity to pursue my degree as a member of this prestigious community. I'd like to especially thank Wes Gruber, one of the program co-directors and my first mentor at Columbia. Your advice and guidance have helped me through many tough times. I'd like to thank all of the members of the Au Lab through the years. Your training and commiserations have always kept me on course. Last, I'd like to extend an especially heartfelt thank you to my family and friends. We did it, fam.

Dedication

One group often goes un-heralded in these works: the animals that make these experiments possible. Therefore, I would like to dedicate this work to all of the animals that I have been fortunate enough to work with and whose sacrifice shall not go herein un-noticed.

Table of Contents

List of Figures and Illustrations

Materials and Methods

Methods.1 Cell culture

Derivation of N/D and N/D/S lines

I derived a mouse parental ES cell line from Dlx6a^{Cre} (Jackson Laboratory Stock No. 008199); Ai9 (Jackson Laboratory Stock No. 007909) E3.5 pre-implantation embryo using previously described methods (Meissner et al., 2009). To this parental line, I stably transfected 2 transgenes, Nestin-Nkx2-1-IRES-tTA^{2}S and either TRE-Dlx2 (N/D) or TRE-Dlx2-St18 (N/D/S) as previously described (Au et al., 2013). Briefly, constructs were linearized and introduced into low-passage parental ES cells on a nucleofector (Lonza) using the mouse ES cell nucleofection kit (Lonza) using protocol A24. Cells were plated at 1:20 density on gelatinized 10cm plates and grown in ES cell media for 48 hours. After this time, hygromycin was added to the media for clone selection. Following 1 week of drug selection, ES cell colonies were clonally selected and expanded on gelatinized 96-well plates and expanded to two plates per clone. One plate was cryopreserved at -80^{0}C while the other was used for genotyping. Clones were screened by PCR for presence of transgenes. Clones were then expanded and differentiated to screen transgene function before use in experiments. ES cell cultures were maintained and screened using standard practices and protocols (Joyner, 2000) and routinely tested for mycoplasma.

ES cell culture

Mouse ES cell lines stably expressing transgenes described above (N/D) and (N/DS) are cultured in 10cm cell culture pre-treated places with .1% gelatin coating. A modified DMEM media is used for to maintain ESC growth and pleuripotency (500mL DMEM, 90mL HIFBS, 6mL each 100x MEM NAA, 100x Sodium Pyruvate, and 100x Glutamax, 1.1mL bimercaptoethanol, and 60uL LIF). ESCs are cultured until confluent and split into two plates. After each plate reaches full confluency, one is frozen using a freezing media (90% modified DMEM ES media and 10% DMSO) and the other is used for downstream differentiation protocol. Passage number and cell line vials are tracked using FreezerPro software.

MS351 treatment

MS351 (Ren et al., 2016 [BOC Sciences CAS 472984-79-5]) was reconstituted to a 3M stock concentration in a solution of 50% water and 50% DMSO (Sigma) per manufacturer specifications. Throughout the entire EB differentiation as well as during the migration assay, or when grown in monolayer cultures, the stock MS351 solution was diluted to 1mM in media or we added an equivalent volume of 50% water/50% DMSO as a vehicle control.

RT-PCR MS351 validation

To verify MS351 efficacy on N/D/S cells, MS351 or vehicle-treated day 12 N/D/S EBs were gathered and spun at 300xg to form pellet, washed with 1x PBS and re-spun at 300xg We then suspended pellet in Trizol (Invitrogen Cat. 15596026) and lysed the cells with vigorous trituration and incubated the cells for 5 minutes at room temperature. We then added 200uL of chloroform (Sigma) and vortexed the lysed cells for 15 seconds before incubating the cells at room temperature for another 3 minutes. Next, the cells were spun at 10,000xg, and we removed the clear, aqueous phase from the Trizol reagent and proceeded with RNA mini-prep using the RNeasy Micro Kit (Qiagen Cat. 74004). We next took eluted RNA and proceeded with reverse transcription to create cDNA libraries for RT PCR. Briefly, we add 200ng of eluted RNA to a mix of water, 1mM dNTP Solution Mix (New England Biosciences Cat. N0447L), and 5uM Oligo(dT)20 Primer (Invitrogen Cat. 18418020) and incubated at 65^0C for 5 minutes. Next, the mixture is cooled on ice for 1 minute before adding reagents for reverse transcription from the SuperScript III Reverse Transcriptase Kit (Invitrogen Cat. 18080093) along with 1 unit of RNaseOUT Recombinant RNase Inhibitor (Invitrogen Cat. 10777019) and 1 mM MgCl2 (Thermo Fisher Scientific Cat. R0971). This mixture was then incubated at 50^0C for 50 minutes before being inactivated at 85^0C for five minutes, completing cDNA synthesis. We used the following primer sequences for p16INK4a (also known as Cdkn2A) (Fwd: CAACGACCGAATAGTTACG Rvs: CAGCTCCTCAGCCAGGTC) GAPDH (Fwd: GAGTCCACTGGCGTCTTC Rvs: GGGGTGCTAAGCAGTTGGT) for amplification of 100ng of cDNA template from N/D/S cells either treated with MS351 or vehicle using Power SYBR Green Master Mix (Thermo Fisher

Scientific Cat. 4368577) qRT PCR protocol (Al-Khalaf and Aboussekhra, 2013). qRT PCR reaction was run on a QuantStudio(TM) 7 Flex System in a 96 well format with associated software performing analysis (Applied Biosystems Cat. 4485701).

Specification of ESCs into MGE progenitors

Differentiation of ES cells to become MGE lineage neurons was adapted from protocols previously described (Au et al., 2013; Watanabe et al., 2005). Briefly, ES cell cultures were maintained for two passages on 0.1% gelatin (Millipore) using modified Dulbecco's Modified Eagle Medium (Gibco), 15% heat-inactivated FBS (HyClone), 1x Modified Eagle Medium Non Essential Amino Acids (Gibco), 1x Sodium Pyruvate (Gibco), and 1x Glutamax (Gibco), 10uM beta-mercaptoethanol (Fisher Scientific), and 104 U/mL ESGRO LIF (Sigma Millipore). N/D and N/D/S line ESCs were dislodged with 0.025% trypsin/1% EDTA (Gibco), dissociated, and suspended at a density of 50,000 cells/well in a non-TC-treated 24 well plate in 800uL of premixed differentiation media (Glasgow's Modified Eagle Medium [Gibco], 1x PenStrep [Gibco], 1x Modified Eagle Medium Non Essential Amino Acids [Gibco], 1x Sodium Pyruvate [Gibco], and 1x Glutamax [Gibco], 10uM beta-mercaptoethanol [Gibco], and 4% Knockout Serum Replacement [Gibco]) as described previously (Au et al., 2013). Briefly, cells were neuralized and directed toward telencephalic identity with Wnt-inhibitor XAV-939 (Tocris, 0.1 uM) from days 0-4. Sonic hedgehog agonist (SAG [Tocris], 1uM) is added to ventralize telencephalic EBs from days 4-6. From day 6 onwards, on SAG is present in the medium until EB differentiation is complete on day 12. Media changes occurred on days 4, 6, and 9 during the protocol, and free floating embryoid bodies (EBs) containing differentiating neurons form spontaneously during the course of the protocol.

2D culture and morphometric analysis of ESC derived differentiated neurons

Mouse cortical feeders were prepared from P0-P4 wild-type Swiss-Webster mice. Briefly, cortices were micro-dissected into chilled Hibernate A media (Hibernate A[Gibco] , 1% Pen/Strep [Gibco]). 1mL of a Papain solution of approximately 20 Units/mL was prepared with Hibernate A dissection media and ~1000 units of DNAseI and added to dissected tissue. Cortical

tissue is agitated at 37^0C for 15 minutes. Papain is quenched with 3mL Hibernate A, after which cortical tissue is triturated with a P1000 pipette tip until fully dissociated (8-10 times). Cells were counted, spun at 200xg for 5 minutes, and re-suspended in modified Neurobasal A to a concentration of 6 $X10^7$ viable cells per mL, and 50uL cell suspensions were plated per well. In parallel, EBs were dissociated in 1mL Papain solution for 15 minutes, 37^0 C with agitation. Cells were then diluted approximately 1/1000 in modified Neurobasal A media in order for labeled cells to be plated at low density for single cell morphological analysis. The EB/cortical feeder mix is plated onto m 24-well optical plastic tissue culture plates (Ibidi) pretreated with 20ug/mL poly-D lysine and rinsed thoroughly with sterile water. Neuronal cultures were maintained in a modified Neurobasal A media (500mL Neurobasal A [Gibco], .01M HEPES [Gibco], 1% PenStrep [Gibco], 1X B27 supplement [Gibco] is added on the day of use). Media is changed on the first day following plating, and every other day subsequent to that before cultures were fixed with 4% PFA in PBS after 12 days of culture. Whole wells were imaged at 100x magnification using a Zeiss Apotome tiling microscope. Whole neuronal morphologies were traced using the Neuro-Anatomy Simple Neurite Tracing plugin in ImageJ (Longair et al., 2011). Morphometric and Sholl analysis were performed on the traces using Neuro-Anatomy plugin (ImageJ). Sholl analysis is performed at a standard radius of 10um (Ferreira et al., 2014).

In vitro migration assay

Individual differentiation day 12 N/D and N/D/S EBs were placed into the center of a m 24-well optical plastic tissue culture plates (Ibidi), using a wide-bore P200 pipette tip. Media was gently removed before EBs were suspended in Matrigel (Corning) droplets (50-100uL) using pre-chilled P1000 pipette tips. EB/droplets were incubated for 30 minutes at 37^0C. Following incubation, solidified Matrigel droplets containing EBs were suspended in Neurobasal media and cultured for four days until fixation using 4% PFA in PBS. Whole EBs were imaged at 200x using a Zeiss confocal microscope. Migration distance is analyzed using straight line tool in ImageJ, measuring the distance a cell traveled perpendicular to the edge of the EB.

Methods.2 Tissue preparation and histology

Embryoid body fixation and histology

Embryoid bodies (EBs) from two rows of a 24-well plate were gathered in a 15mL conical tube and spun down at 200xg for 2 minutes, rinsed with PBS and re-spun. EBs were then re-suspended in 1mL of 4% PFA and incubated for 30 minutes at room temperature. Post-fixation, EBs were rinsed in PBS and re-suspend in 10% sucrose solution in PBS and incubated for 30 minutes, then re-suspended in 30% sucrose solution in PBS and incubated for an additional 30 minutes. Using a P200 wide bore pipette tip, EBs were removed from the tube and placed in the base of a plastic cryomold (Fisher Scientific). Sucrose solution is removed carefully with both a pipette and the folded edge of a Kimwipe until EBs were as dry as possible at the base of the mold. Tissue-Tek OCT (Sakura) is added to the mold and placed on dry ice for flash freezing and then stored at -30^{0}C. Cryosectioning was performed on a Leica cryostat at a thickness of 15um. Sections were permeabilized using a 0.01% Triton X-100 in PBS and blocked overnight with a 5% normal donkey serum (NDS)/PBS solution. Primary antibodies for V5 (Invitrogen Cat. R960-25, 1:200) and St18 (1:1000) were incubated in 5% NDS/PBS overnight at 4^{0}C and secondary antibodies (Jackson Immunoresearch, 1:1000) diluted in 0.01% Triton X-100/PBS for 2 hours at room temperature. Sections were cover slipped with Fluoromount-G (Southern Biotech) and stored at 4^{0}C prior to imaging with Zeiss epifluourescent microscope at 200x.

In vivo tissue preparation and histology

For adult histology, P30-P40 animals older were anesthetized using a cocktail of Ketamine and Xylazine and were sacrificed using a trans-cardiac perfusion of PBS followed by 4% PFA/PBS. Following dissection, brains were post fixed for 24 hours in 4% PFA/PBS at 40C and then mounted in 4% low melt agarose to prep for vibratome sectioning. Brains were sectioned in the coronal plane at a thickness of 50um. Sections were collected in series in 96-well U-bottom plates in an anti-freeze solution (1:1:1 PBS, poly-ethylene glycol, and glycerol) for long term storage at -30^{0}C. For immunohistochemistry, free-floating sections were permeabilized with 0.01%Triton X-100/PBS. Primary antibodies were incubated for three days at 4^{0}C in 5%

NDS/PBS (PV [ImmunoStar Cat. 24428] 1:1000, Npas1 [Gift from the Chan Lab, Northwestern University] 1:1000, FoxP2 [Gift from the Jessel Lab, Columbia University] 1:1000, Er81 [Gift from the Jessel Lab, Columbia University] 1:32000, SST [Millipore Sigma Cat. MAB354] 1:250, s100B [Millipore Sigma Cat. SAB5600115] 1:1000, Nkx2-1 [Abcam Cat. Ab227652] 1:500), and secondary antibodies (Jackson Immunoresearch). Rat-anti St18 antibody was produced as described previous (Hu et al., 2020). Briefly, the N-terminus of St18 (aa 60-298) was fused to a maltose binding protein to generate a purified immunogen. Strategic Bio-Solutions (Newark, DE) used the immunogen to generate rat polyclonal anti-St18 antibody. Free floating sections were mounted by paint brush onto SuperFrost Plus slides in Fluoromount G solution for long term storage.

For embryonic histology experiments, E13.5 timed plugs were prepared using St18 null heterozygous breeders, and pregnant dams were sacrificed using carbon dioxide euthanasia and cervical dislocation prior to embryo dissection. Embryos were immersion fixed in 4% PFA/PBS for 15 minutes, rinsed with PBS, before overnight cryoprotection in 30% sucrose/PBS solution. Following cryoprotection, embryos were mounted in OCT compound and flash frozen on dry ice and stored at -30^{0}C prior to sectioning. Cryosectioning was performed on a Leica cryostat at 15 um thickness, and sections were dried at room temperature for 1 hour before freezing at -30^{0}C. Immunolabeling was performed following a 20 minute wash in PBS to remove excess OCT. Primary antibodies were incubated overnight at 4^{0}C in 5% NDS/PBS (Nkx2-1 [abcam Cat. Ab227652] 1:500, St18, 1:1000, Ki67 [Invitrogen Cat. 14-5698-82] 1:200, Caspase 3 [Novus Cat. 31A1067] 1:500), and secondary antibodies (Jackson Immunoresearch). Sections were cover slipped in Fluoromount G solution for long term storage.

RNAscope

E13.5 timed plugs were dissected and immersion fixed with 4% PFA/PBS for 15 minutes and rinsed with PBS before overnight cryoprotection in 30% sucrose/PBS solution. Following cryoprotection, embryos were mounted in OCT compound and flash frozen on dry ice and stored at -30^{0}C prior to sectioning. Cryosectioning was performed on a Leica cryostat at 15 um thick-

ness in the coronal plane, and sections were dried at room temperature for 1 hour before storage at -30^{0}C. The RNAscope assay for fixed-frozen tissue was performed on the sections using the ACD RNAscope Fluorescent Multiplex Reagent Kit (ACD, Cat. 320293; Wang et al., 2012) and a catalog probe for St18 transcript (Cat. 443271). Sections were imaged on a Zeiss confocal microscope at 200x.

Methods.3 RNA sequencing

RNA preparation and sequencing

Day 12 N/D and N/D/S EBs were collected into a 15mL conical tube and spun down at 200xg for 5 minutes. EBs were rinsed with PBS and then suspended in 500uL 1X AccuMax (Gibco) enzyme solution with 10 Units DNAaseI (Thermo) and incubated for 15 minutes at 37^{0}C. The enzyme was quenched with 5mL HEPES buffered saline and triturated to a single cell suspension using a P1000 pipette tip. Cells were spun at 300xg for 3 minutes and resuspend the pellet in 500uL HEPES buffered saline. The suspension was filtered with a 70um cell strainer for flow cytometry. tdTomato+ cells were sorted (BD Influx System) directly into Trizol (Figure Methods.1). RNA was purified using an RNA miniprep kit (Zymo) and measured with a Bioanalyzer (Agilent) to ensure an RIN score of 7 or greater. mRNA was enriched using a standard poly-A pull-down prior to library construction with Illumina TruSeq chemistry. The library is sequenced using Illumina NovaSeq 6000 at the Columbia Genome Center. Samples were multi-

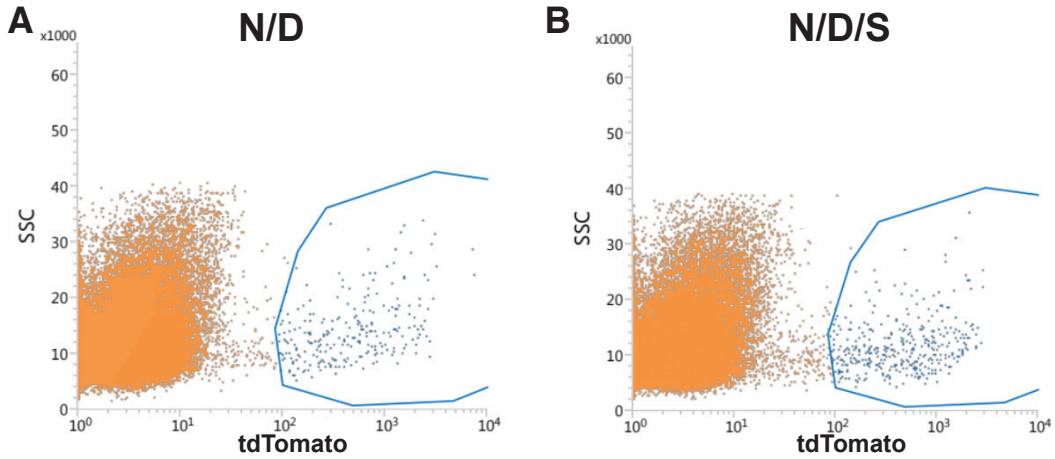

Methods.1 FACS sorting of N/D and N/D/S EBs collects tdT+ differentiated neurons

A) FACS plots of sorted N/D tdT+ neurons. Y axis shows Side Scatter light (SSC) as a measure of cell size. X axis shows the fluorescence for tdTomato (563nm). Sorted cells circled in blue.

B) FACS plots of sorted N/D/S tdT+ neurons. Axes and notations are the same as (A).

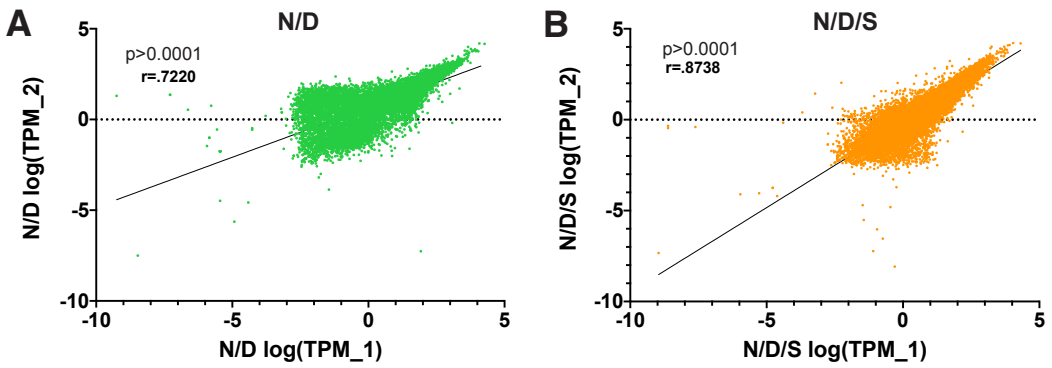

Methods.2 Correlation of N/D and N/D/S RNAseq biological replicates

A) N/D biological replicate RNAseq TPM values plotted against each other (*Pearson's correlation coefficient*).
B) N/D/S biological replicate RNAseq TPM values plotted against each other (*Pearson's correlation coefficient*).

plexed in each lane with yields of paired-end 100bp reads per sample. RTA (Illumina) was used for base calling and bcl2fastq2 (version 2.20) for fastq format conversion. A pseudoalignment was performed to a kallisto index created from the mouse transcriptome using kallisto (0.44.0). We tested for differentially expressed genes using Sleuth, an R package designed for differential gene analysis from kallisto abundance files. Two biological replicates were run per cell line, with a high degree of correlation between the two runs for each the N/D and N/D/S lines (Figure Methods.2).

Single cell RNA sequencing sample preparation

E14.5 embryos generated from a cross of St18+/- x St18+/- parents. Embryos were collected and MGE was microdissected into chilled Hibernate A solution. During the dissection, embryo DNA was obtained using the HOTSHOT protocol (Truett et al., 2000) to allow for rapid PCR genotyping. St18 null and WT MGE were pooled and dissociated separately. Samples were submitted to the Sulzberger Genome Center Single Cell Core at the Columbia University Medical Center for library construction using 10X Genomics chemistry. Sequencing is run on a 10X Genomics platform, and analysis was performed on 10X Genomics' Cellranger software version 5.0.1.

Single cell RNA sequencing data analysis

After alignment and quantification with Cellranger, cells were filtered based on the following criteria: cells with fewer than 200 unique genes detected, or cells with more than

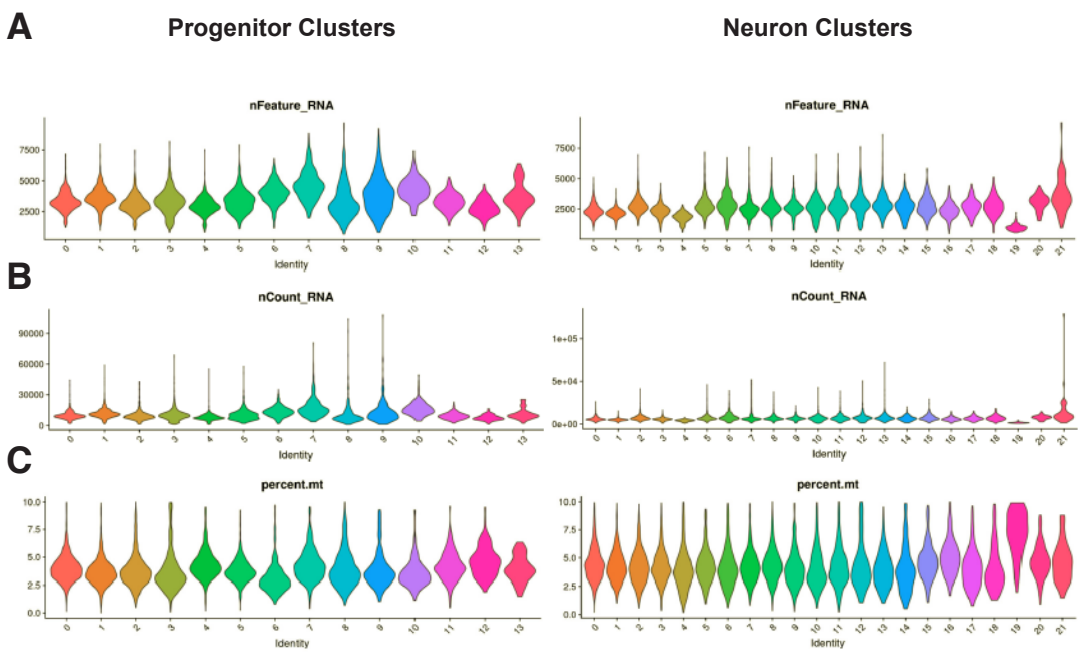

Methods.3 Quality control of single cell RNA-seq dataset

A) Violin plots showing the distribution of unique genes detected per cell. Dataset grouped by cluster.
B) Violin plots showing the distribution of unique molecular identifier (UMI) counts per cell. Dataset grouped by cluster.
C) Violin plots showing the distribution of percent of UMIs mapped to the mitochondrial genome. Dataset grouped by cluster. Cells with low unique genes detected or high percentage of mitochondrial reads were removed prior to clustering.

10% of reads mapping to the mitochondrial genome were excluded from further analysis. After QC (Figure Methods.3), all cells from all experiments were aggregated and clustered using the Seurat package in R, with default parameters, except the following: cell cycle differences among dividing cells were regressed and removed (Mi et al., 2018), and clustering was performed on the 49 principal components with a pvalue less than 0.01, as determined by jackstraw resampling (Macosko et al., 2015), with a resolution of 1.4, based on bootstrapped iterative clustering (Patterson-Cross et al., 2021). After clustering, progenitor and neuronal clusters were identified by plotting the expression of marker genes from (Mi et al., 2018). Subsequently, progenitors and neurons were re-clustered separately. Each cluster was then assessed for statistically significant enrichment or depletion in the WT versus St18 (-/-) groups, using a Fisher's exact test with Bonferroni correction for multiple comparisons. This identified three neuronal clusters with statistically significant differences between the groups in terms of proportions, with the additional constraints of comprising >5% of the total neuronal population and at least two-fold change in proportions between the groups. Differential gene expression among the clusters was performed

using a Wilcoxon rank-sum test in the Seurat package.

Methods.4 Animal handling and genotyping

Animals

The conditional St18 allele was generated by introducing flanking LoxP sites to exons 9 and 10 of St18 (Huang et al., 2018). Cre-mediated recombination causes a frame shift in the coding region and a premature stop codon, resulting in the production of a truncated N-terminal fragment. Using an antibody that recognizes the N-terminus of St18, no signal is detected, likely due to a combination of nonsense mediated mRNA decay and peptide instability (Hu et al., 2020). The St18fl/fl mouse is on a mixed C57Bl/6-ICR background. To generate the St18 null, we crossed St18fl/fl with a germline Cre driver (E2a-Cre Jackson Laboratory Stock No. 003314) Experimental null animals were generated from St18 heterozygote breeders, and wildtype littermates were used as controls. For St18 conditional knockout (cKO) experiments, the St18fl/fl was crossed to an MGE specific Cre driver (Nkx2-1Cre Jackson Laboratory Stock No. 008661) along with the conditional tdTomato reporter (Ai9 Jackson Laboratory Stock No. 007909) or a synaptophysin tagged fate-mapping allele (Ai34 Jackson Laboratory Stock No. 012570) for forward fate-mapping of the Nkx2-1 lineage. Similarly, St18fl/+ breeders were used for St18 cKO experiments to generate St18 cKO and heterozygote littermate controls. All animal experiments were conducted in compliance with and preapproval from Columbia University's Institutional Animal Care and Use Committee.

Animal husbandry

All animal husbandry was performed according to industry standards with help from Columbia University's Institute of Comparative Medicine (ICM) animal care staff. I established breeder cages for desired alleles to produce animals for four generations before replacement with new breeders. For St18 (-/-) experiments, I used heterozygote breeders (St18 (-/+)) to produce Mendellian proportions of progeny. For St18 cKO animals, I used heterozygote breeders (St18 (fl/+)). Fate-mapping alleles (Ai9 and Ai34) were homozygotes to ensure that all progeny in conditional loss of function experiments would carry the fate-mapping allele for experimental

analysis. The presence or absence of Cre is determined by PCR genotyping, as Cre zygosity is difficult to determine.

Genotyping

Animals were genotyped using a ProFlex Thermocycler (Applied Biosystems by Life Technologies). Genotyping primers for Cre are FWD: AGCCTGTTTTGCACGTTCACC RVS: GGTTTCCCGCAGAACCTGAA. Cre presence is determined by either a presence or absence of a band. Genotyping primers for Ai9 are WT FWD: AAGGGAGCTGCAGTGGAGTA WT RVS: CCGAAAATCTGTGGGAAGTC Mut FWD: CTGTTCCTGTACGGCATGG Mut RVS: GGCATTAAAGCAGCGTATCC. Genotyping primers for Ai34 are Mut FWD: GGAGTGTGCCAACAAGACGGAGA Mut RVS: CCAGCCTGTCTCCTTGAACACGA and WT primers are the same as Ai9. Genotyping for St18 loss of function experiments uses WT FWD: TGAGACTGAGACTACTTGTTAGC Mut FWD: GGAGCATGTTCACCTTCTGG RVS: GCTTTCTGGGTTTCATTTCTG. All PCR products were run on 2% agarose gel at 150V.

Methods.5 Microscopy and image analysis

All imaging was performed at 200x using either a Zeiss scanning confocal microscope or a Zeiss epifluourescent tiling microscope at specific ROIs based on the Allen Brain Institute Reference Atlas. All adult histology (PV, Npas1, Nkx2-1, Er81, FoxP2, SST, and s100B) and tdTomato analysis was performed following imaging with the Zeiss epifluourescent scope at 200x, and representative images for figures were taken with the Zeiss confocal microscope at 200x. Image analysis was performed blind using the Blind Analysis Tool in ImageJ. Images were post-processed using combination of custom ImageJ macros for maximum z-projection, background subtraction (rolling ball radius=20 microns), brightness and contrast adjustments, thresholding, and particle analysis for semi-automated cell and object counting. All embryonic histology (Nkx2-1, Ki67, Casp3, and St18) was performed following imaging with the Zeiss epifluourescent scope at 200x, and representative images for figures were taken with the Zeiss confocal microscope at 200x. Image analysis was performed blind as with adult tissue. Images

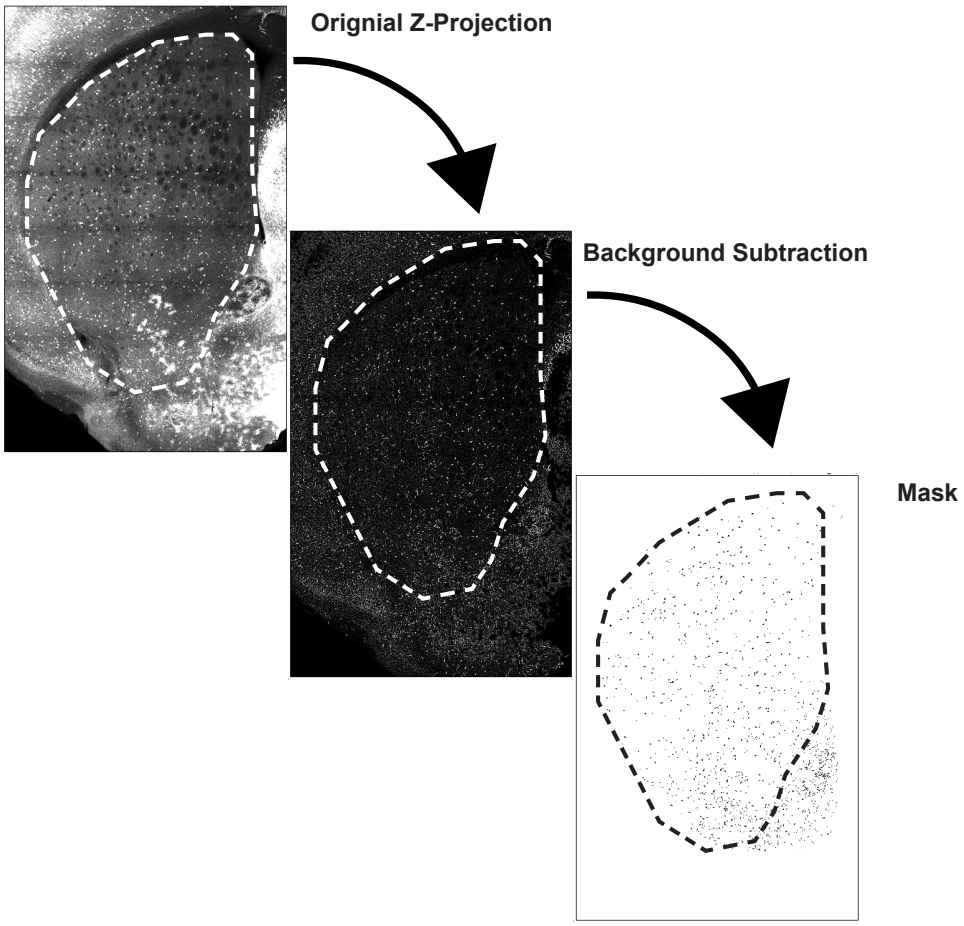

Methods.4 Workflow of image processing for semi-automated cell counting.
Sample workflow of image analysis pipeline. First image is a Z-projection of an image of the striatum labelled by tdT. The next image shows a background subtraction. The next image shows the mask of objects for automated counting.

were post-processed using a combination of custom ImageJ macros for maximum z-projection, background subtraction (rolling ball radius=5 microns), brightness and contrast adjustments, thresholding, and particle analysis for semi-automated cell and object counting. All Ai34 synaptic puncta image analysis were performed following imaging at 200x on a Zeiss confocal microscope. Images were post-processed using a combination of custom ImageJ macros for Z-stack slice selection, background subtraction (rolling ball radius=2 microns), brightness and contrast adjustments, thresholding. Synaptic puncta were quantified by particle analysis for semi-automated object counting (ImageJ). All imaging cell counts were normalized to the area of the section being counted. Semi-automated cell counting was done using the same approach in each experiment with adjustments being made for the size and relative signal present in each case.

A sample of the image analysis pipeline is exemplified using a striatal tdTomato image (Figure

Methods.4).

Methods.6 Behavior experiments

All behavior experiments were performed at the Columbia Neurobiology Motor Behavior Core with consultation on experimental design and data analysis from the facility's staff.

Developmental Milestones

Pups are tattooed in the paws for identification on P2. Developmental milestone tests are conducted on alternated days to avoid over handling. Developmental milestones in pups are important readouts of developmental delays. We measure body weight, righting reflex (the latency to right oneself from a belly-up position to be on all fours), negative geotaxis (on a wire mesh screen, the latency to turn 90 degrees or 180 degrees from a downward-facing start position), and vertical screen holding (the latency too fall off a vertically positioned wire mesh screen). To begin the test, each pup is gently removed from the nest and placed on a clean piece of bench protector. The cage lid is immediately and gently placed back, to reduce agitation in the nest. All assessments are completed within 3 min. At the end of the session, the pup is quickly returned to the nest.

Rotarod

Motor performance in adults was assessed using a mouse accelerating rotarod (Ugo Basile). Mice were placed on the rotating drum that accelerated from 5 to 40 rpm over 5 min. Mice were tested for three trials a day, for 2 consecutive days. The inter-trial interval was 1 h. Rotarod scores were scored for latency to fall or ride the rod around for all three cohorts.

Open Field Test

The open field test is the most commonly used general test for locomotor activity. Each mouse is gently placed in the center of a clear Plexiglas arena (27.31 x 27.31 x 20.32 cm, Med Associates ENV-510) lit with dim light (~5 lux), and is allowed to ambulate freely for 60 min. Infrared (IR) beams embedded along the X, Y, Z axes of the arena automatically track distance moved, horizontal movement, vertical movement, stereotypies, and time spent in center zone. At the end of the test, the mouse is returned to the home cage and the arena is cleaned with 70%

ethanol followed by water and wiped dry.

Catwalk Experiments

The CatWalk XT system (Noldus) was used to record normal, uninterrupted gait in mice. Briefly, an enclosed walkway on a glass plate is traversed by a mouse from one side of the walkway to the other. Footprints and step cycles are measured as green light that enters at one edge of the glass plate is scattered by contact by a paw of a mouse. A high speed camera captures these events at 100 frames/second and, using Noldus Catwalk XT software, various gait parameters are obtained. Mice are removed from their home cage and gently placed at the beginning of the glass catwalk plate. Mice freely traverse the walkway until three compliant trials are completed (determined by the direction of travel and time it takes to complete a run), upon which the mouse is returned to its home cage. The glass plate is cleaned between each mouse with 70% ethanol followed by water.

Methods.7 Stereotax injection experiments

Stereotax injection experiments were done using standard techniques previously described (Abecassis et al., 2020). PND 30 mice were used for injection experiments. Animals were anesthetized using a cocktail of ketamine, xylazine, and acepromazine per IACUC guidelines and approval. Anesthetized animals were immobilized on a stereotaxic frame (David Kopf Instruments), and a dental drill (Osada) was used to make small craniotomy (~1mm diameter) at coordinates typically used for GPe injections, allowing for a calibrated micropipette (Hamilton Cat. 65461-02) to be inserted to the location of the GPe (AP= -0.34 ML= 1.80 DV= -3.60; Allen Brain Institute). I injected 1uL of adeno associated virus (AAV) AAV-CAGS-GFP obtained from the Columbia University Virology Core at a rate of .5uL per minute. I left the pipette *in situ* for 12 minutes post injection to maximize virus retention and to reduce the amount of capillary spread of virus upon pipette withdrawal. I withdraw the pipette .5mm at a time, with a 5 minute wait between each movement to further minimize unintended viral spread. Following removal of the pipette, animals were observed post-operation for any negative effects and then given Carprofen as a post-operative analgesic.

Two weeks post injection, animals were sacrificed via transcardiac perfusion as earlier described, and then animals were prepared for free floating tissue preparation and sectioned in the sagittal plane to optimize visualization of the indirect pathway. I collected serial sections from lateral to medial on the injected side of the brain. I collected the first five sections to sample the striatum which I stained with a GFP antibody (Abcam Cat. Ab13970). I collected the next 24 sections for GPe sampling, which I stained with GFP and alternatively PV or Npas1 to sample prototypic and arkypallidal neurons in the GPe. I collected the next six sections to sample the STN and SNr, which I stained only with GFP. I then imaged all samples at 200x on a Zeiss Epifluorescent scope. I hand counted the number of virally labelled PV or Npas1 neurons in the GPe samples. I used my method for semi-automated puncta quantification for GFP signal in the striatum, STN, and SNr. I normalized the amount of GFP signal in the striatum and STN/SNr to the number of Npas1+ and PV+ cells in the GPe, respectively.

Introduction

Introduction.1 Diversity and function in the nervous system

In the late 19th century, Santiago Ramon y Cajal founded modern neuroscience with his study of the functional units of the nervous system, neurons. Using golgi staining and immaculate illustrations of hundreds of bizarrely shaped cells, Ramon y Cajal uncovered perhaps the most striking feature of mammalian biology: the nervous system is comprised of functional units, each with a unique shape and structure. He hypothesized that these functional units communicate with one another in ways determined by the effect that they might have on mammalian behavior. He further speculated that the shapes of the cells themselves are formed to fit the functional needs of the nervous system. Of course, he would not live to see his hypothesis proven, but his work is foundational in how I understand neuroscience as a field. To understand behavior and function, one must study the brain's functional units in high resolution. Only then will it be possible to make conclusions about the role of any given neuron on animal behavior and circuit function.

One of the most profound challenges facing neuroscience as a field is the pressing need to understand the origins of neural diversity. The mammalian brain is capable of driving a remarkable number diverse functions and behaviors, including, but not limited to, vocalization, locomotion, sensory perception, memory formation, and, in human beings, conscious thought. This breadth is underwritten by the myriad of distinct cell types that constitute the brain's repertoire of neurons. Indeed, our nervous system contains 100 billion neurons with a myriad of identities, morphologies, patterns of connectivity, and functions. Vast neural diversity underlies the complex functional capability of the nervous system, and each discrete cell type in the mature nervous system is thought to be responsible for contributing particular aspects to the brain's overall function. Furthermore, some of the most pressing and costly obstacles to bridging the gap between the lab and the clinic is the lack of understanding of the genetic antecedents of specific neuronal populations in the brain. In the lab, identifying the genes necessary for the specification of specific neuronal populations would allow for greater genetic access to the circuits and con-

nections that define behavior fundamentally. In the clinic, this could help identify susceptibility genes and generate new, targeted treatments tailored to specific, vulnerable neuronal populations in a variety of disease states. Therefore, the focus of this work will be on studying the adoption of cell features and fates throughout developmental time. I will then show the value of this approach by demonstrating the physiological role of a specific neuronal population in mouse behavior following identification of a transcription factor involved in the specification of a discrete neuronal population.

Introduction.2 The MGE lineage epitomizes the diversity of the nervous system

The medial ganglionic eminence (MGE) is a neurogenic progenitor zone in the mouse ventral telencephalon responsible for the generation of a majority of the GABAergic cells that distribute throughout the mouse brain. Indeed, the MGE produces dozens of different neuronal cell types that distribute broadly throughout the brain (Wichterle et al., 2001; Xu et al., 2008). While the MGE is best known for generating the majority of the GABAergic interneurons in the cortex, it also produces inhibitory neurons that populate the hippocampus and striatum as well as subcortical nuclei, including the globus pallidus pars externa (GPe) and medial amygdala (MeA) (Bupesh et al., 2011; Nobrega-Pereira et al., 2010; Puelles et al., 2000; Wichterle et al., 2001; Xu et al., 2008). MGE neural progenitors are defined by their expression of the transcription factor Nkx2-1 (Butt et al., 2008; Du et al., 2008; Sussel et al., 1999). However, as cell progress through developmental time and space, immature MGE neurons begin to express distinct gene repertoires en route to terminal differentiation (Mayer et al., 2018; Mi et al., 2018). Therefore, the challenge that remains is to link the expression of these early transcriptional antecedents with mature neuronal identity beyond their specification as MGE progenitors with the expression of Nkx2-1. Given the remarkable diversity of the MGE lineage, I believe that it therefore is the ideal system to study the genetic specification of different neural subtypes within a restricted lineage.

Introduction.3 Neuron specification within the nervous system and MGE

To begin understanding the development of discrete cell type features and morphologies during MGE neuronal development, it is crucial to first examine how neurons get specified

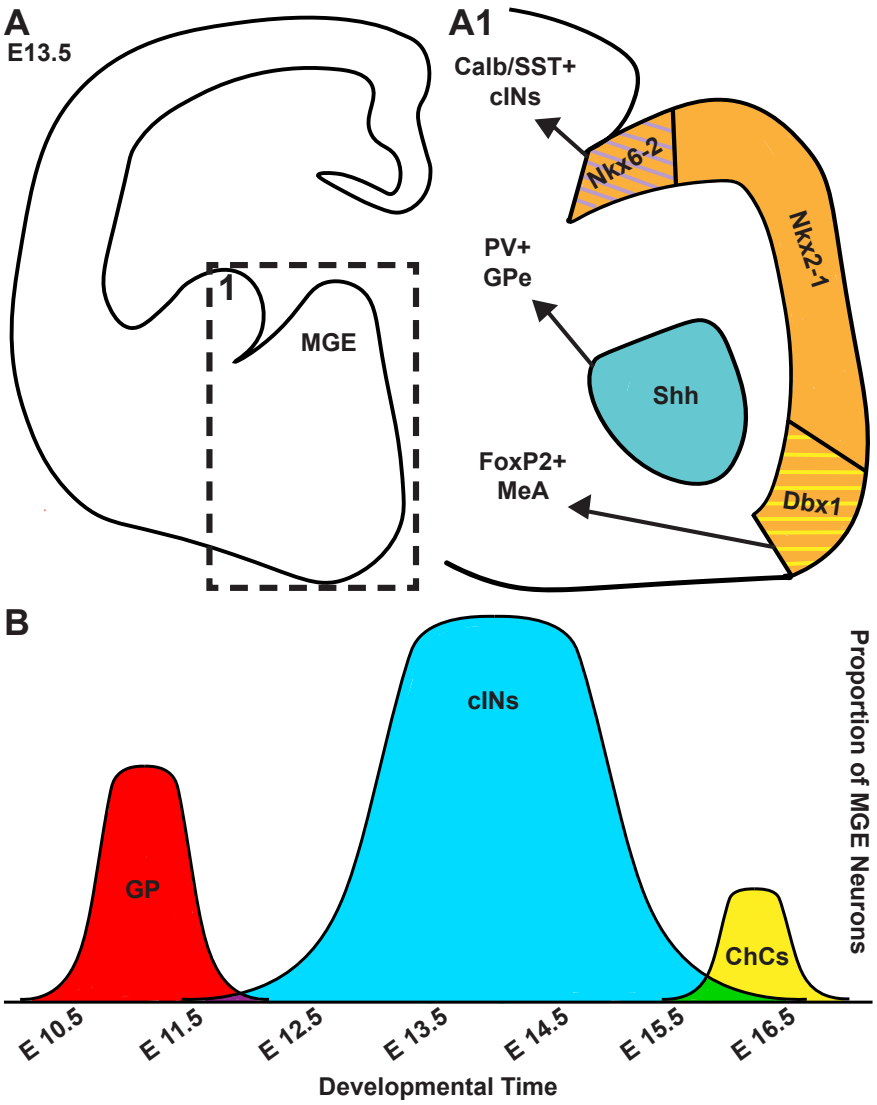

Introduction.1 Models of neuronal development within the MGE

A) Schematic of an E13.5 coronal mouse embryonic telencephalon with the MGE labeled. Inset (1) is a higher power schematic of the MGE with various different regions characterized by gene expression delineated in different colors. Arrows indicate different MGE lineage cardinal cell types that are produced in these spatially restricted regions of the MGE. Adapted from (Hu et al., 2017).

B) Schematic of the temporal control of MGE neurogenesis. Different cardinal cell types born in the MGE are produced at different time points during neurogenesis. Adapted from (Lim et al., 2019).

during developmental time. Firstly, there are two competing models for how neurons get specified during developmental time. The first model states that different neuronal subtypes develop according to the spatial distribution of progenitor cells during development. This model is exemplified in the spinal cord, where different motoneurons, sensory neurons, and interneurons are specified based on the distribution of progenitor cells on the ventral to dorsal axis relative to secreted sonic-hedgehog (Shh) emanating from the spinal cord floor plate (Jessel, 2000). Within the MGE, there is evidence that elements of this model are recapitulated (Introduction.1 A).

Indeed, there are a number of different factors expressed along the ventral-dorsal axis that define different sub-divisions within the MGE progenitor zone beyond ventricular expression of Nkx2-1 (Hu, J. et al., 2017). Nkx6-2 is expressed in a restricted, dorsal portion of the MGE, which gives rise primarily to somatostatin (SST)/calretinin cortical interneurons (Sousa et al., 2009). Shh is expressed ventrally to this, and its expression defines a portion of the ventral MGE that gives rise to mostly sub-cortical projection neurons and interneurons (Flandin et al., 2010). Ventral to this, Dbx1 is expressed, specifying MeA neurons within the MGE lineage (Lischinsky et al., 2017). Elements of MGE neuronal differentiation, then, are determined primarily by the spatial distribution of various genes and factors.

A second, competing model of nervous system development states that neuronal differentiation occurs as a temporal procession of neuronal progenitors, with different neuronal subtypes being born only at specific times during development. This model is best exemplified in the developing fruit fly, where neuroblasts pass through a series of asymmetric divisions, producing different neuronal classes sequentially based on the number of divisions the parent neuroblast has undergone (Kohwi and Doe, 2013). The MGE lineage also exemplifies features of this temporal competence model (Introduction.1 B). Indeed, nascent globus pallidus neurons are born early during neurogenesis, preceding the generation of cohorts of SST and paravalbumin (PV) expressing cortical interneurons (Lim et al., 2018; Inan et al., 2012). Following these waves, near the end of neurogenesis, chandelier cells are preferentially produced around E16.5 (Taniguchi et al., 2013). Together, this means that many aspects of MGE neuronal differentiation are controlled along the temporal axis during neurogenesis.

Therefore, within the MGE, there is a hybrid of these two models of neuronal specification in action. Specifically, there are both spatial and temporal elements controlling the differentiation of the dozens of cell types within the MGE lineage. Indeed, there is evidence that within the MGE lineage, individual neuronal progenitors can either give rise to a dedicated sub-population of neuron or give rise to a diverse set of neurons within the MGE lineage (Mayer et al., 2015). Specifically, using a viral linage tracing approach to label discrete neuronal progenitors as

they progress through developmental time and space, it has been shown that single MGE progenitors can delineate a specific neuronal population, like cortical interneurons (Mayer et al., 2015). Alternatively, single MGE neuronal progenitors can also produce a heterogeneous neuronal cohort that crosses the boundaries of subtype and anatomical structure (Mayer et al., 2015). This means that a single MGE progenitor has the capacity to become either, for example, a cortical interneuron or a GPe projection neuron (Mayer et al., 2015). There are likely uncharacterized factors, then, that are dynamically expressed during developmental time, and in a spatially restricted manner, that further specify the remarkable diversity of the MGE neuronal lineage beyond the timing and placement of progenitor cell birth and mitosis.

Introduction.4 Transcriptional specification of MGE neuronal diversity

Along with the spatial and temporal factors that shape MGE differentiation, there are a host of other factors that determine the fate of a neuronal progenitor during development. Indeed, another axis of development that determines the ultimate fate and function of a neuronal cell from the MGE lineage is the cohort of factors that are expressed in a combinatorial fashion for the adoption of the various cell-type specific features that determine a neuron's form and function. Some features of MGE development are determined at the onset of neurogenesis. Nkx2-1 expression is required throughout neurogenesis for the proper development of MGE neuronal cohorts, with loss of Nkx2-1 resulting in trans-fated progenitors that resemble the neighboring lateral ganglionic eminence progenitor domain (Nobrega-Pereira et al., 2008; Sandberg et al., 2016). Other cardinal features of MGE neural populations are adopted following transcription factor expression downstream of Nkx2-1. This includes the regulation of PV cortical interneuron migration by Sp8/Sp9 (Tao et al., 2019) and the allocation and maturation of SST cortical interneurons by Satb1 (Close et al., 2012). Yet more features of mature MGE lineage neurons are controlled by a combination of cell-intrinsic and cell-autonomous factors that act to shape neuronal shape, distribution and function. This includes, for example, the allocation of MGE lineage striatal neurons via Nkx2-1 induced expression of Nrg1/ErbB4, attracting migrating interneurons into the striatum in concert with chemo-repulsive responses controlled by EphB/erphrinB

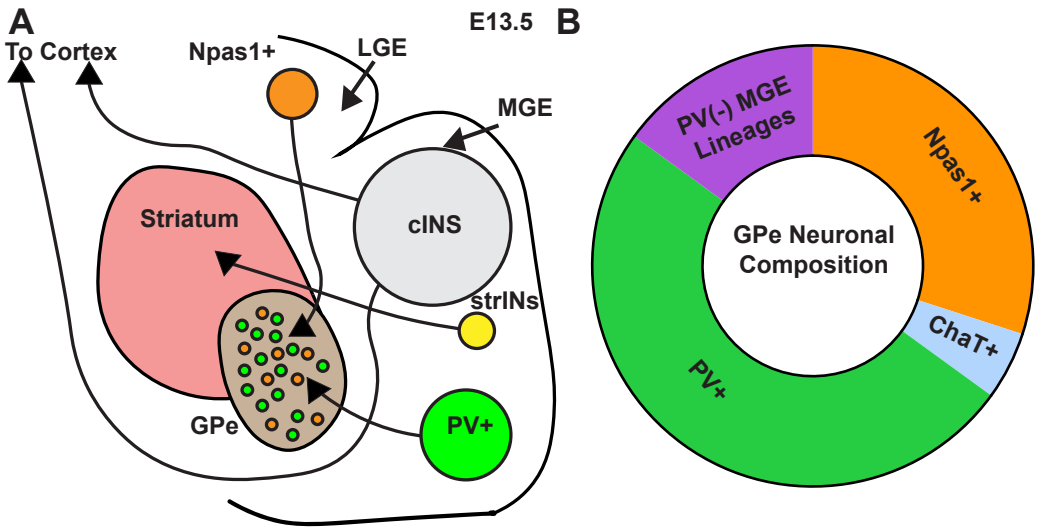

Introduction.2 Transcriptional specification of the GPe

A) Schematic of the E13.5 mouse embryonic LGE and MGE, highlighting the specification of the neuronal populations of the GPe. Relative size of the neuronal cohorts born in each progenitor zone represented by the size of the circles. Arrows indicate the migratory paths of various neuronal lineages. cINs=cortical interneruons. strINs=striatal interneurons. Adapted from (Nobrega-Pereirra et al., 2010).

B) Graphical representation of the relative proportions of neuronal populations in the GPe. Adapted from (Abecassis et al., 2020).

signalling (Villar-Cervino et al., 2015). These cardinal cellular features of mature MGE lineage neurons, including progenitor identity, post-mitotic identity, and migration, are conferred by the expression of various factors throughout MGE neurogenesis. However, there are many MGE lineage cell types that are further specified from the rest of the lineage by a host of other uncharacterized factors that are expressed during development.

Introduction.5 GPe development is poorly understood within the MGE

The globus pallidus pars externa (GPe) is one such MGE lineage; the factors that are expressed during MGE development that specify the GPe from the rest of the lineage are unknown. While much is known about MGE production of cortical interneurons (Kepecs and Fishell, 2014), the process by which the MGE generates its various projection neuron lineages is still poorly understood. The MGE produces a vast majority of the PV+ projection neurons of the GPe, with the rest of the neuronal cohort of the GPe coming from the LGE (Introduction.2 A) (Nobrega-Pereira et al., 2010; Hernandez et al., 2015). The majority of MGE born GPe neurons, known as prototypic neurons, make up approximately half of the neuronal population of the GPe (Introduction.2 B) (Abecassis et al., 2020). Furthermore, these neurons are a key feature of the canonical basal ganglia indirect pathway, a circuit that broadly regulates voluntary movement and

locomotion (Freeze et al., 2013; Holgado et al., 2010; Neumann et al., 2018; Sani et al., 2009; Windels et al., 2005; Cucca et al., 2016; Evans et al., 2020; Joel and Weiner, 1997). Prototypic neurons receive inhibitory input from the striatum and project a high frequency, tonic inhibitory projection onto the sub-thalamic nucleus (STN) (Carpenter et al., 1968; Carter and Fibiger, 1978; Holgado et al., 2010). Given the relevance of this circuit to locomotor behavior, understanding the developmental origins of the different cohorts of GPe neurons could shed light both on the broader mechanisms of neuronal differentiation within the MGE as well as the function of this critical neuronal population.

A key feature of GPe prototypic neuron development within the MGE is that it peaks early, between E11 and E13, in the ventral portion of the MGE that co-expresses Shh (Lim et al., 2018; Flandin et al., 2010) (Introduction.1). Indeed, it has been shown that upon Nkx2-1 deletion within the ventral MGE using the Shh-Cre driver line, the embryonic globus pallidus fails to form altogether (Flandin et al., 2010). Furthermore, other SVZ expressed genes, like Lhx6 and Lhx8, are expressed along with Shh and are known to be critical for the development of the GPe. For example, double knockout of Lhx6 and Lhx8 produces a disorganization of the embryonic globus pallidus, with ectopic neurons migrating past the structure into the striatum and cortex (Flandin et al., 2011). Furthermore, fate-mapping of the Lhx8 lineage shows that 100% of PV+ projection neurons in the adult GPe are labeled by Lhx8 fate-map (Mayer et al., 2018). However, beyond our current knowledge that a large cohort of PV+ neurons are specified by being of ventral MGE fate, as determined by the combinatorial expression of Nkx2-1, Shh, Lhx6 and Lhx8, the transcriptional landscape that specifies multipotent MGE lineage progenitors as GPe neurons is unknown.

Introduction.6 St18 is expressed in the MGE and could specify GPe neruons

Neuronal progenitors in the MGE are multipotent and can adopt a diverse set of fates, determined by migratory pattern, morphological characteristics, and electrophysiological properties. Studies into the diversification of this lineage are nascent and primarily focused on the relatively large cohort of cortical interneurons produced in the MGE (Lim et al., 2018; Kepecs

and Fishell, 2014). Therefore, one of the challenges to testing the hypothesis that any particular gene is involved in the development of a non-typical MGE lineage like the GPe is that many in the field are not screening for these non-typical lineages in the first place. Therefore, it is necessary to identify a putative gene involved in the specification of the GPe to begin to characterize the development of the locus at all.

Indeed, one set of factors that could regulate MGE development and potentially GPe development is the Myelin Transcription Factors (Myt TFs) gene family. They include three paralogs, Myt1 (Nzf2), Myt1L (Myt2 or Nzf1), and St18 (Nxf3 or Myt3) that are highly expressed in the progenitor cells of the neural and neuroendocrine lineages (Kim and Hudson, 1992; Vasconcelos et al., 2016; Wang et al., 2007). They can either activate or repress transcription depending on cellular context (Manukyan et al., 2018). In humans, Myt TF mutations have been associated with cancer (Jandrig et al., 2004), neuronal dysfunction (Kepa et al., 2017; Kroepfl et al., 2008), and neuroendocrine abnormalities (Blanchet et al., 2017; Loid et al., 2018). In model organisms, Myt1 and Myt1L were reported to regulate endocrine/neuronal differentiation or transdifferentiation by repressing non-neuronal genes (Mall et al., 2017; Vasconcelos et al., 2016), while the family together or St18 alone regulate pancreatic islet cell function and survival (Hentry et al., 2014; Hu et al., 2020; Tennant et al., 2012).

St18, in particular, is an interesting member of the Myt TF family given its expression pattern in the MGE throughout development. Previous work has shown that St18 has the most restricted expression of any Myt TF, dynamically peaking between E10 and E14 in a relatively spatially restricted portion of the ventral MGE (Matsushita et al., 2014; Allen Brain Institute). Interestingly, this time window overlaps with the known time course of GPe neuronal development (Lim et al., 2017). St18 is known to be expressed as well in the marginal zone of the developing cortical plate as well (Matsushita et al., 2014; Allen Brain Institute). Indeed, when examined by RNAscope, I find that St18 RNA is present in the MGE sub-ventricular zone and mantle at E13.5 (Introduction.3 A). This finding is recapitulated by immunohistochemistry at E13.5, which shows that St18 protein is present wherever St18 RNA is present (Introduction.3 B,C). Intriguingly,

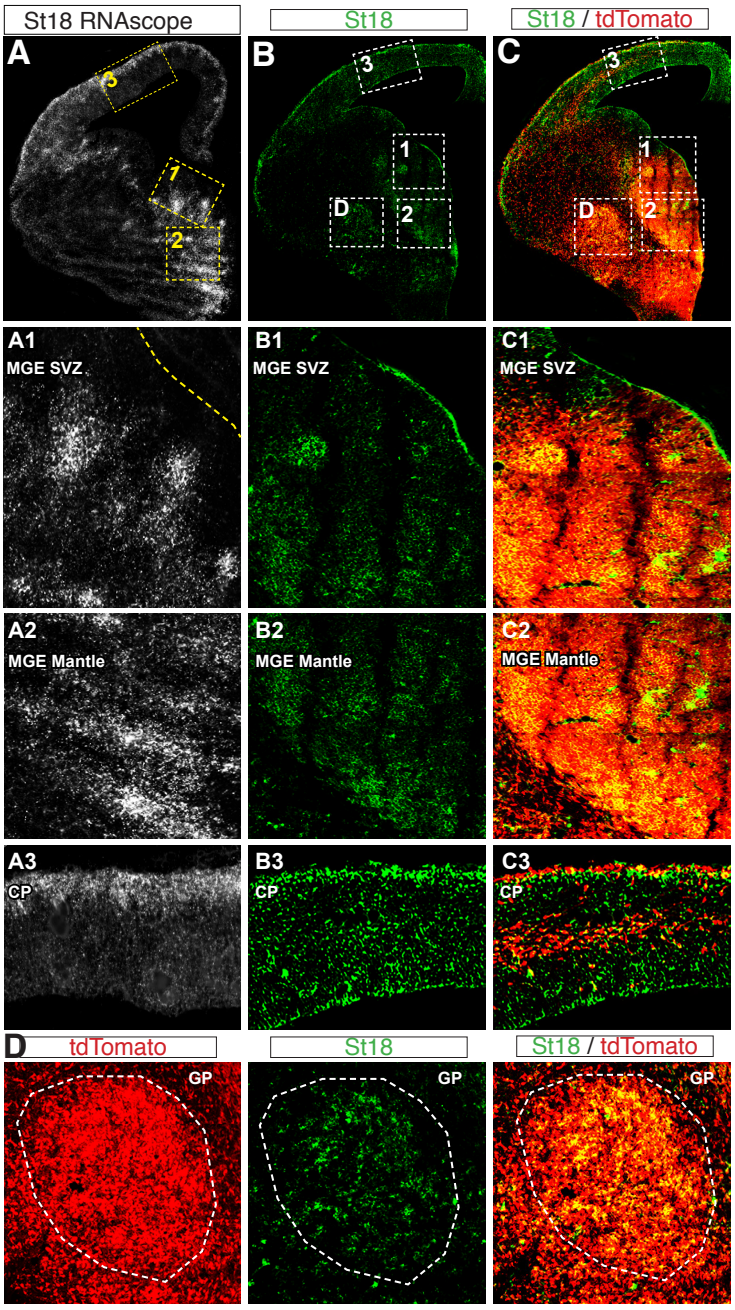

Introduction.3 *In vivo* expression pattern of St18

A) E13.5 WT embryo with RNAscope for St18 RNA expression. Insets indicate higher power images of the MGE VZ (1) MGE Mantle (2) cortical plate (CP; 3) and globus pallidus (GP; D).
B) E13.5 WT embryo with immunolabelled St18. Insets indicate higher power images in the same way as (A).
C) E13.5 WT embryo with (B) merged with MGE lineage fate map (Nkx2-1^{Cre}; Ai9). Insets indicate higher power images in the same way as (A).
D) High power image of WT embryonic GP with MGE lineage fate map, immunolabelled St18, and a merged image of the other two channels.

St18 protein is also present in the nascent globus pallidus (GP) in a region lateral and ventral to the MGE and is overlapped with fate-mapped MGE lineage neurons (Introduction.3 D). This shows, then, that St18 is a factor that is expressed in the temporal window during which GPe

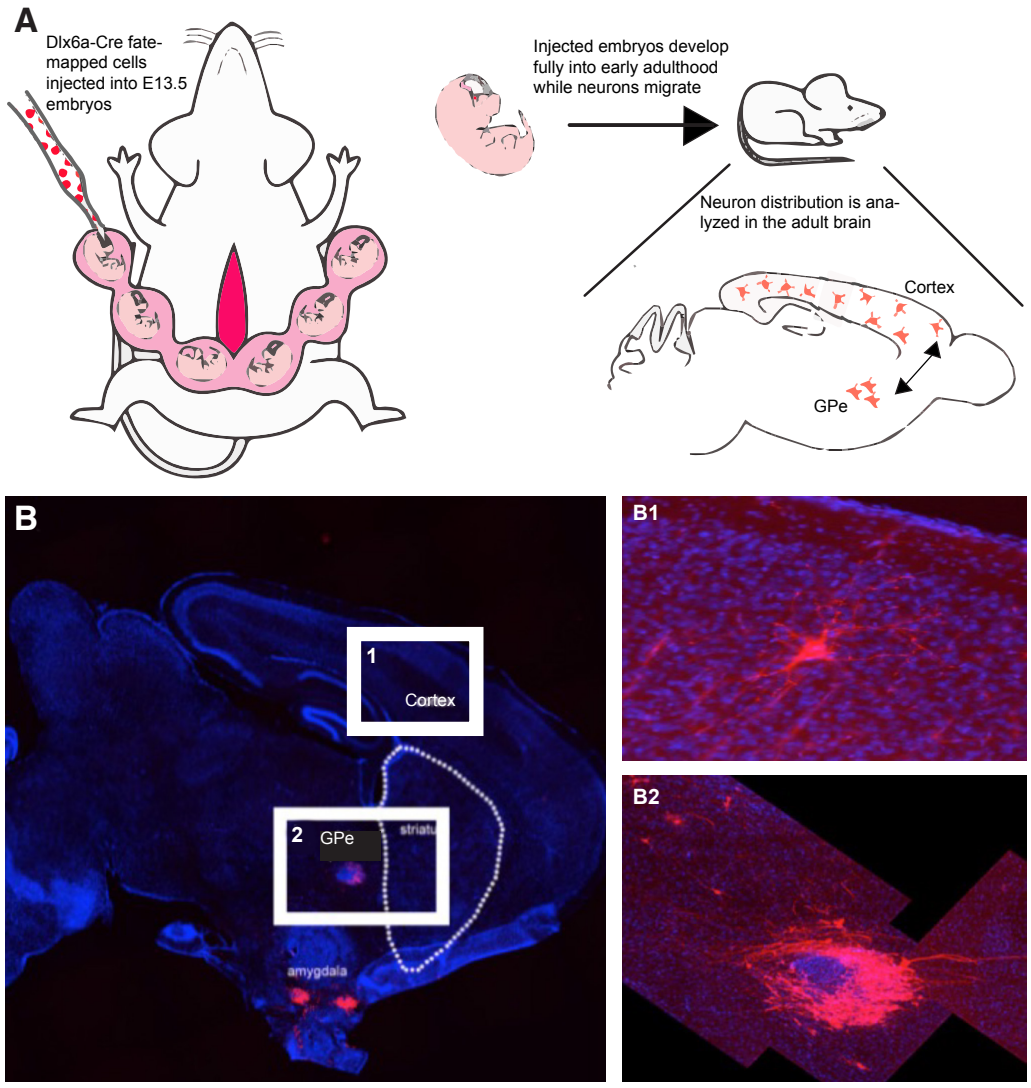

Introduction.4 St18 expression in MGE progenitors causes cells to migrate almost exclusively to the GPe

A) Schematic of UBM transplant experimental paradigm. Briefly, neurons are transplanted following differentiation into MGE lineage neurons in parallel with transgenic overexpression of St18. Fate-mapping is done with a conditional tdTomato reporter under control of Cre recombination in GABAergic MGE lineages ($Dlx6a^{Cre}$; Ai9). Differentiated neurons are injected into E13.5 embryos using ultrasound, and embryos are then allowed to develop to early adulthood, where the distribution of fate-mapped neurons is analyzed in brain tissue.

B) Representative image of an adult mouse brain in the sagittal plane following embryonic injection with MGE lineage cells programmed with St18 expression. Insets show higher power images of the cortex (1) and GPe (2).

neurons are born and within the anatomical region that GPe are born in. Furthermore, previous work has shown that, when overexpressed in MGE progenitors that are then transplanted into the *in vivo* MGE, St18 specification produces neurons that migrate primarily to the GPe instead of the cortex (Introduction.4). This is a strikingly specific migratory pattern that is not recapitulated by the presence of any other gene in MGE progenitors. This suggests that St18 may have a dis-

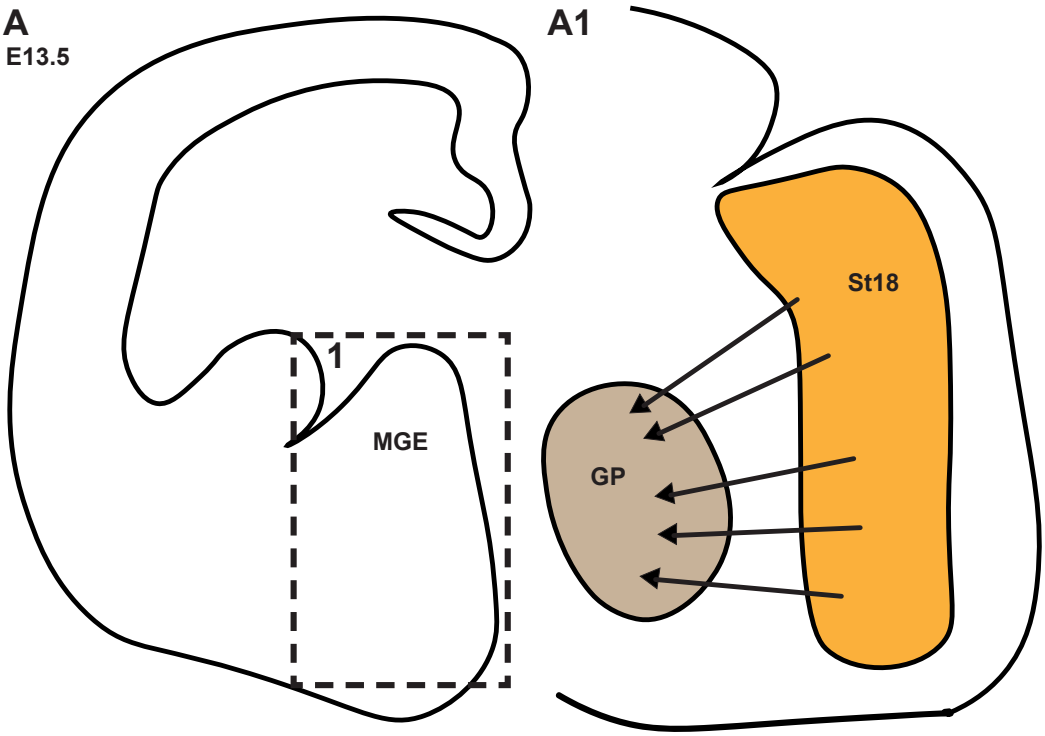

Introduction.5 St18 could specify GPe neurons within the MGE

A) Schematic of a coronal section of an E13.5 mouse embryo. Inset shows a higher power schematic of the E13.5 MGE that highlights the St18 expression pattern observed within the MGE. This scheme also highlights the hypothesis that St18 expression leads to the specification of GPe neuronal lineages.

crete role in the embryonic specification of the GPe neuronal lineage, specifically in the delineation of the GPe lineage from the rest of the heterogeneous MGE neuronal component. This, taken together with St18's expression pattern, shows that St18 is likely involved in the specification of MGE lineage GPe neurons (Introduction.5). Studying St18 will shed light into the development of a GPe neuronal cohort of previously unknown genetic origins and thereby grant genetic access to a previously uncharacterized neuronal population.

Introduction.7 Project overview

St18 is an MGE transcription factor that is expressed in a temporal-spatial pattern that overlaps with GPe neurogenesis, making St18 a prime candidate to be a factor that specifies GPe lineages within the MGE. Therefore, my dissertation will show my work studying St18's role in the specification of GPe prototypic projection neurons from the MGE.

In this study, I will show that I tested the function of the transcription factor St18 using a combination of an ES cell-based model of MGE development (Au et al., 2013) and *in vivo*

loss-of-function. I show that, upon transcriptional specification with St18, ES derived MGE neurons adopt a projection neuron-like identity, as defined by migration and morphology. I next show by gene expression analysis on ES derived MGE neurons specified by St18 that Cbx7 is an essential downstream effector gene of St18. I then show that Cbx7 is essential for St18-mediated projection-neuron migration while it plays no part in projection neuron morphogenesis. Next, by genetic loss-of-function, I show that St18 is essential for the specification of the PV+ cohort of GPe neurons and that St18 plays no role in the specification of other MGE neuronal populations. I then determine that St18 is exerting its effect on the neuronal output of the MGE during development and not on the makeup of the progenitor pool by using single cell RNA sequencing (scRNAseq) on St18 genetic loss-of-function animals. I then show that this loss of a specific GPe PV+ neuronal population following the loss of St18 produces a specific loss of prototypic projections in the STN. Last, I show that the loss of this prototypic projection induces a locomotor gait phenotype, whereby animals lacking St18 can no longer produce functional walk cycles. Taken together, I will show that St18 is essential for the development of MGE lineage PV+ prototypic GPe neurons, and I will show that these neurons form a crucial link in the circuit that controls and coordinates locomotor gait.

Chapter 1: St18 gain of function produces MGE lineage projection neurons *in vitro*

To first begin assessing the role of St18 in the development of MGE neuronal lineages, I utilized established methods to drive the expression of St18 in a controlled, replicable model of MGE development. Using this ES-based system, I demonstrate that St18 drives MGE neuronal progenitors down a distinct migratory and morphological pathway during development that makes it unique from generic MGE lineage neurons: St18 specifies projection neuron fate within an *in vitro* model of MGE development.

1.1 MGE lineage neurons specified with St18 are projection-like neurons

To test the function of St18 in the MGE, I employed an *in vitro* ES cell differentiation model of MGE development. This tool was developed to systematically test transcription factors expressed in the MGE (Au et al., 2013; McKenzie et al., 2019). Briefly, I start with a parental ES reporter line (Dlx6a-Cre; Ai9; Monory et al., 2006) that fate maps neuronal lineages born in the subpallium. This line is sequentially transcriptionally specified downstream of the Nestin promotor by Nkx2-1 and Dlx2. Nkx2-1 imparts MGE identity (Butt et al., 2008; Sussel et al., 1999) while Dlx2 further specifies GABAergic neuronal lineages (Anderson et al., 1999; Anderson et al., 19997; Le et al., 2017). The system makes use of a bidirectional Tet-O cassette that allows me to test candidate transcription factors in gain of function alongside Nkx2-1 and Dlx2 (Figure 1.1.1 A). This gain of function (GOF) system allows me to progress a multi-potent ES cell through specification as a neural stem cell, an MGE progenitor cell, and a GABAergic MGE progenitor before fate-mapping post-mitotic MGE lineage neurons (Figure 1.1.1 B). Using this system, I generated two lines: one control line for generic GABAergic MGE lineages using Nkx2-1 and Dlx2, which I named N/D, and a second line with Nkx2-1, Dlx2, and St18 (with a V5 tag), named N/D/S, to test how St18 impacts MGE neuronal output (Figure 1.1.1 C).

To verify St18 induction in the N/D/S line, I tested St18 and V5 expression by immunohistochemistry in N/D and N/D/S lines differentiated into embryoid bodies (EBs). I found colocalized labeling for St18 and V5 in the N/D/S line (Figure 1.1.2 B). In contrast, St18 was detect-

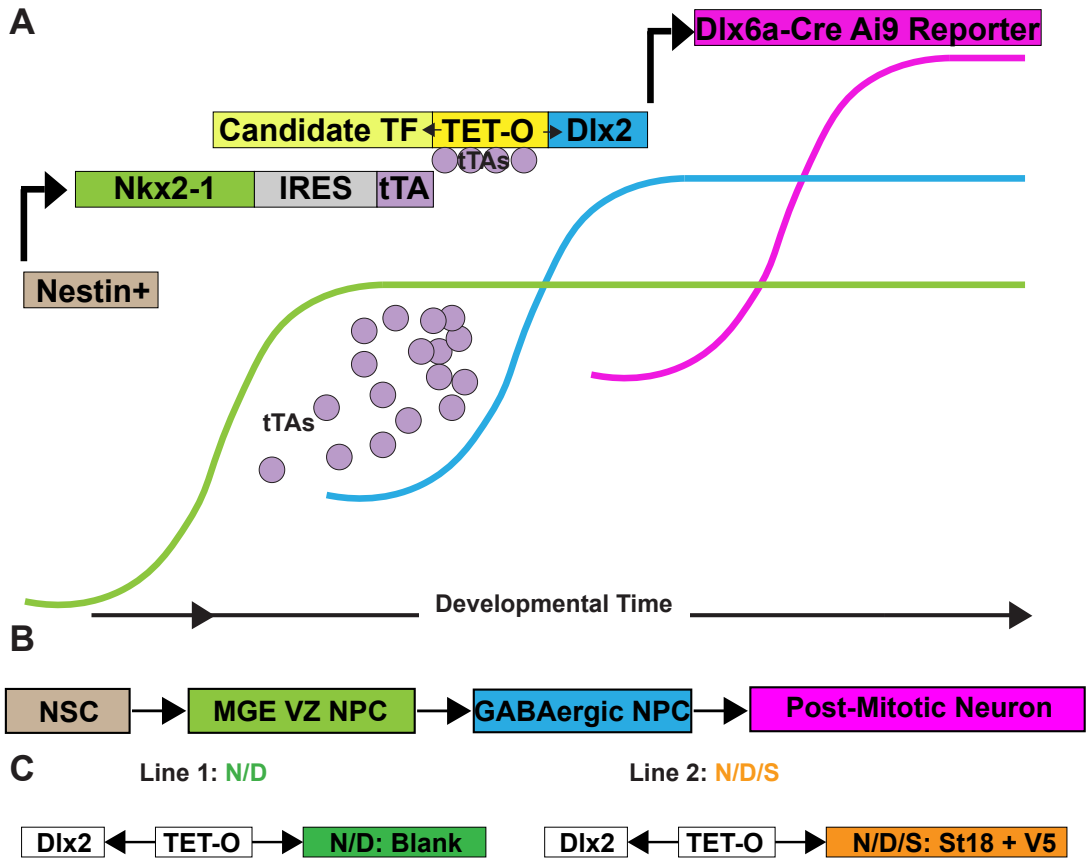

1.1.1 **ES gain of function constructs and paradigm to model MGE development *in vitro***

A) Schematic of the gain of function constructs used to test the role of various transcription factors in an *in vitro* model of MGE neurogenesis. Briefly, downstream of the Nestin promotor, Nkx2-1 is expressed along with a inter-ribosomal entry site (IRES) that controls the expression of tetracycline trans activator elements (tTAs) that accumulate over developmental time. tTAs then bind to the bi-directional tet-operon (TET-O), driving simultaneous expression of Dlx2 and additional transcription factors. Once cells exit the cell cycle, Dlx6a-Cre recombines a conditional tdTomato reporter, allowing for fate-mapping of post-mitotic, differentiated neurons.

B) Schematic illustrating the progression of cells through this model of MGE development. Cells are neuralized as neural stem cells (NSC) and then specified as MGE ventricular zone neural progenitor cells (MGE VZ NPC). Dlx2 then specifies these cells as GABAergic NPCs before the cells become post-mitotic neurons.

C) Schematic illustrating the two lines created for this study.

ed only sparsely with an absence of V5 expression in N/D EBs (Figure 1.1.2 A). Furthermore, tdTomato induction was not grossly affected by St18 induction (Figure 1.1.2). Next, I differentiated N/D and N/D/S EBs and dissociated them into monolayer cultures to examine tdTomato+ neurons. Here, I noticed a dramatic change: tdTomato fate-mapped N/D neurons were multipolar with complex morphologies reminiscent of interneurons, and consistent with previous studies (Au et al., 2013; McKenzie et al., 2019) while tdTomato+ N/D/S neurons appeared to have less complex morphologies and bore longer processes, similar to projection neurons (Figure 1.1.3).

The MGE generates both short range interneurons as well as long range projection neu-

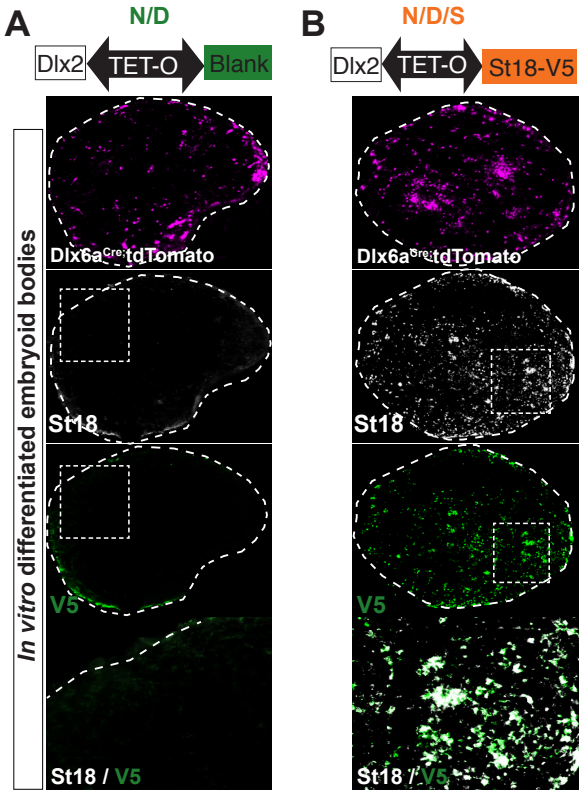

1.1.2 Verification of St18 GOF following differentiation *in vitro*

A) Schematic of transcriptional GOF in N/D line. N/D ES cell line is differentiated over 12 days into EBs. Sectioned, differentiated EBs from N/D condition shown below the schematic with conditional fate-map (Dlx6aCre; Ai9) and immunolabeling for St18 and V5 tag.

B) Schematic of transcriptional GOF in N/D/S line. N/D/S ES cell in is differentiated in the same way as N/D line. N/D/S EBs are shown below the schematic with conditional fate map (Dlx6aCre; Ai9) and immunolabeling for St18 and V5 tag.

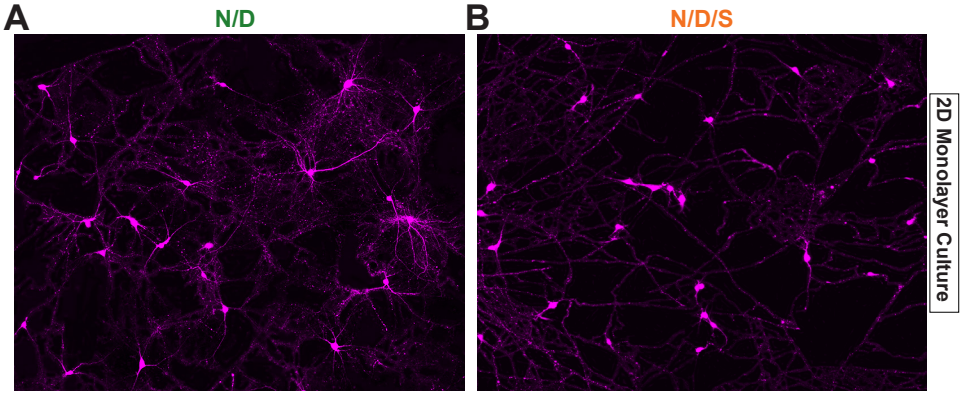

1.1.3 MGE progenitors specified with St18 have projection neuron-like morphologies

A) 2D monolayer cultures from dissociated N/D EBs with conditional fate-map (Dlx6aCre; Ai9). EBs are gently dissociated and then plated at high density to optimal survival and then cultured for 12 days before imaging.

B) 2D monolayer cultures from dissociated N/D/S EBs. Reporter and culture conditions are the same as in (A).

rons (Wichterle et al., 2001; Xu et al., 2008). The apparent difference between N/D and N/D/S cells raises the intriguing possibility that St18 may direct MGE progenitors towards projection neuron identity. To carefully test this hypothesis, I examined N/D/S neurons and N/D neurons by

the two principle features that delineate interneuron and projection neuron identities: migration and morphology.

1.2 N/D/S cells do not migrate to the same extent as N/D cells

A defining characteristic of MGE-derived interneurons is their long-distance tangential migration from their birthplace in the ventral telencephalon into the cortex (Figure 1.2.1 A) (Hu et al., 2017). In contrast, MGE-derived projection neuron migrate shorter distances, where they remain subcortical and populate nuclei in the basal ganglia and amygdala (Figure 1.2.1 B) (Bupesh et al., 2011; Dodson et al., 2015; Nobrega-Pereira et al., 2010; Puelles et al., 2000; Xu et al., 2008). Thus, if St18 instructs MGE progenitors to become projection neurons, I would expect that N/D/S neurons will migrate less than N/D neurons before they become adult sub-cortical projection neurons while N/D neurons will migrate long distances in a migratory pattern reminiscent of cortical interneurons (Figure 1.2.2 A). To test this, I embedded N/D and N/D/S EBs in

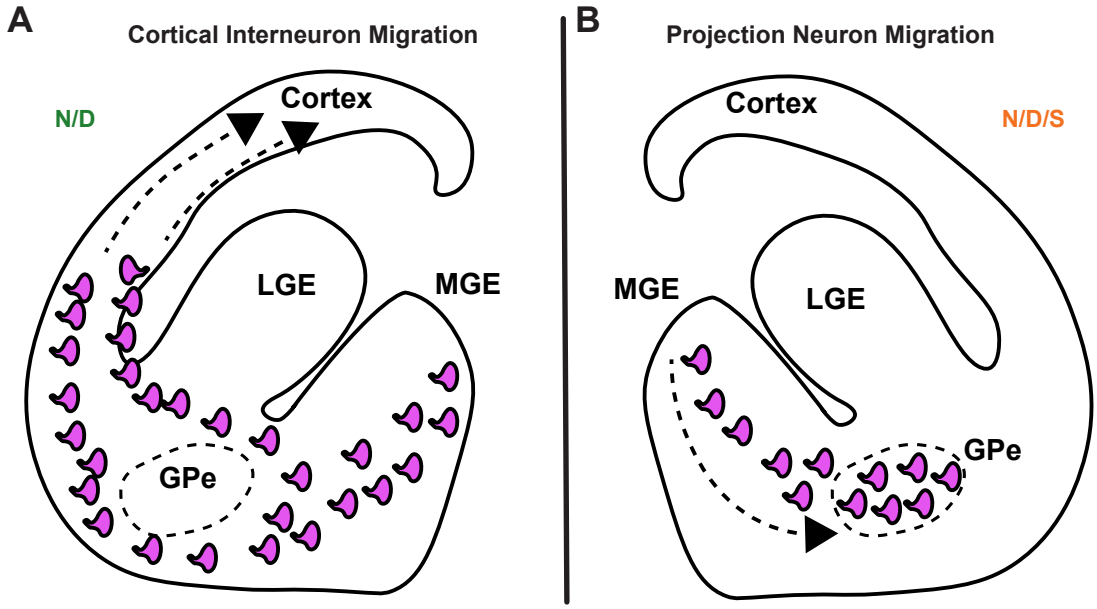

1.2.1 Projection neurons migrate less distance from the MGE than do interneurons

A) Schematic illustrating the long distance tangential migration of MGE derived cortical interneurons into the cortex.

B) Schematic illustrating the short distance migration of MGE derived GPe projection neurons from the MGE.

Matrigel and measured the capacity of Dlx6a^{Cre}; Ai9 fate-mapped neurons to migrate out of the EB (Figure 1.2.2 B). Using this assay, I found that N/D neurons robustly migrate out of EBs long distances radially into the Matrigel (Figure 1.2.2 C). Conversely, N/D/S neruons migrate shorter

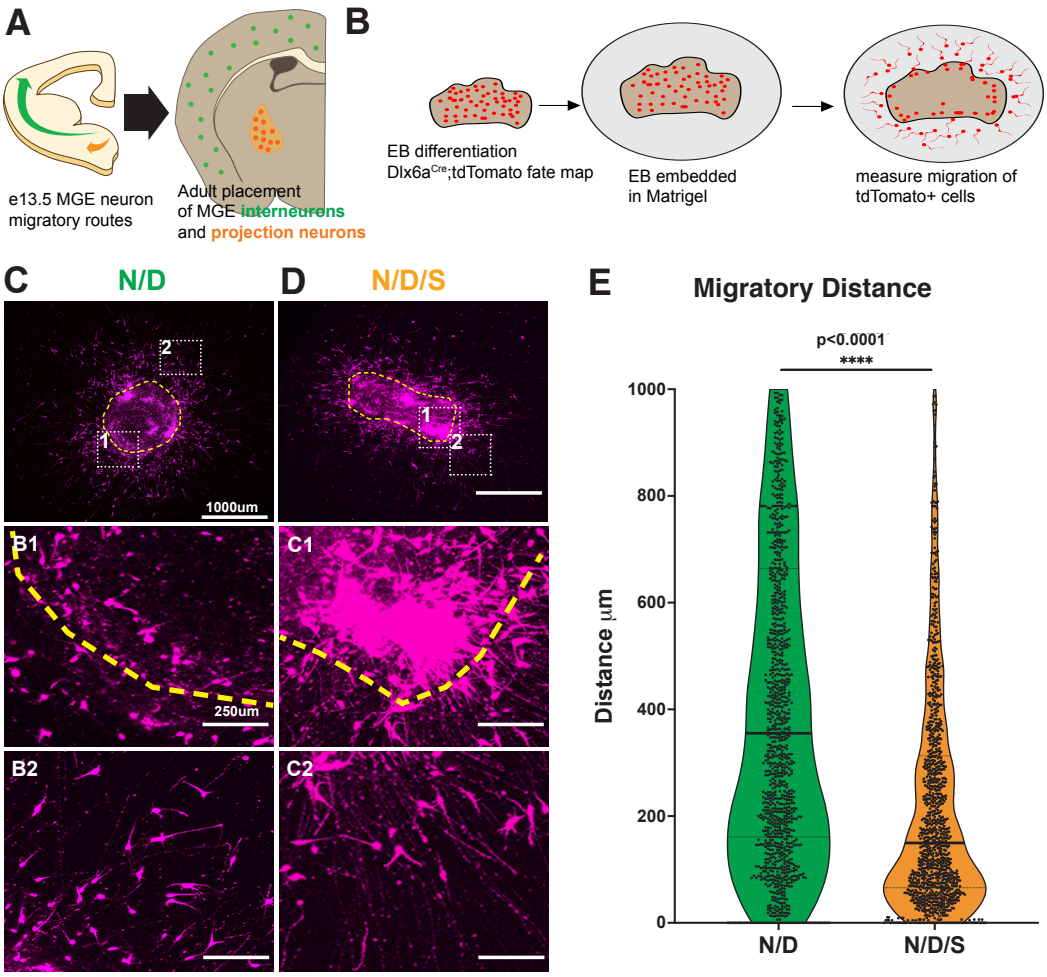

1.2.2 N/D/S cells migrate less than N/D neurons *in vitro*

A) Schematic representation (left) of MGE lineage neurons that adopt divergent migratory paths en route to (right) their final position in the adult brain. Cortical intenruons in green, GPe neurons in orange to parallel N/D and N/D/S cell line color scheme, respectively.

B) Experimental design for Matrigel embedding experiments. N/D and N/D/S lines are differentiated into EBs for 12 days after which they are embedded in Matrigel. Fate-mapped neurons (Dlx6a^{Cre}; Ai9) are allowed to migrate radially into Matrigel for 4 days before quantification.

C) Representative image of N/D EB. Yellow dashed line indicates edge of EB. Insets show EB edge (1) and migrating fate-mapped neurons (2).

D) Representative image of N/D/S EB. Yellow dashed line indicates edge of EB. Insets show neurons failing to migrate out of EB (1) and elaborated long processes (2).

E) Quantification of neuronal migration in (B) and (C): Migratory distance (*Mann-Whitney U Test*). Dataset represents cells assayed from 6 EBs per condition; 1,137 N/D/S cells and 1,156 N/D cells.

distances than N/D controls, oftentimes failing to leave the EB altogether (Figure 1.2.2 D). Furthermore, numerous N/D/S neurons that failed to migrate out of the EB produced long processes that emanated from the edge of the EB whereas migratory N/D neurons had leading unipolar and branched processes reminiscent of migratory interneurons (Figure 1.2.2 C,D, inset 2). When quantified, I find that N/D neurons migrate greater than two-fold distance farther than do N/D/S neurons, suggesting that N/D/S neurons are projection neurons when assessed by their migratory

patterns (Figure 1.2.2 E).

1.3 N/D/S cells have a projection-neuron-like morphology

This finding prompted me to examine the morphologies of N/D and N/D/S neurons in greater detail. To begin, it is crucial to first understand the salient morphological differences between a cortical interneuron and a sub-pallial projection neuron. To begin, an interneuron is defined by short range, multipolar projections that radiate from a centrally local cell body (Figure 1.3.1 A) (Ofer et al., 2020; Kepecs and Fishell, 2014). In contrast, a projection neuron is characterized primarily by a polarized morphology with long range axonal collaterals that target specific, distal synaptic partners (Figure 1.3.1 B) (O'Leary and Koester, 1993). Therefore, when determining how a cell fits into these broad categories, one must first determine the extent to which a cell adheres to these general criteria.

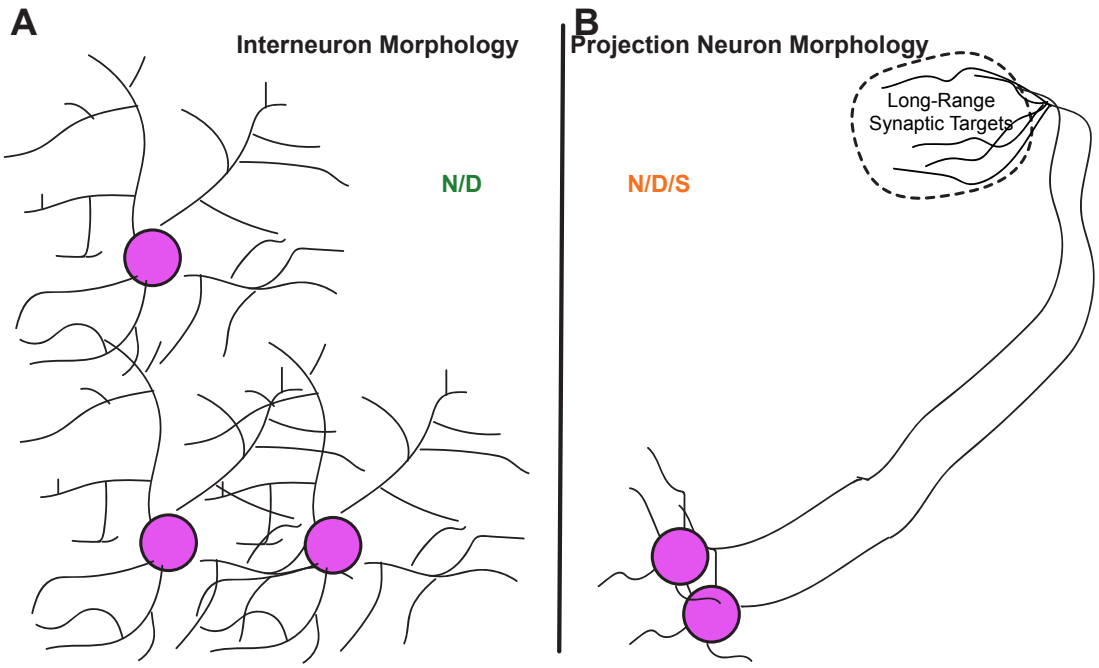

1.3.1 Interneurons and projection neurons have distinct morphologies

A) Schematic of typical interneuron morphology. Briefly, interneurons have multi-polar, locally projecting morphologies that underlie their integrative functions.

B) Schematic of a typical projection neuron morphology. Briefly, projection neurons have polarized morphologies characterized by long axonal projections that target specific, distal synaptic targets.

To do this, I dissociated N/D and N/D/S EBs and plated them sparsely onto cortical feeders. This allows for long-term 2D culture of tdTomato+ neurons, which can be analyzed morpho-

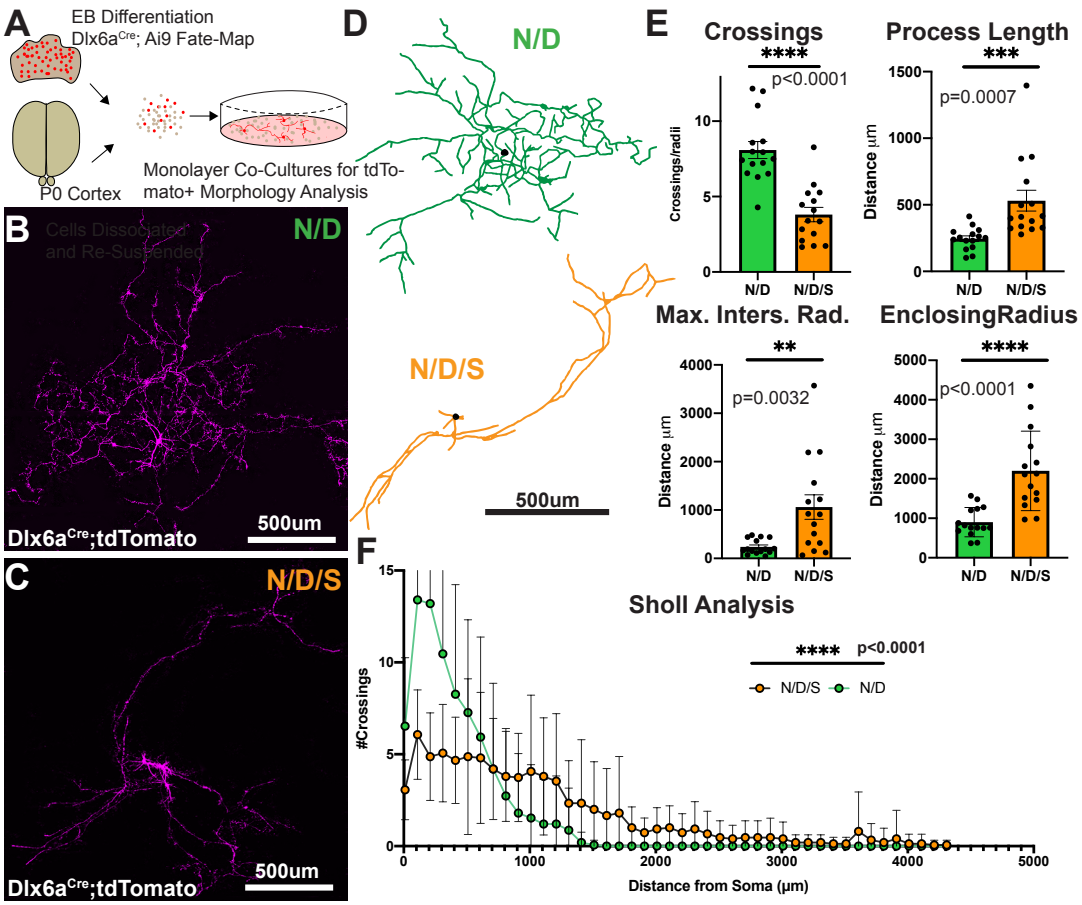

1.3.2 N/D/S cells are projection neuron-like compared to N/D interneuron morphologies

A) Experimental design of 2D monolayer tracing experiments. N/D and N/D/S lines are differentiated into EBs and dissociated into single cell suspensions. Concordantly, P0 corticies are dissociated and combined with low density EB suspensions for plating and whole cell tracing following fate-mapping (Dlx6a^{Cre};Ai9).

B) Sample N/D neuron plated at low density with fate-mapping (Dlx6a^{Cre};Ai9).

C) Sample N/D/S neuron plated at low density with fate-mapping (Dlx6a^{Cre};Ai9).

D) Representative tracings of N/D and N/D/S neurons.

E) Sholl analysis curves for tracings in (D) (*Two-Way ANOVA*).

F) Quantification of Sholl Crossings, Process Length, Maximum Intersection Radius, and Enclosing Radius (*Un-paired t-test*). Dataset represents 15 reconstructed neurons per line. Briefly, Sholl Crossings is a proxy for neuronal complexity; projection neurons have fewer crossings. Maxiumum intersection radius, enclosing radius, and process length are summary statistics that exemplify neuronal arbor size; projection neurons have longer neuronal arbors.

logically in isolation (Figure 1.3.2 A). I found that N/D/S neurons bear far longer primary processes as well as longer average process length when compared with N/D neurons (Figure 1.3.2 B,C,F). Next, I reconstructed N/D and N/D/S neurons and assayed morphological complexity by Sholl analysis, the benchmark tool for characterizing neuronal morphologies *in vitro*. I found that N/D/S neurons are significantly less branched with longer, less complex processes compared to N/D neurons (Figure 1.3.2 E, F). This striking difference between N/D and N/D/S cells is robustly recapitulated across all reconstructed cells in each condition (Figure 1.3.3), cementing the difference between N/D interneurons and N/D/S projection neurons.

Thus, I find that N/D/S neurons are less migratory than N/D neurons and that N/D/S neurons exhibit a projection-like morphology (less-branched with longer processes) that are significantly difference from the multipolar, shorter, complex morphologies of N/D neurons. Taken together, these findings suggest that St18 may be involved in specifying MGE projection neuron lineages.

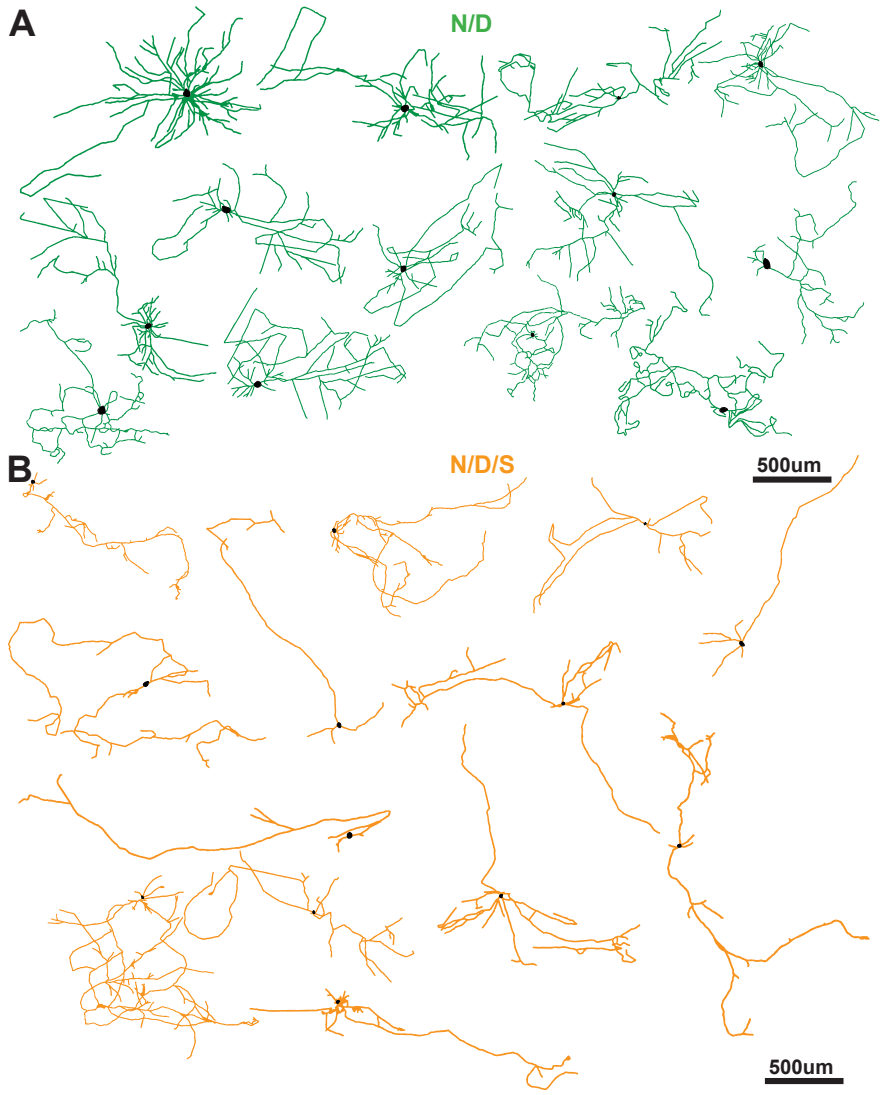

1.3.3 Additional morphological reconstructions of N/D and N/D/S neurons

A) Additional 2D tracings of N/D ES-derived MGE neurons cultured in isolation on unlabeled cortical feeders in green.

B) Additional tracings of N/D/S neurons in orange.

Chapter 2: Cbx7 acts downstream of St18 to specify projection neuron migration

After establishing that St18 GOF induces projection neuron fate in MGE neuronal progenitors as judged by migration and morphology *in vitro*, I next sought to understand the transcriptional regulation downstream of St18 expression that specifies projection neuron fate. In order to do this, I performed an RNA sequencing experiment to compare the differentially expressed genes in differentiated N/D/S and N/D neurons. I found a sizeable list of genes regulated by St18, and I followed up on a particularly well studied and drugable target, Cbx7, as a putative downstream effector gene of St18. Following pharmacological knockdown of Cbx7, I find that N/D/S projection neuron migration, but not morphology, is regulated by Cbx7. Cbx7, then, is a downstream effector of St18, regulating projection neuron migration.

2.1 RNAseq of N/D/S cells shows St18 related upregulation in Cbx7

Given the finding that N/D/S cells resemble MGE lineage projection neurons that are distinct from generic MGE lineage neurons, I next wanted to determine how St18 regulates projection neuron identity in MGE progenitors. To do this, I examined differential gene expression between N/D and N/D/S neurons using bulk RNA seq (RNAseq) *in vitro*. Brielfy, I differentiated N/D and N/D/S lines and then, using the tdTomato reporter that delineates transcriptionally specified neurons, sorted the programmed cells and batch prepared the cells from each line for sequencing. N/D/S cells differentially expressed a large cohort of genes compared to generic MGE lineage N/D cells (Figure 2.1.1 A). Following the differential gene expression analysis, I found that there were 901 upregulated genes in N/D/S cells and 674 downregulated genes in N/D/S cells based on log2FC criteria. Among the genes that were upregulated in N/D/S cells were genes associated with cessation of migration (Cbx7) (Bao et al., 2017; Nawaz et al., 2016; Ni et al., 2017), establishment of neuronal polarity (Wwp2) (Ambrozkiewicz et al., 2018), and neurite and axonal growth (Rnf157, Zfyve27, Plcg1, Mef2D) (Matz et al., 2015; Ohnishi et al., 2017; Pantakani et al., 2011; Raiborg et al., 2015; Kang et al., 2018; Lam and Chawla, 2007). Meanwhile, genes that were downregulated in N/D/S cells included genes involved in neuronal

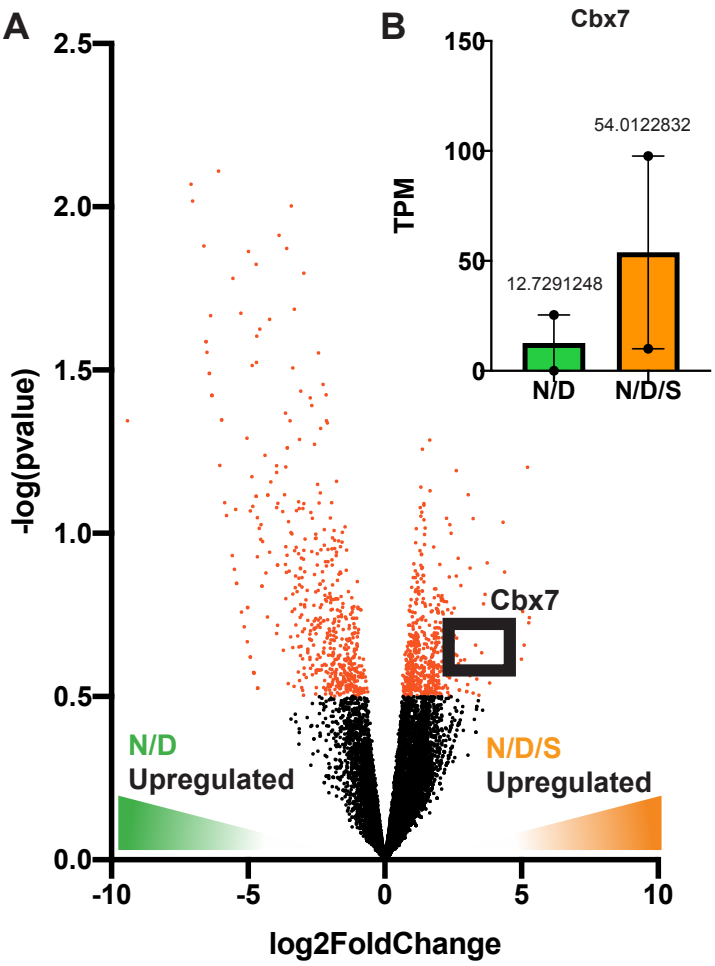

2.1.1 Differential gene expression shows that Cbx7 is upregulated in N/D/S cells

A) MA plot showing differential gene expression analysis of N/D/S vs. N/D cells following bulk RNAseq. Statistical significance is plotted against log2FC, and these criteria were used to determine significantly differentially expressed genes (Red) versus non-significantly differentially expressed genes (Black). Cbx7 is highlighted in a black box on the MA plot. Orange gradient marks genes upregulated in N/D/S cells and green gradient marks genes upregulated in N/D cells.

B) B) Cbx7 TPM plot showing biological replicates of sequencing experiment. Mean TPM showed above the column plots for N/D and N/D/S cells, respectively.

migration (Wnk1, Adgrl3, Mllt10) (Friedel et al., 2015; Sun et al., 2006; Lu et al., 2015; Kennedy et al., 2014), neurite multipolarity (Kif23) (Lin et al., 2012; McNeely et al., 2017), and decreased neurite extension or increased complexity and branching (Pcdh11x, Dock10) (Wu et al., 2015; Zhang et al., 2014; Jaudon et al., 2015). These initial insights suggest that MGE lineage neurons programmed with St18 GOF are fundamentally different neurons than generic MGE lineages. Furthermore, examining the differentially expressed genes in more detail could explain how N/D/S neurons are genetically distinct from N/D neurons.

In order to examine the transcriptional changes in N/D/S neurons compared with N/D

GO TERM	GO ID #	P-Value	Gene List
Neuron Differentiation	GO:0030182	4.50E-05	HES5, CREB1, NKX6-2, ATG7, ISL1, PBX3, FIG4, WNT7A, VASP, STAT3, NKX2-2
Regulation of Transcription	GO:0045449	3.15E-04	EGR1, SETDB1, CREB1, POU6F2, MTA3, CBX2, ISL1, TAF6L, CBX7, JUNB, STAT3, JRK, TARBP2, MEF2D, HES5, DBP, NKX6-2, GATAD2A, TEF, KDM4A, KCNH2, PBX3, NKX2-2, SERTAD1, KDM5C
Cell Fate Commitment	GO:0045165	0.00108199	HES5, NKX6-2, DLL3, TGFB1I1, ISL1, NKX2-2
Behavior	GO:0007610	0.00131326	EGR1, GNB1L, ATG7, TSC2, UBR3, ITGA3, PBX3, FIG4, STAT3
Chordate Embryonic Development	GO:0043009	0.00167849	SETDB1, SFRP2, GRN, TSC2, GATAD2A, DLL3, UBR3, VASP, JUNB
Regulation of Transcription: DNA Dependent	GO:0006355	0.00364017	EGR1, CREB1, POU6F2, MTA3, CBX2, ISL1, JUNB, STAT3, MEF2D, HES5, DBP, NKX6-2, GATAD2A, TEF, KCNH2, PBX3, NKX2-2
Regulation of RNA Metabolic Process	GO:0051252	0.00424732	EGR1, CREB1, POU6F2, MTA3, CBX2, ISL1, JUNB, STAT3, MEF2D, HES5, DBP, NKX6-2, GATAD2A, TEF, KCNH2, PBX3, NKX2-2
Regulation of Neurogenesis	GO:0050767	0.00525813	HES5, NKX6-2, ISL1, WNT7A, NKX2-2
Cell Projection Organization	GO:0030030	0.02692074	CREB1, ATG7, TSC2, MTOR, ISL1, VASP
Synapse Organization	GO:0050808	0.0277398	DRP2, WNT7A, F2R
Wnt Receptor Signalling Pathway	GO:0016055	0.03163499	SFRP2, TGFB1I1, WNT7A, BCL9
Transmission of Nerve Impulse	GO:0019226	0.03184426	NKX6-2, SYN3, LIN7B, TAC1, WNT7A
Plasma Membrane Part	GO:0044459	0.00159958	KCNC1, GABRB2, LIN7B, STXBP2, ITGA3, RIMS2, VASP, RND2, GPC2, SYN3, LRFN1, OPHN1, SYT13, MTOR, TGFB1I1, EHD1, JAM2, KCNH2
Synapse	GO:0045202	0.00449366	GABRB2, SYN3, LRFN1, LIN7B, OPHN1, RIMS2, F2R
TORC1 Complex	GO:0031931	0.01456519	MTOR, RPTOR
Synaptosome	GO:0019717	0.04113437	LIN7B, ITGA3, RIMS2

2.1.2 GO terms for genes upregulated in N/D/S cells

Table outlining the biologically relevant, statistically significant GO terms from the list of differentially expressed genes in N/D/S cells.

neurons in greater detail, I next examined the list of genes upregulated by gene ontology (GO) analysis. I did this to parse the developmental pathways and gene cascades St18 may be influencing to produce the effect of St18 GOF seen in N/D/S cells. I found among the most significantly differentially expressed GO terms were terms and genes related to neuron differentiation, synaptic development, and established pathways involved in nervous system organization (Figure 2.1.2). One of the genes that is identified as both biologically significant in our GO analysis and is also significantly differentially expressed is Cbx7 (Figure 2.1.1 A). Indeed, I found that Cbx7 was one of the most differentially expressed genes ins N/D/S cell compared to N/D cells; it was strongly upregulated in the N/D/S line (Figure 2.1.1 A,B) ($\log_2$FC = 2.09, ~4.25-fold).

Briefly, Cbx7 is a component of the Polycomb repressor complex 1 (PRC1), which broadly enacts transcriptional repression (Vandamme et al., 2011). Cbx7, via its association with the PRC1, is involved in both the early embryonic development of neural tissue (Morey et al.,

2013) as well as in post-mitotic differentiation of maturing neurons (Duan et al., 2018), making it an attractive candidate to further investigate as a potential downstream effector of St18 *in vitro.* Because of its documented involvement in various developmental processes, Cbx7 was an intriguing hit from the N/D/S differential gene expression analysis. Indeed, when deciding which downstream effector genes to test downstream of St18 GOF, I believed that promising targets would have a confluence of novelty in neural development processes, strong levels of upregulation in St18 GOF, and otherwise established roles in transcriptional control. Cbx7, having satisfied these criteria, was the target I decided to investigate downstream of St18 GOF.

2.2 Inhibition of Cbx7 causes loss of N/D/S projection neuron migration phenotype

In order to investigate the role of Cbx7 in mediating projection neuron fate in N/D/S neurons, I utilized a pharmacological inhibitor of Cbx7-mediated repression, MS351 (Ren et al., 2016). Briefly, MS351 works by inhibiting PRC1 binding to H3K27me3 methylation sites, which is involved in broad, generalized transcriptional repression and control, by inhibiting Cbx7's binding to methylation sites (Figure 2.2.1 B) (Ren et al., 2016). First, to test the efficacy of MS351, I assayed P16^{INK4A} transcript levels by qPCR (Al-Khalaf and Aboussekhra, 2013)

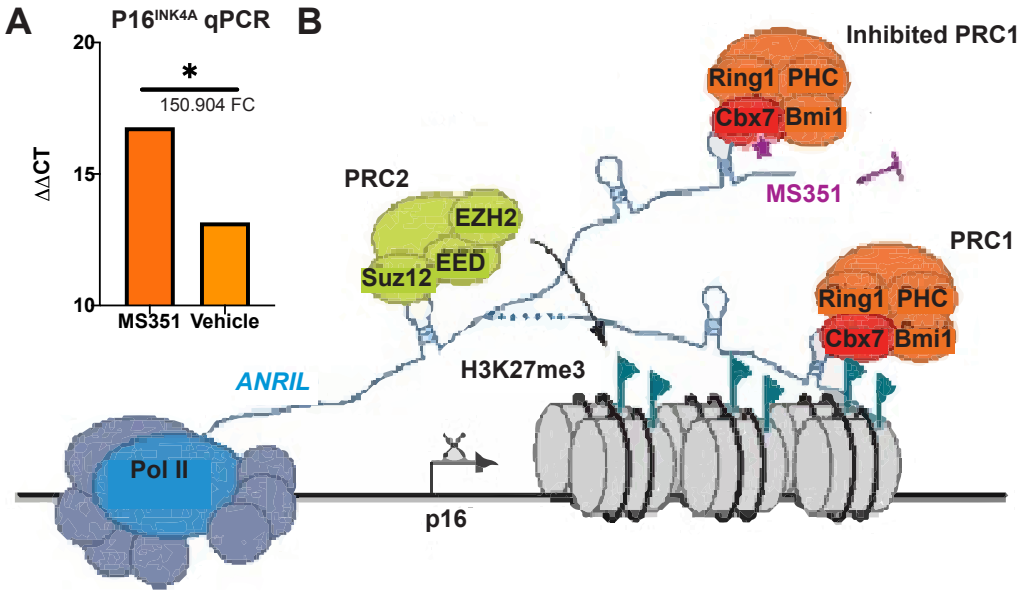

2.2.1 MS351 inhibits Cbx7 mediated transcriptional repression

A) RT qPCR validation of efficacy of MS351 pharmacological blockade of Cbx7 mediated PRC1 function. Briefly, P16^{INK4A} expression is higher when PRC1 function is blocked as a result of a loss of H3K27me3 methylation.

B) Schematic of the role of Cbx7 in the PRC1 in noncoding RNA *ANRIL* and H3K27me3-mediated gene transcriptional repression and the mode of action of MS351 (purple pentagon) in modulating Cbx7 in this functional context. Adapted from (Ren et al., 2016).

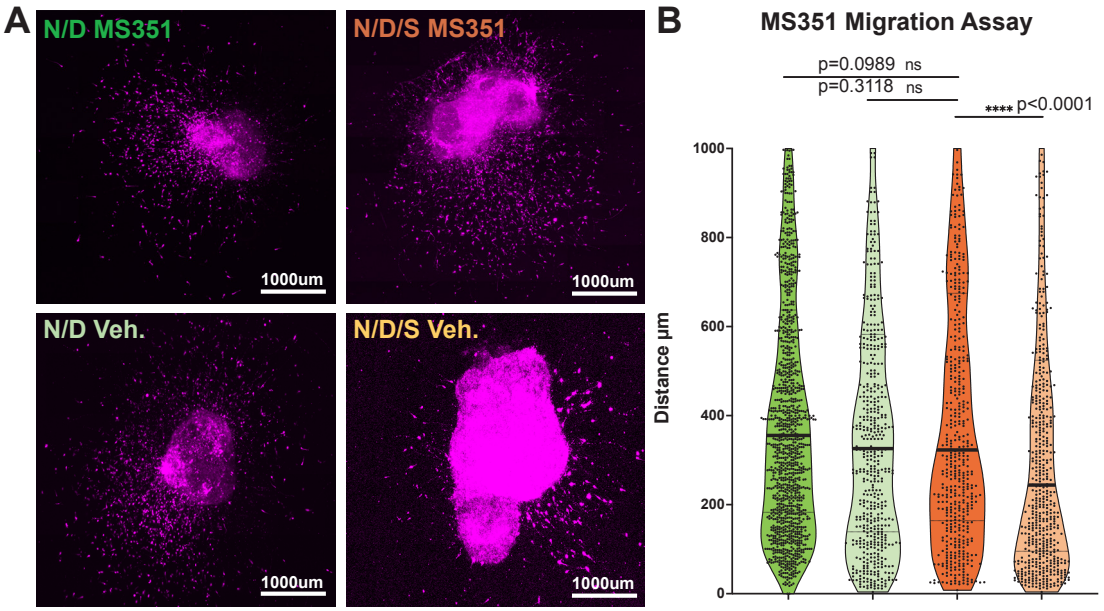

2.2.2 MS351 treatment induces interneuron-like migration in N/D/S cells

A) Representative images of N/D and N/D/S EBs treated with either MS351 or Vehicle during differentiation. Images capture four days following embedding in Matrigel and culture to allow for migration.

B) Quantification of MS351 migration assay (*Mann-Whitney U Test*). Dataset represents 3 EBs per condition; 531 N/D/S MS351 cells, 614 N/D/S Veh. cells, 1,301 N/D MS3451 cells, and 567 N/D Veh. cells.

in N/D/S neurons. This assay will test the efficacy of MS351 because $P16^{INK4A}$ transcription is negatively regulated by Cbx7-mediated PRC1 activity (Bernard et al., 2005). I found that N/D/S cells treated with MS351 had higher levels of $P16^{INK4A}$ compared to N/D/S cells treated only with vehicle (Figure 2.2.1 A).

Having established that MS351 works as expected, I next tested if MS351 treatment affects the *in vitro* migratory phenotype of N/D/S cells, specifically testing if Cbx7 is involved in N/D/S induced projection neuron migration. To test this, I used the Matrigel migration assay that I introduced in the previous chapter. During this assay, I applied MS351 or vehicle to differentiating EBs and during the culture paradigm to inhibit Cbx7 throughout the experiment. Recall that N/D neurons migrate significantly further than N/D/S neurons in my *in vitro* migration assay. However, following application of MS351, I find that N/D/S neurons now migrate significantly further than vehicle-treated N/D/S neurons (Figure 2.2.2). Intriguingly, N/D/S neurons treated with MS351 migrate as far as N/D neurons either treated with MS351 or with vehicle (Figure 2.2.2). Furthermore, N/D/S neurons treated with vehicle fail to migrate in the same fashion as N/D/S neurons from my earlier experiment, instead producing processes that emanate from the

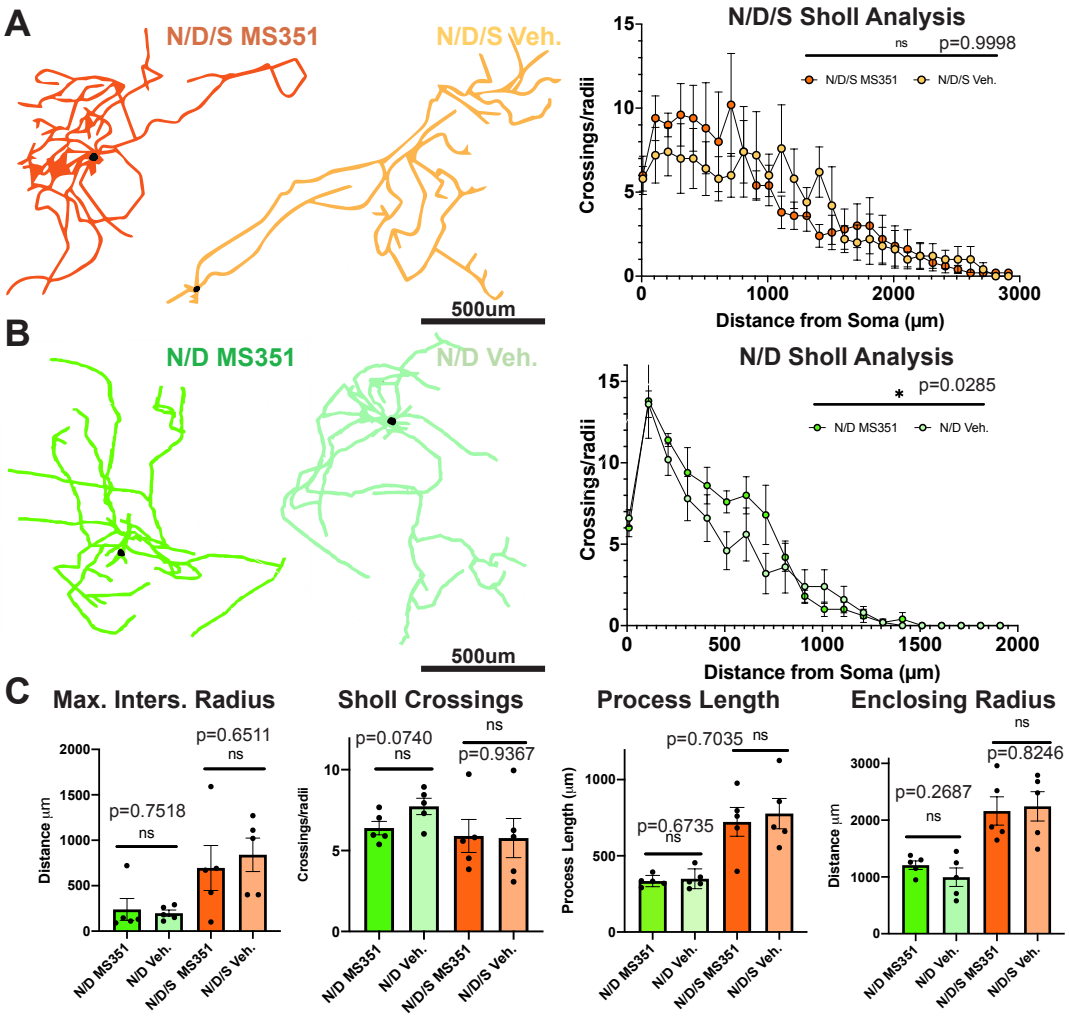

2.3.1 MS351 treatment does not affect MGE lineage neuronal morphology

A) Sample neuronal reconstructions in N/D/S MS351 and N/D/S vehicle conditions. Sholl analysis was performed and curves are shown to the right of the reconstructions (*2 way ANOVA*).

B) Sample neuronal reconstructions in N/D MS351 and N/D vehicle conditions. Sholl analysis was performed and curves are shown to the right of the reconstructions (*2 way ANOVA*).

C) Sholl summary statistics for all conditions shown above (*Un-paired t-test*). Dataset represents five reconstructed neurons per condition.

edge of the EB (Figure 2.2.2 A). This result suggests that N/D/S neurons treated with MS351 lose projection neuron-like migratory behavior and, instead, migrate in a more interneuron-like manner. Cbx7, then, is integral to projection neuron migratory behavior observed in N/D/S neurons downstream of St18 programing of MGE lineage neural progenitors.

2.3 Inhibition of Cbx7 does not affect N/D/S projection neuron morphology

Given that Cbx7 appears to be a downstream effector gene of St18, producing projection neuron migratory behavior of N/D/S neurons, I next wanted to determine if Cbx7 is also responsible for the morphological phenotype of N/D/S projection neurons. To test this, I used the 2D

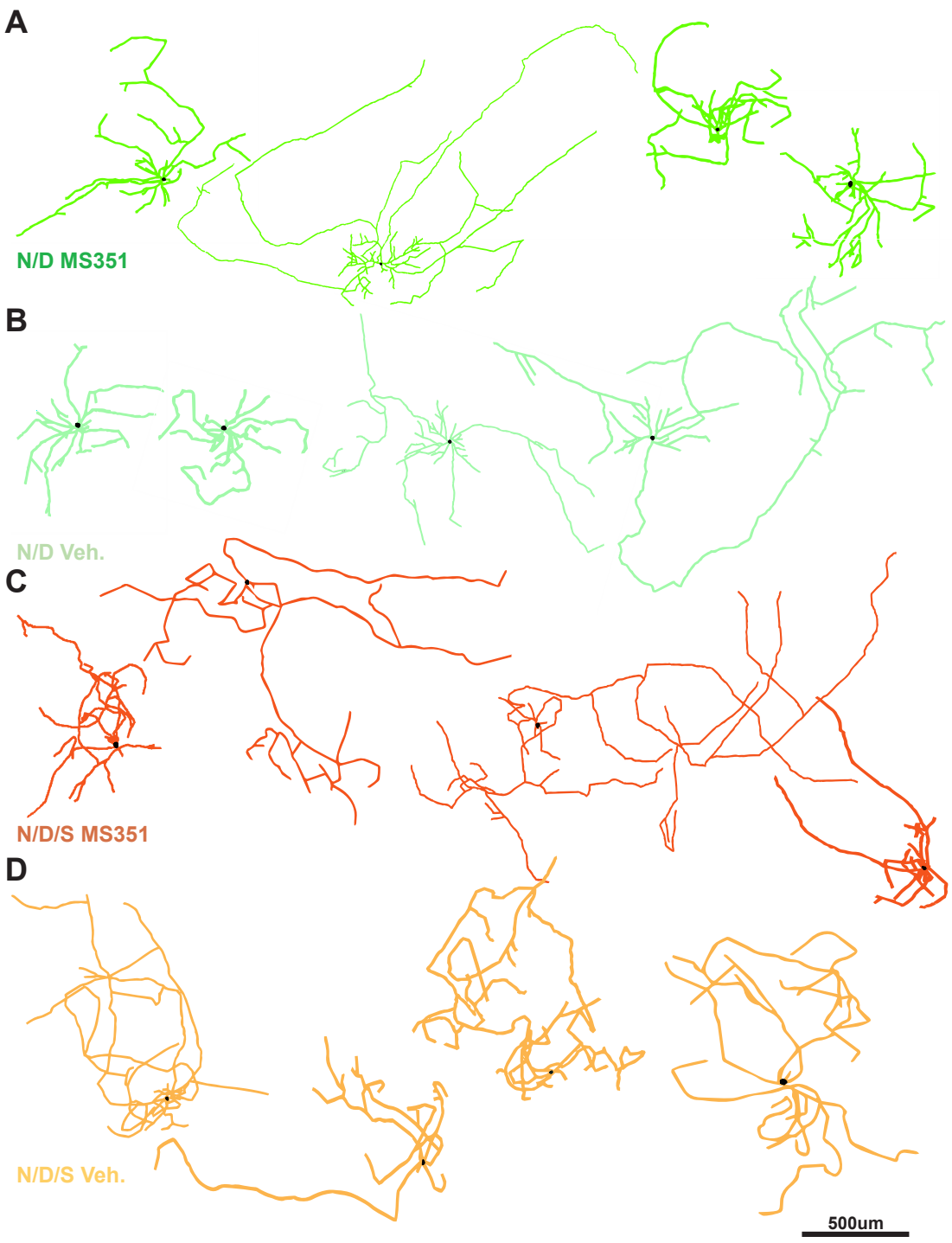

2.3.2 Additional neuronal reconstructions for N/D and N/D/S cells treated with MS351

A) Neuronal reconstructions for N/D MS351 condition.
B) Neuronal reconstructions for N/D Vehicle condition.
C) Neuronal reconstructions for N/D/S MS351 condition.
D) Neuronal reconstructions for N/D/S Vehicle condition.

culture assay of neuronal reconstructions by Sholl analysis introduced in the previous chapter.

During this assay, I applied MS351 or vehicle to differentiating EBs and during the culture para-

digm to inhibit Cbx7 throughout the experiment. Recall that N/D/S neurons have less-complex, more polarized neuronal morphologies that resemble projection neurons compared to interneuron-like N/D neurons. Following MS351 treatment, I found no change in N/D/S neuronal morphology compared to vehicle treated neurons (Figure 2.3.1 A). There is also little overall change in N/D neuronal morphology following MS351 treatment, as the cells maintain their complexity and process length features with little shift in the Sholl curves (Figure 2.3.1 B). The morphological characteristics defining N/D/S neurons compared to N/D neurons remain in-tact following MS351 treatment (Figure 2.3.1 C; Figure 2.3.2). This means that projection neuron morphology is maintained following Cbx7 inhibition. There must be another gene or group of genes, then, that operates downstream of St18 in N/D/S cells to produce projection neuron morphology.

Chapter 3: St18 loss of function produces a loss of projection neurons in the GPe

Based on my *in vitro* findings that St18 is regulating a transcriptional cascade that produces MGE lineage projection neurons, I believed that the next logical step would be to test if St18 is regulating MGE lineage projection neuron development *in vivo*. To do this, I generated a whole animal St18 knockout (St18 (-/-)) mouse and a mouse with a conditional ablation of St18 in the MGE lineage (cKO). I found that these genetic manipulations had no effect on the early proliferation, cell death, and patterning of the MGE but instead led to a specific loss of St18 RNA and protein. Downstream of this loss of St18 in both whole animal knockout and conditional knockout animals, I found a specific loss of MGE lineage PV+ GPe projection neurons. St18, then, is essential for the proper development of a specific MGE lineage projection neuron population *in vivo*.

3.1 St18 conditional allele produces a decrease in St18 RNA and a loss of protein

Given my *in vitro* findings showing that St18 specifies projection neurons within a model of MGE development, I next sought to test the function of St18 in *in vivo* MGE lineage projection neuron development. To do this, I used a conditional St18 loss-of-function allele that was generated by introducing flanking LoxP sites to exons 9 and 10 of the St18 genetic locus (Huang et al., 2018). Briefly, Cre-mediated recombination causes a frame shift in the coding region along with a premature stop codon, resulting in the production of a truncated N-terminal fragment of the St18 protein. Using this conditional loss-of-function allele, I generated St18 null (St18 (-/-)) and St18 MGE lineage specific conditional knockout animals (cKO).

Briefly, St18 (-/-) animals were generated by crossing St18 conditional loss of function animals to a germline driver line (E2a-Cre). Genotypes used in St18 (-/-) experiments were St18 null homozygotes and St18 null heterozygote littermate controls (-/- ; +/-). St18 cKO animals were generated by crossing St18 conditional loss of function animals to an MGE-lineage-specific driver line (Nkx2-1-Cre). Genotypes used for St18 cKO experiments were cKO homozygotes with heterozygote controls ($St18^{fl/fl}$;$Nkx2\text{-}1^{Cre}$; $St18^{fl/+}$;$Nkx2\text{-}1^{Cre}$).

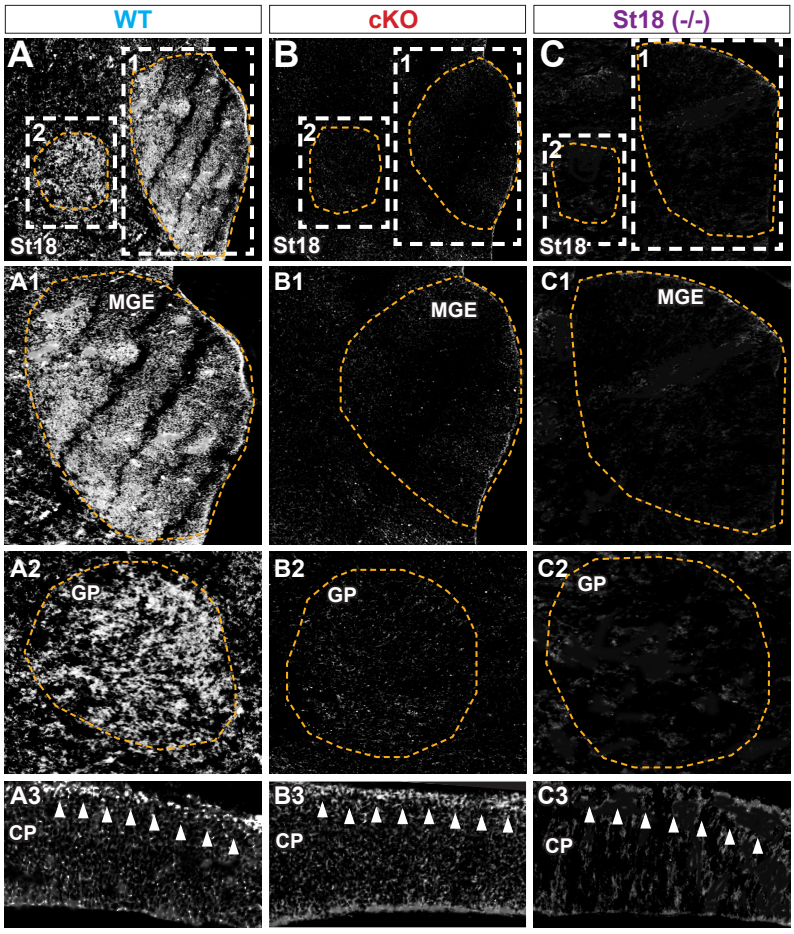

3.1.1 Histological validation of St18 (-/-) and cKO genetic knockout strategies

A) WT E13.5 MGE immunolabelled with St18 antibody. Insets indicate MGE (1) and GP (2). CP (3) shown below with arrowheads indicating location of St18 immuno-labelling in the marginal zone.
B) St18 cKO E13.5 MGE immunolabelled with St18. Subsets are the same as (A).
C) St18 (-/-) E13.5 MGE immunolabelled with St18. Subsets are the same as (A).

To test the efficacy of these genetic knockout strategies, I examined St18 (-/-) and cKO embryonic brain tissue at embryonic day E13.5 by St18 histology and compared to WT embryos. Recall that St18 RNA and protein is present in the MGE SVZ and in the nascent globus pallidus (GP) as well as in the marginal zone of the cortical plate (CP) in WT embryos (Figure 3.1.1 A). I found that St18 protein was not detectable throughout St18 (-/-) embryos (Figure 3.1.1 C). Next, I found that St18 protein was absent in the cKO MGE and GP, since these structures express Nkx2-1 and therefore also express Cre to ablate St18 (Figure 3.1.1 B). However, St18 is present in the CP in cKO embryos, as this structure does not express Cre in cKO animals (Figure 3.1.1 B). Importantly, these findings are consistent with previous work characterizing the St18 conditional allele and St18 antibody (Hu et al., 2020; Huang et al., 2018). Taken together with previ-

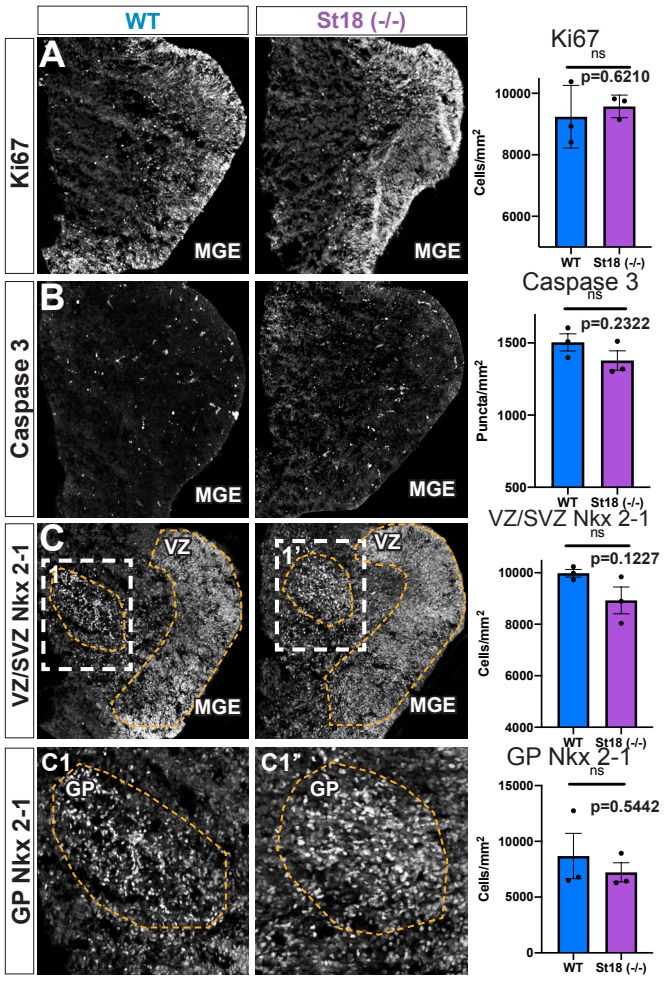

3.2.1 St18 (-/-) has no effect on MGE proliferation, cell death, or early progenitor patterning

A) WT and St18 (-/-) E13.5 MGE with immunolabelled Ki67 (*Unpaired t-test*).
B) WT and St18 (-/-) E13.5 MGE with immunolabelled Casp3 (*Unpaired t-test*).
C) WT and St18 (-/-) E13.5 MGE with immunolabelled Nkx2-1. VZ is outlined in orange. Inset shows higher-powered imaged GP (*Unpaired t-test*). All datasets represent N=3 per genotype.

ous work, this indicates that the St18 genetic knockout strategies used in the upcoming experiments work as anticipated.

3.2 St18 (-/-) does not cause a change in MGE cell-death or proliferation at E13.5

Before investigating the effect of St18 genetic ablation on a specific MGE projection neuron lineage *in vivo*, I first wanted to determine if St18 loss of function has any gross developmental phenotypes. To test this, I first examined MGE proliferation and cell death in St18 (-/-) embryos by immunohistochemistry. To test proliferation, I examined WT and St18 (-/-) E13.5 embryos by Ki67 antibody staining. I found that there was no discernable, significant difference between WT and St18 (-/-) with regards to Ki67 staining (Figure 3.2.1 A). To test cell death, I

examined WT and St18 (-/-) E13.5 embryos by cleaved-Caspase3 antibody staining. Again, I found that there was no difference between WT and St18 (-/-) with regards to Caspase3 signal (Figure 3.2.1 B). I next tested whether St18 (-/-) embryos exhibited defects in early MGE patterning by examining Nkx2-1+ cells in either the MGE VZ/SVZ or ventrally in the developing globus pallidus (GP) (Flandin et al., 2010). I found that there is no difference in either the MGE or GP between St18 (-/-) and WT embryos (Figure 3.2.1 C). Together, I conclude that St18 loss of function does not produce changes in proliferation, cell-death, or early MGE patterning.

3.3 St18 (-/-) and St18 cKO cause a loss of PV+ projection neurons in the GPe

The MGE produces GABAergic neurons that populate the cortex, hippocampus, striatum, medial amygdala (MeA), and globus pallidus pars externa (GPe) (Xu et al., 2008). Given that

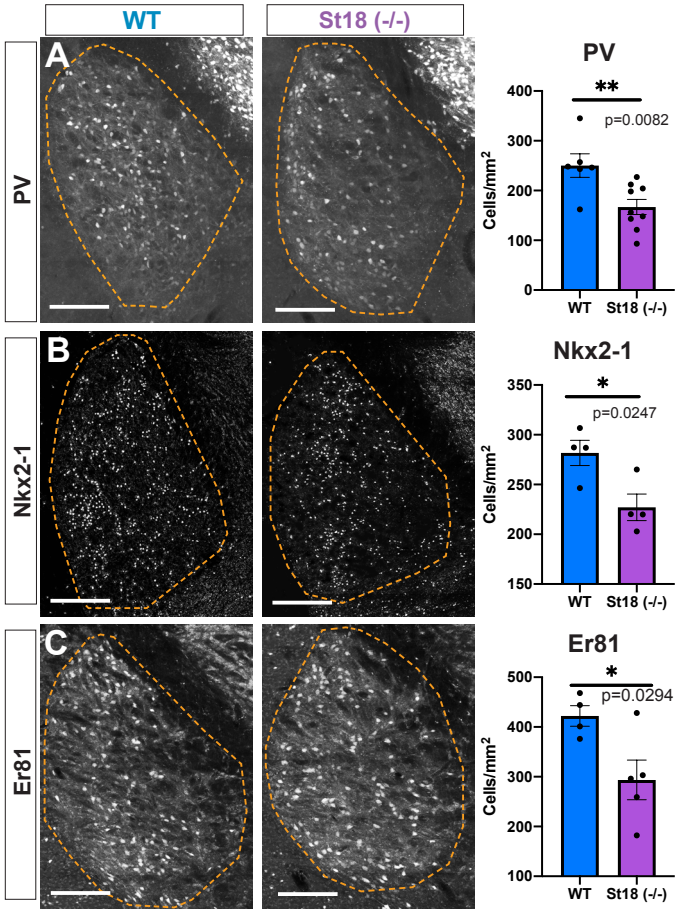

3.3.1 St18 (-/-) causes a loss of MGE lineage prototypic neurons in the GPe

A) Representative images of WT and St18 (-/-) GPe with PV immunolabelling. Quantification to the right of the images (*Unparied t-test*). N= 6 WT and 9 St18 (-/-).

B) Representative images of WT and St18 (-/-) GPe with Nkx2-1 immunolabelling. Quantification to the right of the images (*Unparied t-test*). N= 4 WT and 4 St18 (-/-).

C) Representative images of WT and St18 (-/-) GPe with Er81 immunolabelling. Quantification to the right of the images (*Unparied t-test*). N= 4 WT and 5 St18 (-/-).

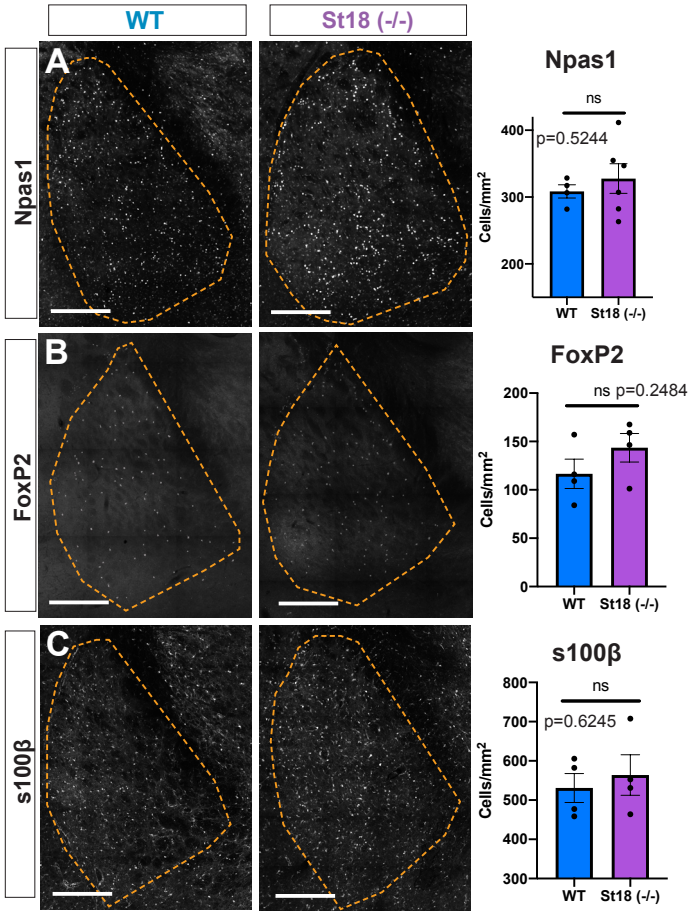

3.3.2 St18 (-/-) does not cause a loss of arkypallidal neurons or glial cells in the GPe

A) Representative images of WT and St18 (-/-) GPe with Npas1 immunolabelling. Quantification to the right of the images (*Unparied t-test*). N= 4 WT and 6 St18 (-/-).

B) Representative images of WT and St18 (-/-) GPe with FoxP2 immunolabelling. Quantification to the right of the images (*Unparied t-test*). N= 4 WT and 4 St18 (-/-).

C) Representative images of WT and St18 (-/-) GPe with s100B immunolabelling. Quantification to the right of the images (*Unparied t-test*). N= 4 WT and 4 St18 (-/-).

St18 expression leads to the adoption of projection neuron migration and morphology in an *in vitro* model of MGE development, I believed that examining St18 loss of function phenotypes in loci populated by MGE lineage projection neurons would be a fruitful starting point to determining the effect of St18 loss of function on MGE lineage development. The GPe is a nucleus that is densely populated by MGE lineage projection neurons where, during development, I observed St18 expression at E13.5. Therefore, I decided to first investigate the GPe following St18 genetic ablation.

To determine the effect of St18 genetic loss of function on MGE lineage GPe projection neuron development, I surveyed the number of MGE-derived prototypic neurons, determined by PV, Nkx2-1, and Er81 expression (Nobrega-Pereira et al., 2010; Abdi et al., 2015). I also

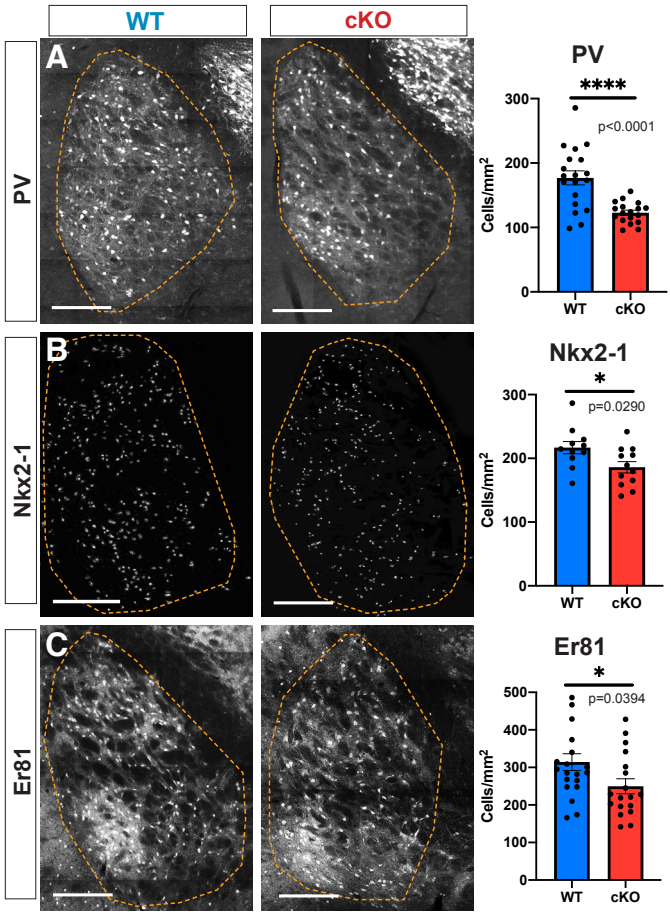

3.3.3 St18 cKO causes a loss of MGE lineage prototypic neurons in the GPe

A) Representative images of WT and St18 cKO GPe with PV immunolabelling. Quantification to the right of the images (*Unparied t-test*). N= 19 WT and 18 St18 cKO.

B) Representative images of WT and St18 cKO GPe with Nkx2-1 immunolabelling. Quantification to the right of the images (*Unparied t-test*). N= 11 WT and 12 St18 cKO.

C) Representative images of WT and St18 cKO GPe with Er81 immunolabelling. Quantification to the right of the images (*Unparied t-test*). N= 20 WT and 18 St18 cKO.

surveyed the number of LGE-derived arkypallidal neurons, determined by Npas1 and FoxP2 expression (Dodson et al., 2015; Hernandez et al., 2015; Nobrega-Pereira et al., 2010). I also surveyed the GPe cohort of astrocytes, determined by S100B. I began by first characterizing the GPe in St18 (-/-) animals, as this manipulation is the broadest and most comprehensive loss of St18 RNA and protein. In St18 (-/-) animals, I found that there was a significant decrease in PV+, Nkx2-1+, and Er81+ prototypic neurons in the GPe (Figure 3.3.1). Interestingly, we observed no significant difference in any other neuronal or glial component of the GPe (Figure 3.3.2). Therefore, St18 (-/-) produces a significant loss of MGE lineage PV+ prototypic neurons in the GPe.

To next determine to extent to which this effect was due to a defect in MGE lineage specification, I recapitulated my characterization of the GPe using St18 cKO specifically in the MGE.

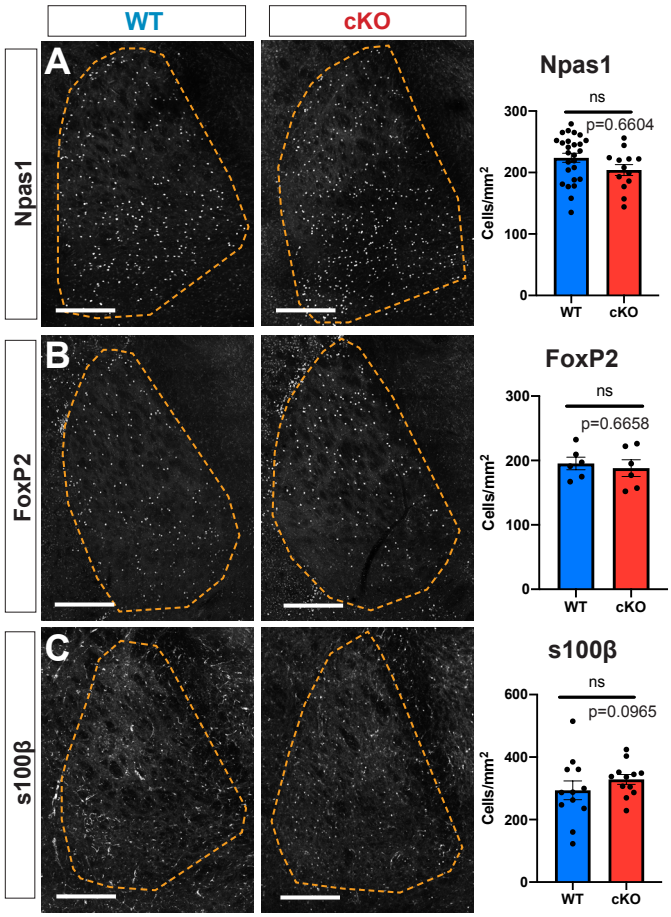

3.3.4 St18 cKO does not cause a loss of arkypallidal neurons or glial cells in the GPe

A) Representative images of WT and St18 cKO GPe with Npas1 immunolabelling. Quantification to the right of the images (*Unparied t-test*). N= 26 WT and 13 St18 cKO.

B) Representative images of WT and St18 cKO GPe with FoxP2 immunolabelling. Quantification to the right of the images (*Unparied t-test*). N= 6 WT and 6 St18 cKO.

C) Representative images of WT and St18 cKO GPe with S100B immunolabelling. Quantification to the right of the images (*Unparied t-test*). N= 12 WT and 12 St18 cKO.

In St18 cKO animals, I found the same, significant decrease in PV+, Nkx2-1+, and Er81+ neurons in the GPe (Figure 3.3.3). St18 cKO animals also show no loss of other neuronal and glial components of the GPe (Figure 3.3.2 D-F). Therefore, St18 ablation, either in the whole animal or in the MGE lineage specifically, produces a dramatic loss of PV+ prototypic projection neurons. This result shows that St18 is involved in the specification of projection neurons *in vivo*.

3.4 St18 (-/-) and St18 cKO does not change other MGE lineage populations

Since St18 (-/-) and cKO animals exhibit a loss of MGE lineage GPe prototypic projection neurons, I next sought to determine if St18 is also responsible for the specification of other MGE neuronal lineages, projection neuron or otherwise. In order to do this, I crossed St18 cKO animals with a conditional fate-mapping allele, Ai9. This allows for simultaneous tdTomato+

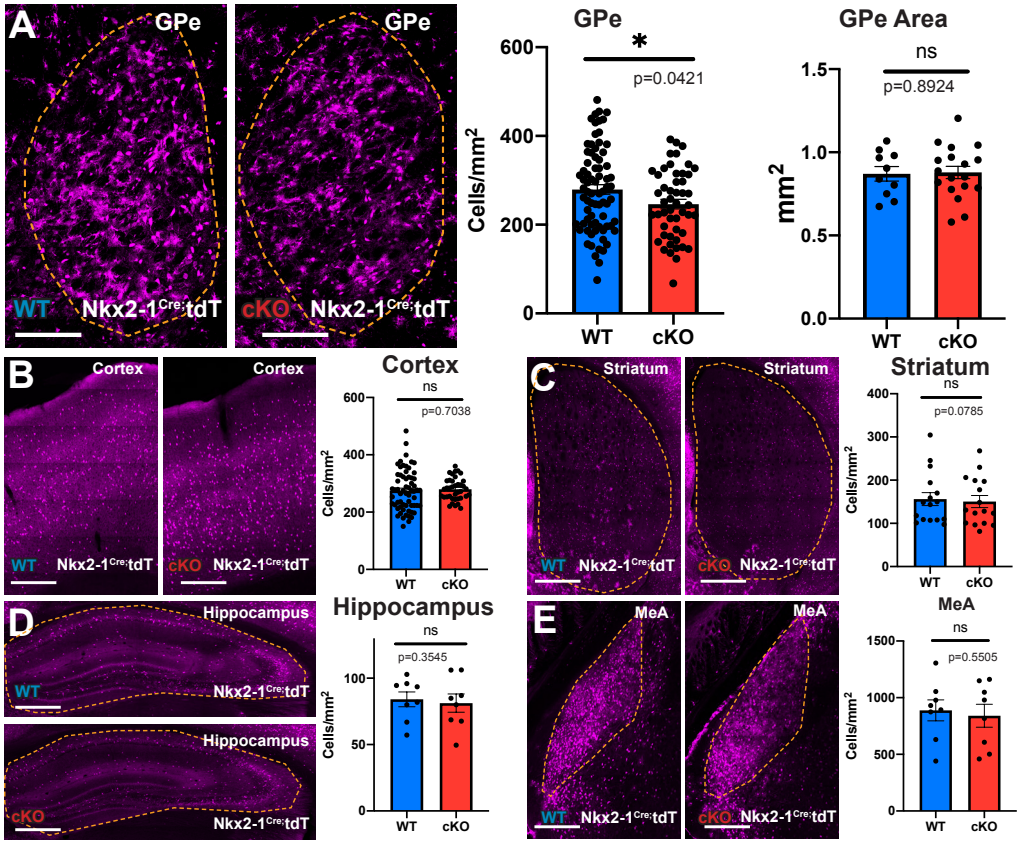

3.4.1 St18 cKO causes a reduction in MGE lineage neurons only in the GPe

A) WT and St18 cKO GPe with MGE lineage fate-map (Nkx2-1 Cre ; Ai9) (*Unpaired t-test*). N= 76 WT and 50 cKO.

B) WT and St18 cKO Cortex with MGE lineage fate-map (Nkx2-1 Cre ; Ai9) (*Unpaired t-test*). N= 63 WT and 38 cKO.

C) WT and St18 cKO Striatum with MGE lineage fate-map (Nkx2-1 Cre ; Ai9) (*Unpaired t-test*). N= 16 WT and 16 cKO.

D) WT and St18 cKO Hippocampus with MGE lineage fate-map (Nkx2-1 Cre ; Ai9) (*Unpaired t-test*). N= 8 WT and 8 cKO.

E) WT and St18 cKO MeA with MGE lineage fate-map (Nkx2-1 Cre ; Ai9) (*Unpaired t-test*). N= 16 WT and 16 cKO.

fate-mapping of the MGE lineage both with and without St18 genetic ablation. Using this approach, I next quantified the number of fate-mapped tdTomato+ neurons throughout various regions in the adult brain to determine the effect of St18 cKO on the development and distribution of other MGE lineages. Recall that the MGE, along with producing projection neurons in the GPe, also produces interneurons of the cortex, striatum, and hippocampus as well as various neuron types in the medial amygdala (MeA). I found that the number of tdTomato+ neurons in St18 cKO animals was not significantly different in any region other than the GPe (Figure 3.4.1). Importantly, in the GPe, the observed decrease in tdTomato+ neuron density is not due to a change in total GPe area (Figure 3.4.1 A).

To examine the MGE neuronal lineages in greater resolution, I next surveyed the MGE

neuronal cohort by immunohistochemistry in St18 (-/-) and cKO genetic manipulations. Briefly, I examined PV+ and SST+ neurons in the cortex, hippocampus, and striatum. I also tested the MGE lineages in the MeA, labeled by SST+ and FoxP2+ signal (Carney et al., 2010; Keshavarzi et al., 2014; Lischinsky et al., 2017). In St18 (-/-), I found that there was no significant difference in any MGE derived neural lineage throughout the brain (Figure 3.4.2). In St18 cKO, I recapitulated the St18 (-/-) phenotype, finding no significant difference in any MGE lineage cohort throughout the various MGE populated loci (Figure 3.4.3). Together with the loss of MGE derived PV+ GPe neurons, I can therefore conclude that St18 is necessary for a specific neuronal lineage from the MGE.

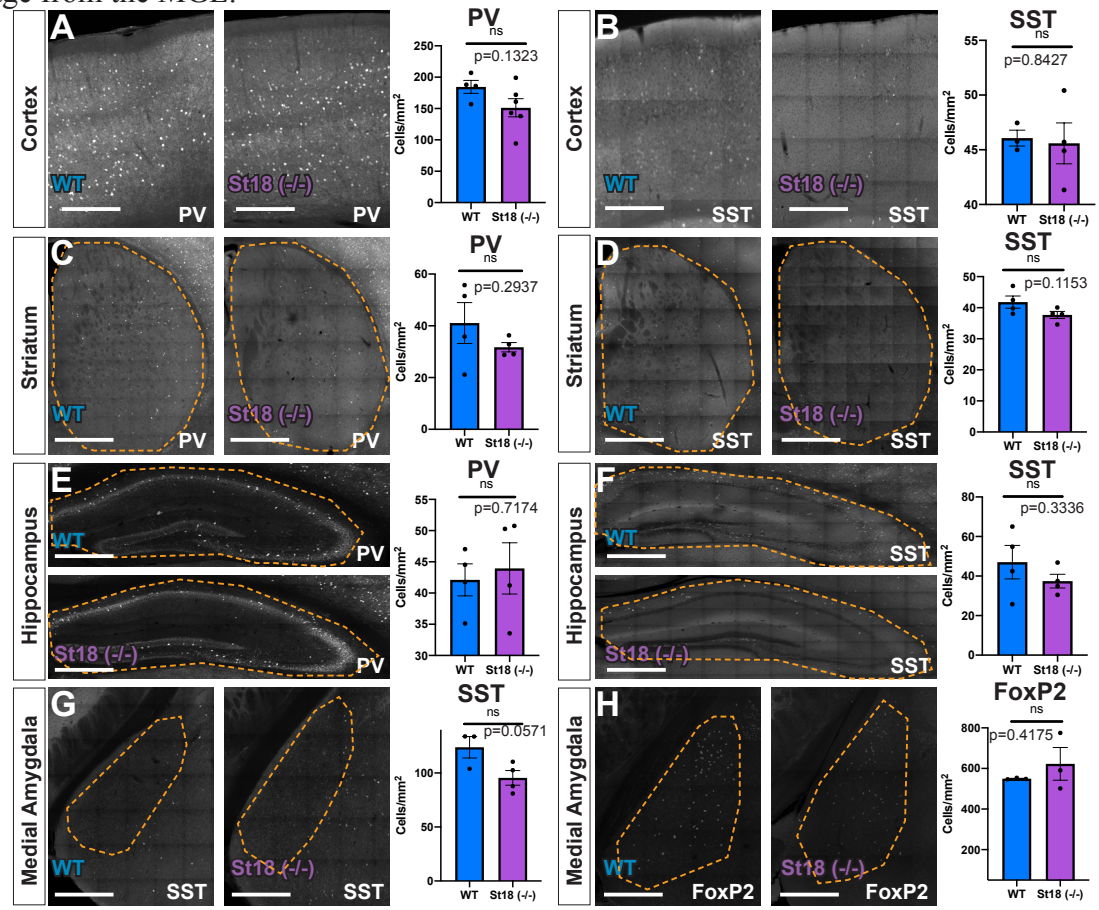

3.4.2 St18 (-/-) does not affect MGE lineages of the cortex, striatum, hippocampus, and MeA

A) WT and St18 (-/-) cortex with PV immunolabelling (*Unpaired t-test*). N= 4 WT and 6 St18 (-/-).
B) WT and St18 (-/-) cortex with SST immunolabelling (*Unpaired t-test*). N= 3 WT and 4 St18 (-/-).
C) WT and St18 (-/-) striatum with PV immunolabelling (*Unpaired t-test*). N= 4 WT and 4 St18 (-/-).
D) WT and St18 (-/-) striatum with SST immunolabelling (*Unpaired t-test*). N= 4 WT and 4 St18 (-/-).
E) WT and St18 (-/-) hippocampus with PV immunolabelling (*Unpaired t-test*). N= 4 WT and 4 St18 (-/-).
F) WT and St18 (-/-) hippocampus with SST immunolabelling (*Unpaired t-test*). N= 3 WT and 4 St18 (-/-).
G) WT and St18 (-/-) MeA with SST immunolabelling (*Unpaired t-test*). N= 3 WT and 4 St18 (-/-).
H) WT and St18 (-/-) MeA with FoxP2 immunolabelling (*Unpaired t-test*). N= 3 WT and 3 St18 (-/-).

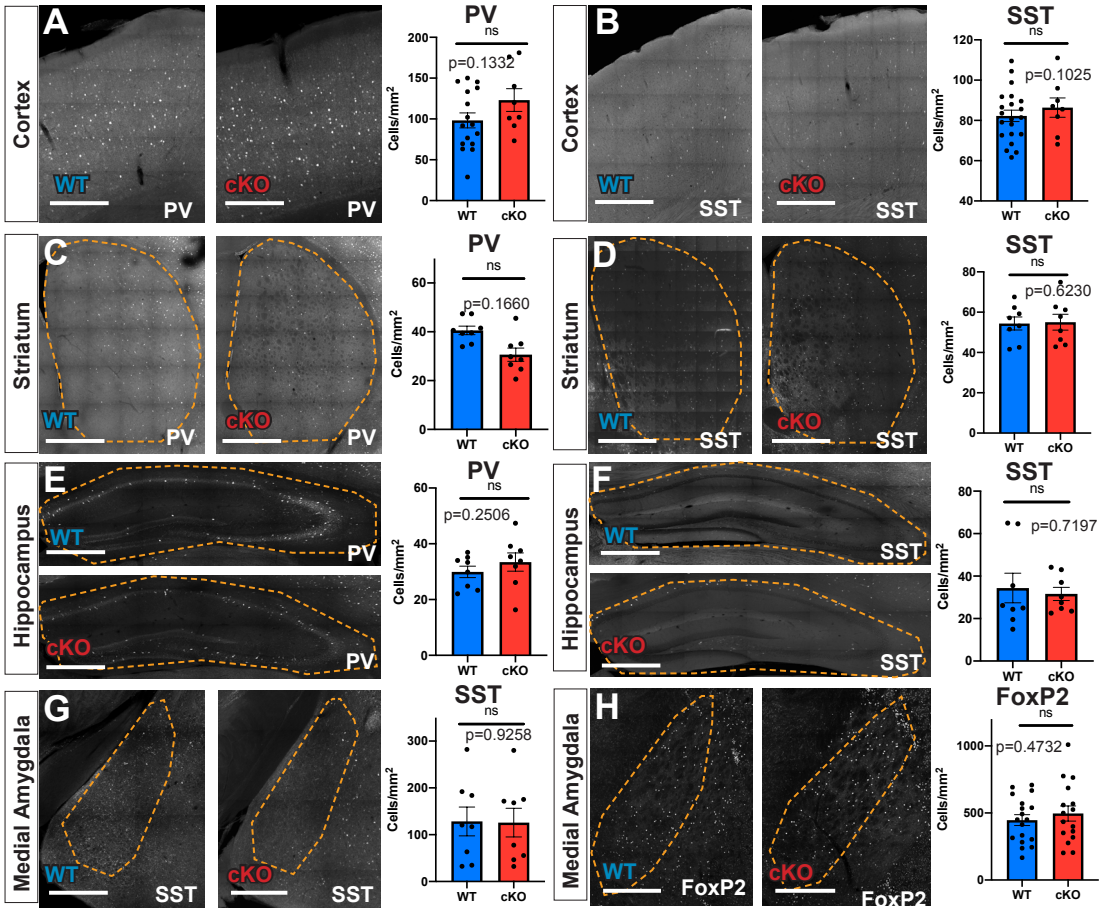

3.4.3 St18 cKO does not affect MGE lineages of the cortex, striatum, hippocampus, and MeA

A) WT and St18 cKO cortex with PV immunolabelling (*Unpaired t-test*). N= 16 WT and 8 St18 cKO.
B) WT and St18 cKO cortex with SST immunolabelling (*Unpaired t-test*). N= 21 WT and 8 St18 cKO.
C) WT and St18 cKO striatum with PV immunolabelling (*Unpaired t-test*). N= 8 WT and 8 St18 cKO.
D) WT and St18 cKO striatum with SST immunolabelling (*Unpaired t-test*). N= 8 WT and 8 St18 cKO.
E) WT and St18 cKO hippocampus with PV immunolabelling (*Unpaired t-test*). N= 8 WT and 8 St18 cKO.
F) WT and St18 cKO hippocampus with SST immunolabelling (*Unpaired t-test*). N= 8 WT and 8 St18 cKO.
G) WT and St18 cKO MeA with SST immunolabelling (*Unpaired t-test*). N= 8 WT and 8 St18 cKO.
H) WT and St18 cKO MeA with FoxP2 immunolabelling (*Unpaired t-test*). N= 18 WT and 18 St18 cKO.

Chapter 4: St18 loss of function causes a shift in the neural output of the MGE lineage

Having established that St18 genetic loss of function leads to the loss of a specific population of MGE derived GPe neurons, I next wanted to establish how St18 genetic loss of function changes MGE lineage differentiation from a transcriptional perspective to produce this cellular phenotype in the adult brain. To do this, I performed a single cell RNA sequencing (scRNAseq) experiment on St18 (-/-) embryonic MGE. I found that St18 whole animal loss of function leads to a shift in the neuronal output of a small proportion of the MGE lineage while the progenitor stage and other lineages remain unchanged. This finding further cements the notion that St18 specifies a specific portion of the MGE neuronal cohort.

4.1 St18 (-/-) does not affect the MGE progenitor pool at E14.5

Given the highly specific reduction in GPe prototypic projection neurons observed in St18 mutant mice, I next examined how this cell loss occurs within the MGE. Recall that I previously showed that overall proliferation, cell death, and Nkx2-1+ progenitor numbers were not significantly altered in the mutant MGE. Therefore, I wanted to next explore the possibility that St18 directs the cell fate of GPe prototypic neurons during progenitor cell specification within the MGE. To do this, I performed scRNAseq on E14.5 St18 (-/-) and WT littermate control MGE (N =2 biological replicates per group; median of ~9,500 cells passing quality control per biological replicate). Briefly, I decided to examine the effect of St18 (-/-) on MGE specification at E14.5 because St18 has been previously shown to be a diagnostic marker gene for specific clusters of MGE progenitors at this age (Mi et al., 2018). Also, I chose to examine St18 (-/-) instead of cKO MGE to guard against incomplete recombination of the St18 allele in Nkx2-1^{Cre}, which is unable to fully recombine the MGE/LGE sulcus region (Fogarty et al., 2007). I dissected and genotyped St18 (-/-) and WT embryos to prepare samples for dissociation and sequencing by the core facility at Columbia.

Sequencing data was analyzed in a similar manner to a previous study of MGE progeni-

tors and neurons (Mi et al., 2018). Briefly, after filtering cells with fewer than 200 genes detected, I performed a standard clustering analysis using the Seurat package in R (Butler et al., 2018). I then identified high variance genes, followed by principal component analysis (retaining 49 PCs) and Louvain-based community detection clustering. I then subclustered neurons and progenitors. Briefly, progenitor and neuronal clusters were identified by plotting the expression of marker genes at E14.5 (Figure 4.1.1) (Mi et al., 2018). Following subclustering of neurons and progenitors, I identified 13 progenitor cell clusters (3.039 total cells in WT, 4.018 total cells in St18 (-/-)) and 21 neuronal clusters (5,104 total cells in WT, 5,904 total cells in St18 (-/-)) (Figure 4.1.1).

Next, using this sequencing data, I examined the St18 expression levels between WT and St18 (-/-) MGE. I found that St18 transcript was still present in St18 (-/-) samples, although at significantly lower levels in cells classified as neurons (Figure 4.1.2 A; Figure 4.2.1 A). Crucially, this finding is consistent with previous work describing the St18 conditional allele where the

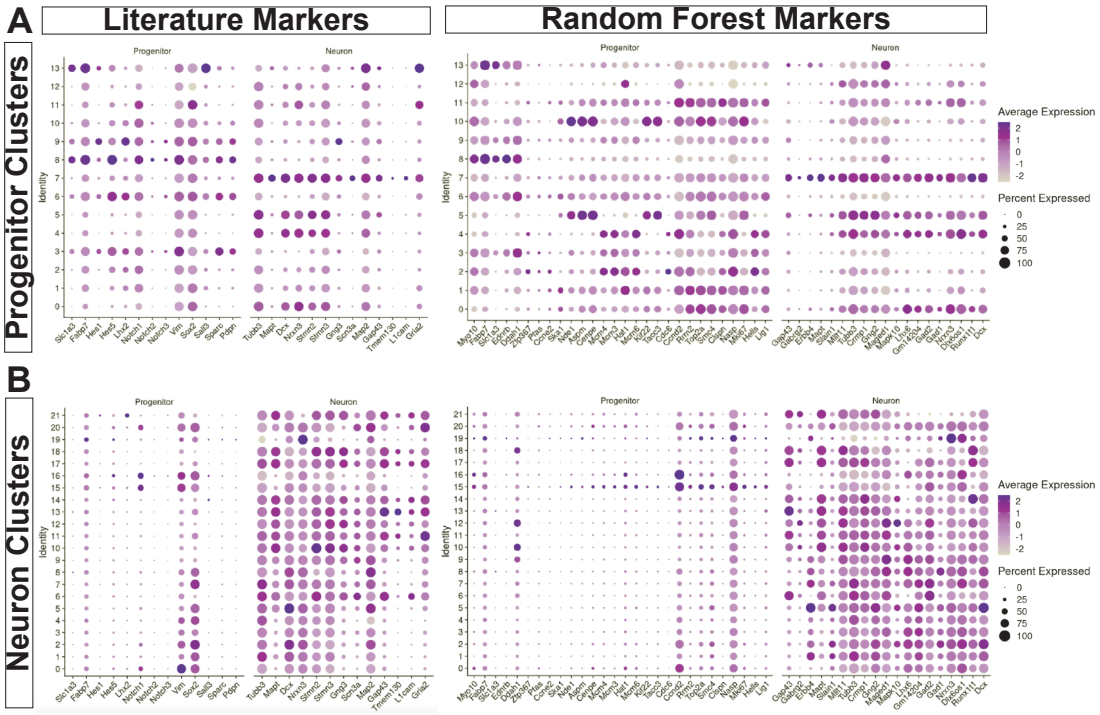

4.1.1 Classification of neuronal and progenitor clusters

A) Dot plots showing scaled average expression of genes from (Mi et al., 2018) distinguishing neuron and progenitor clusters. This row shows clusters identified as progenitors. Left column shows established diagnostic markers for progenitor and neuron clusters from the literature. Right column shows neuron and progenitor classifiers selected by a random forest classifier.

B) Dot plots showing scaled average expression of genes from (Mi et al., 2018) distinguishing neuron and progenitor clusters. This row shows clusters identified as neurons. Columns are the same as in (A).

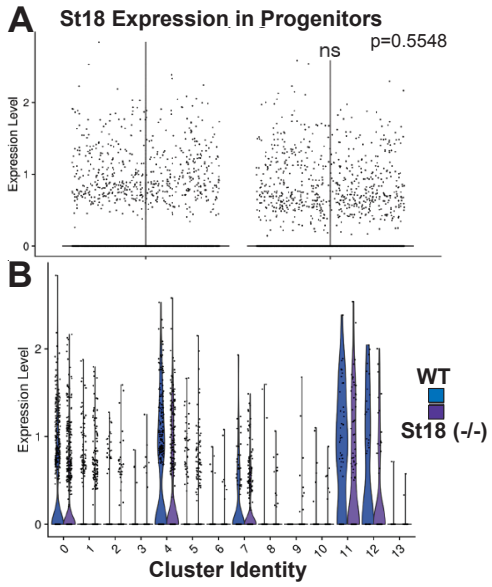

4.1.2 St18 expression in scRNAseq neuron and progenitor clusters

A) Violin plot showing log-normalized expression of St18 in WT and St18 (-/-) progenitors (*Wilcoxon sum-rank test*).

B) Violin plots of log-normalized St18 expression in WT and St18 (-/-) progenitors, grouped by cluster.

transcript is still detectable after recombination, but at lower levels and likely reflects a degree of nonsense-mediated decay (Hu et al., 2020; Huang et al., 2018). Also, as I previously showed, there is no protein detected in St18 (-/-) by immunohistochemistry. Given this antibody recognizes the N-terminus of the St18 full-length protein, the N-terminal fragment of St18 that is encoded by the recombined St18 transcript is not detectable, likely due to protein instability (Hu et al., 2020). I also note that there are certain progenitor clusters that express St18 at different levels (Figure 4.1.2 B). This suggests that St18 expression is regulated across MGE progenitors domains in WT and ST18 (-/-) conditions.

Next, I sought to visualize the differences in progenitor cell clustering to determine if St18 is having an effect on MGE progenitor differentiation. A UMAP visualization of progenitor cell clusters in WT and St18 (-/-) samples indicates that there are only subtle differences in clustering between the two samples. Indeed, the relative proportions of clusters remains largely unchanged, with only slight increases in progenitor clusters 7 and 9 in St18 (-/-) (Figure 4.1.3). This, together with the earlier finding that St18 (-/-) does not alter cell proliferation, cell death, or MGE progenitor patterning, suggests that St18 (-/-) does not effect MGE lineage progenitors en route to the adult loss of GPe projection neurons.

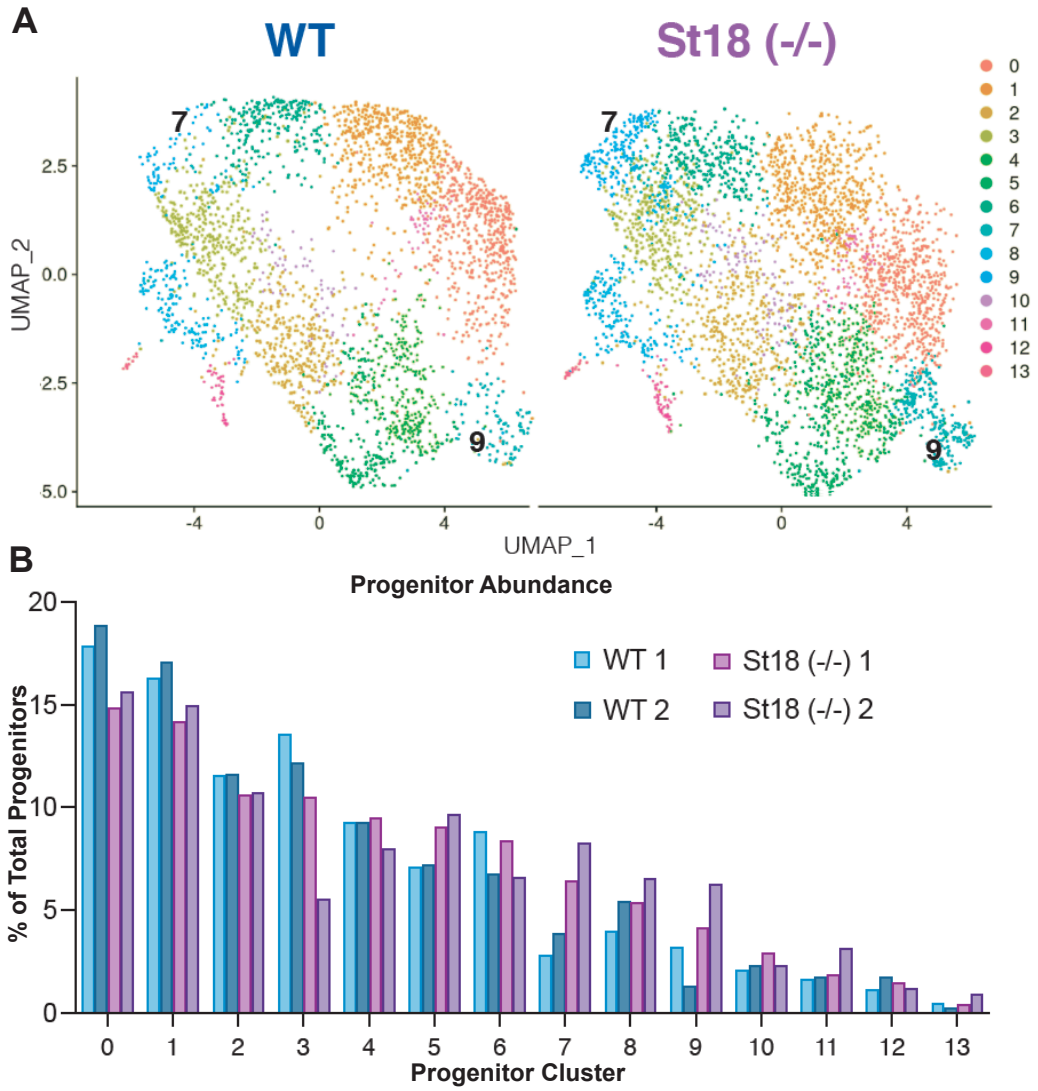

4.1.3 scRNAseq shows only modest changes in MGE progenitor clustering in St18 (-/-)

A) UMAP visualization of 13 progenitor clusters identified in WT (left) and St18 (-/-) (right) E14.5 MGE. Clusters 7 and 9 are noted, as these have the most pronounced difference between the two conditions.

B) Relative proportions of each progenitor cluster with biological replicates plotted separately. Dataset represents 2 biological replicates per genotype, 8,143 WT cells and 9,922 St18 (-/-) cells that pass quality control measures.

4.2 St18 (-/-) causes a shift in the MGE lineage neuronal output at E14.5

After establishing that St18 (-/-) only subtly affects MGE progenitors at E14.5, I next sought to determine whether or not E14.5 neuron clusters are affected by St18 (-/-). Firstly, I find that St18 transcript is expressed at significantly lower levels in St18 (-/-) neuron clusters (Figure 4.2.1 A). I also find, similarly to in progenitor clusters, that in both WT and St18 (-/-) E14.5 MGE, St18 is expressed at different levels in different neuron clusters, further indicating that St18 expression is regulated across different pools of MGE progenitors and neurons (Figure 4.2.1 B). Next, to visualize the effect of St18 whole animal knockout on MGE lineage neuron

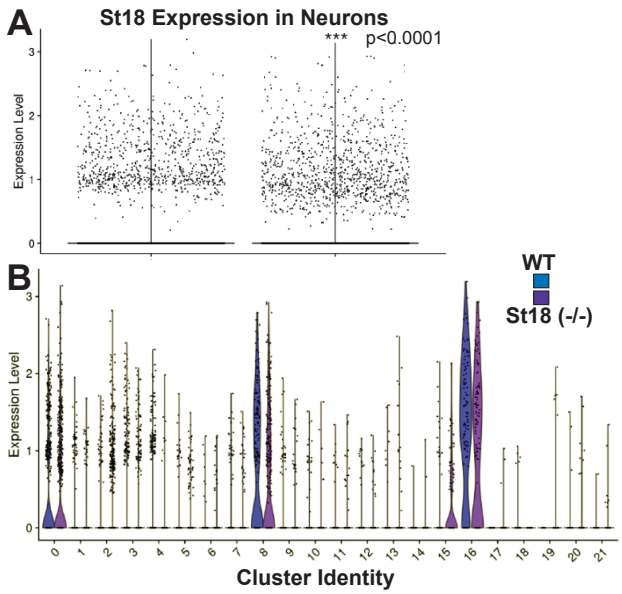

4.2.1 St18 expression in scRNAseq neuron progenitor clusters

A) Violin plot showing log-normalized expression of St18 in WT and St18 (-/-) neurons (*Wilcoxon sum-rank test*).

B) Violin plots of log-normalized St18 expression in WT and St18 (-/-) neurons, grouped by cluster.

production at E14.5 in higher resolution, I produced a UMAP plot of neuron clusters in WT and St18 (-/-) MGE (Figure 4.2.2 A). In this plot, as opposed to the plot for progenitor clusters, I find a pronounced different in neuronal cluster representation between WT and St18 (-/-). This visual change in cluster appearance is substantiated by statistical analysis of cluster proportions (Figure 4.2.2 B). Indeed, statistical analysis using a Fisher exact test identified that the proportion of cluster 4 neurons, as a fraction of total neurons, was reduced 4.72-fold in St18 (-/-) compared to WT (Figure 4.2.2 B). I also find that the proportion of cluster 2 neurons was increased 4.74-fold, and the proportion of cluster five neurons was increased 2.35-fold in St18 (-/-) compared to WT MGE (Figure 4.2.2 B). Therefore, St18 (-/-) causes a shift in the neuronal clusters in the E 14.5 MGE.

Next, I sought to understand the genes differentially expressed in the neuronal clusters that are statistically altered in St18 (-/-) and WT MGE. Analysis of gene expression in neuron clusters 2 and 5 reveals enrichment for interneuron-related genes over cluster 4, for example: Maf (c-Maf) (McKinsey et al., 2013; Pai et al., 2020; Pai et al., 2019), Zeb2 (Zfhx1b, Sip1) (McKinsey et al., 2013; van den Berghe et al., 2013), EphA4 (Zimmer et al., 2011), Ackr3 (CxcR7) (Sanchez-Alcaniz et al., 2011; Wang et al., 2011), and ErbB4 (Flames et al., 2004)

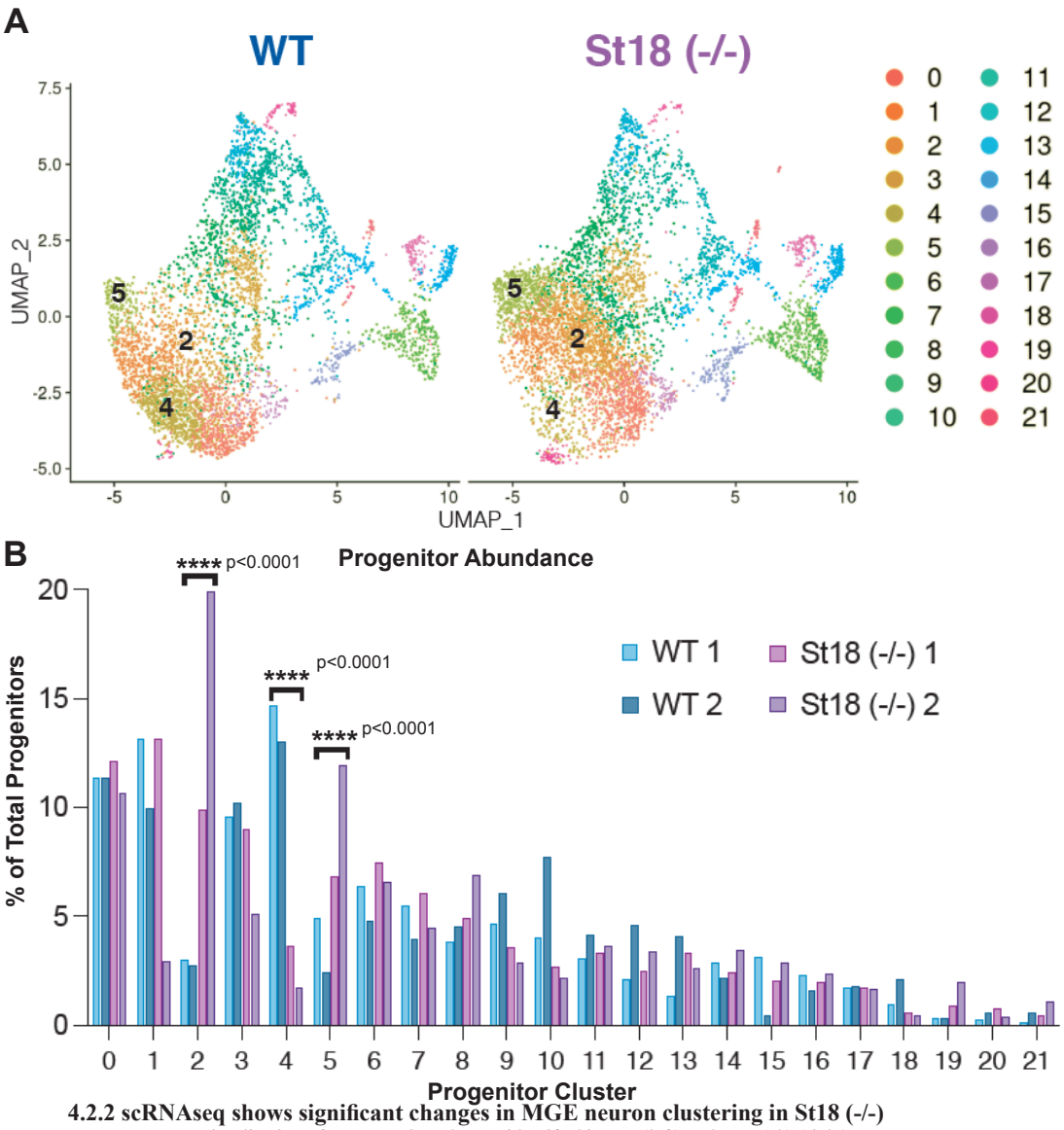

4.2.2 scRNAseq shows significant changes in MGE neuron clustering in St18 (-/-)

A) UMAP visualization of 21 progenitor clusters identified in WT (left) and St18 (-/-) (right) E14.5 MGE. Clusters 2, 4, and 5 are noted, as these have the most pronounced difference between the two conditions.

B) Relative proportions of each neuron cluster with biological replicates plotted separately. Dataset represents 2 biological replicates per genotype, 8,143 WT cells and 9,922 St18 (-/-) cells that pass quality control measures. (*Fisher's Exact test*).

(Figure 4.2.3). Genes enriched in cluster 4 have a less distinction than the interneuron related genes expressed in clusters 2 and 5, but there are several genes upregulated in cluster 4 involved in sub-pallial development and neurite growth, for example: Rnd2 (Heng et al., 2015), Cox5a (Jiang et al., 2020), and Nkx2-1 (Nobrega-Pereira et al., 2010) (Figure 4.2.3).

A more complete accounting of the most differentially expressed genes shows how these distinct neuron clusters express unique cohorts of genes that reflects how early neuron clustering at E14.5 is informative on the mature identity of differentiating neurons (Figure 4.2.4). Given

that St18 is not expressed at particularly high levels in neuron clusters 2, 4, or 5, this means that the loss of St18 in St18 (-/-) affects progenitor cell production of neuron classes, resulting in the observed shift in neuronal output towards clusters 2 and 5 and away from cluster 4. Indeed, taken together, my analysis of St18 (-/-) scRNAseq shows that the loss of St18 causes the specific loss of a specific cluster of nascent MGE lineage neurons. This mirrors the observed loss of MGE lineage GPe PV+ prototypic neurons in St18 (-/-) and St18 cKO in the previous chapter. The relative lack of change in other neuronal lineages also mirrors the St18 loss of function phenotype, namely that St18 loss of function does not alter additional neuronal lineages other than PV+ GPe neurons.

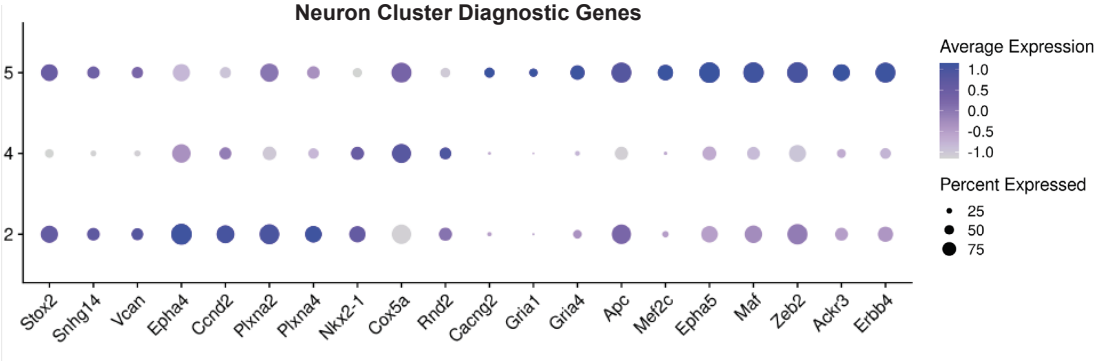

4.2.3 Diagnostic marker genes for neuron clusters 2, 4, and 5

Dot plot showing scaled average expression of differentially expressed genes in neuron clusters 2, 4, and 5. Briefly, clusters 2 and 5 express genes involved in cortical interneuron developmental processes. Cluster 4 is less well defined, but some genes are involved in putative GPe development.

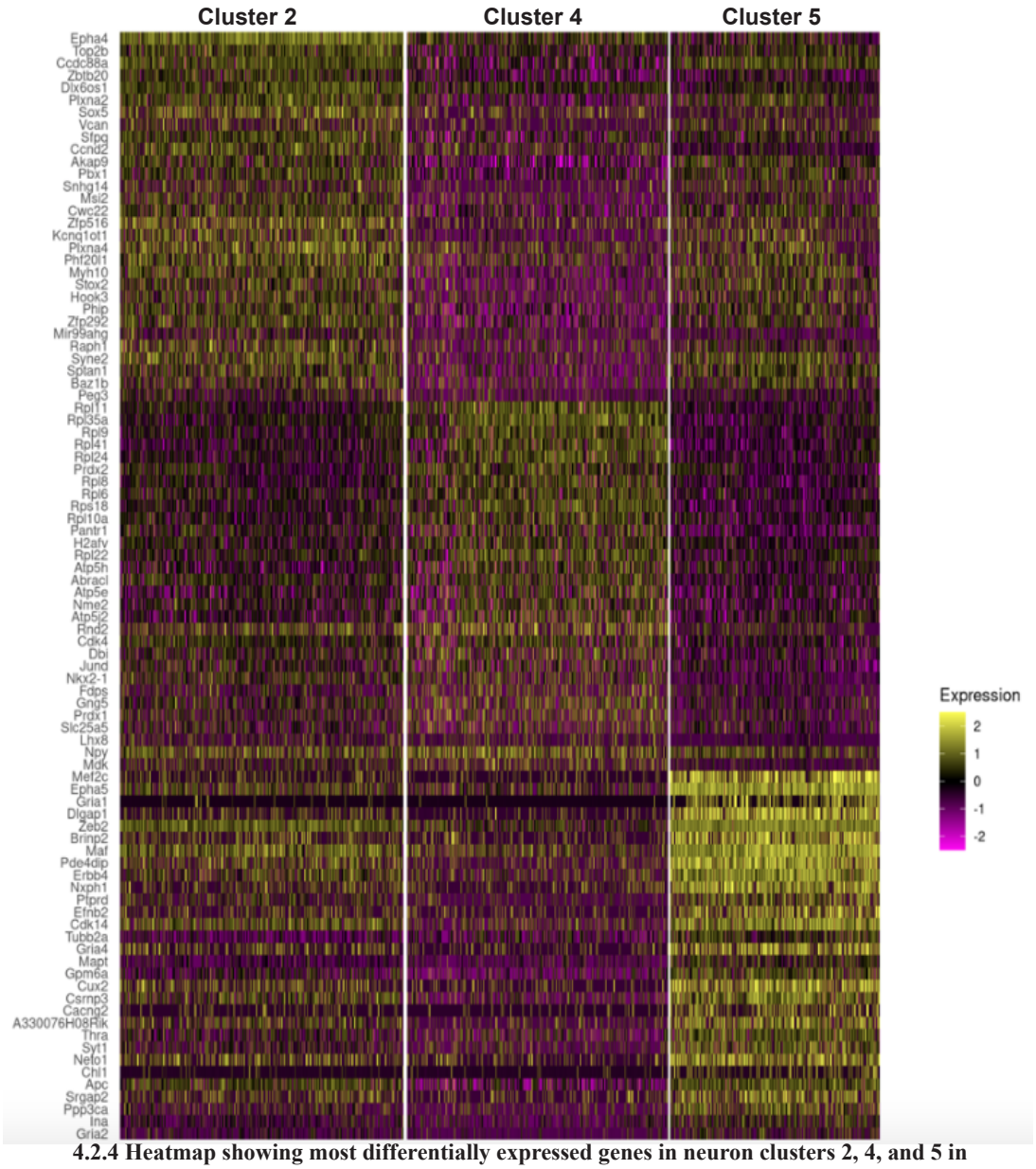

4.2.4 Heatmap showing most differentially expressed genes in neuron clusters 2, 4, and 5 in E 14.5 MGE

Heatmap shows the relative expression of most differentially expressed genes in the neuron clusters identified as affected by St18 (-/-).

Chapter 5: St18 loss of function leads to decreased prototypic innervation of the STN

St18 expression induces projection neuron cell migration and morphology *in vitro*. St18 loss of function *in vivo* leads to the loss of a specific population of MGE lineage projection neurons in the GPe. Therefore, St18 appears to be an essential transcription factor for the development of MGE lineage GPe PV+ projection neurons. Given this, I next wanted to investigate the effect of the loss of PV+ prototypic neurons on the canonical basal ganglia indirect pathway of which PV+ prototypic neurons are a key constitutive neural component. To do this, I utilized the St18 cKO allele described earlier to assay the connectivity of GPe neurons in a variety of ways. By measuring the area and amounts of target innervation by whole cell fate-mapping, synaptic labelling, and stereotax injection, I find that St18 conditional loss of function leads to a loss of GPe prototypic neuron innervation on expected primary synaptic targets in the sub-thalamic nucleus (STN) and substantia nigra pars reticulata (SNr) with little change elsewhere. Therefore, the loss of GPe prototypic neurons as a result of St18 loss of function leads to a deficient prototypic projection onto the STN and SNr.

5.1 St18 cKO causes decreased fate-mapped innervation in the STN

PV+ prototypic neurons in the GPe are an essential component of the basal banglia indirect pathway. Crucially, these are also the class of neuron that is depleted following St18 loss of function. Prototypic neurons of the GPe project caudally primarily to the STN but also some-

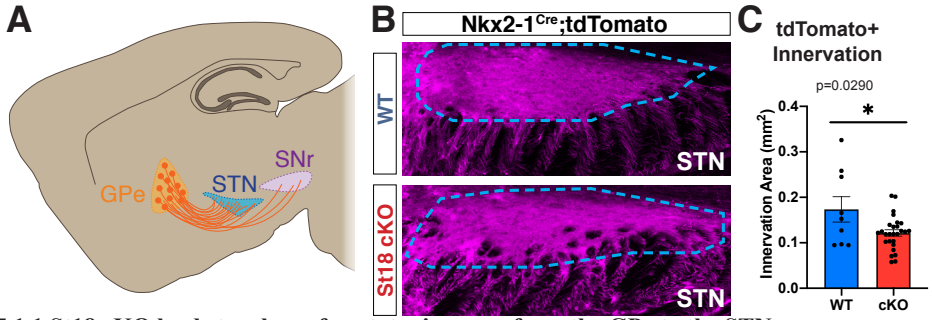

5.1.1 St18 cKO leads to a loss of prototypic axons from the GPe to the STN

A) Schematic showing the anatomy of PV+ prototypic projections from the GPe to the STN and SNr.
B) WT and St18 cKO STN (outlined in orange) with MGE lineage whole cell labelled fate map (Nkx2-1^{Cre}; Ai9).
C) Quantification of innervation area of fate-mapped axons in the STN (*Unpaired t test*). N= 9 WT and 27 St18 cKO.

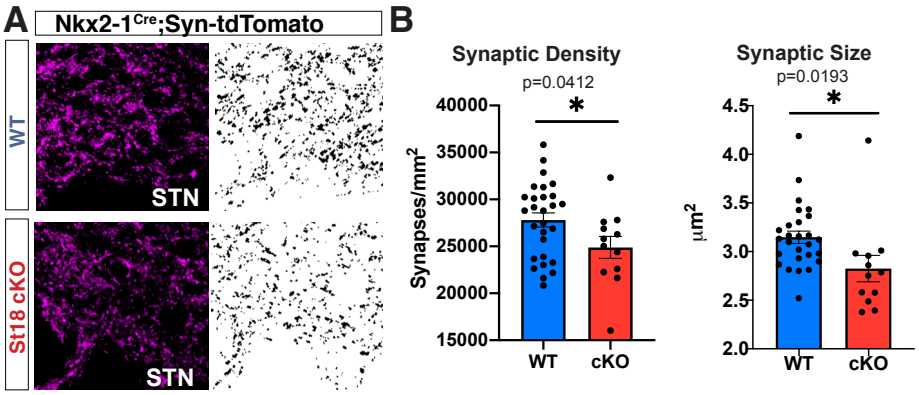

5.1.2 St18 cKO causes a decrease in prototypic neuron synaptic density and size in the STN

A) High powered image of WT and St18 cKO STN (outlined in orange) with MGE lineage synaptophysin labelled fate mapping (Nkx2-1^{Cre}; Ai34). Below, sample segmented images that demonstrate how synaptic density and size were calculated from the above images.

B) Quantification of synaptic puncta density and size (*Unparied t test*). N= 27 WT and 12 St18 cKO.

what to the SNr (Figure 5.1.1 A). These regions then project to the motor thalamus and the spinal cord to regulate movement (Freeze et al., 2013). To determine the extent to which an St18 loss of function induced reduction in PV+ prototypic neurons effects this crucial neural circuit, I first tested whether loss of PV+ GPe neurons in St18 cKO animals resulted in a loss of innervation in the STN. Briefly, the Ai9 reporter fills axonal processes, allowing me to examine projections from fate-mapped prototypic GPe neurons to their target in the STN. When I do this, I find a significant decrease in tdTomato+ axons in the STN in St18 cKO animals compared to WT controls (Figure 5.1.1 B).

Next, to visualize synaptic innervation directly, I utilized a different reporter line, Ai34, that conditionally expresses a fused synaptophysin-tdTomato (syn-tdT) upon Cre recombination. Syn-tdT puncta were then segmented and quantified in the STN in WT and St18 cKO animals. I found that puncta density and average puncta size were significantly reduced in St18 cKO (Figure 5.1.2). As a control against issues with this analysis approach, I examined Ai34 puncta density in the dorsal striatum (dStr) and the GPe, regions that are not primary targets of PV+ prototypic neurons. When examined in these regions, I find no significant difference in puncta density or morphology between WT and St18 cKO animals (Figure 5.1.3). Taken together, St18 cKO results in reduced innervation of the STN due to reduced axonal projections, reduced synaptic density, and reduced synaptic size. Importantly, this result tracks with a reduction of PV+ prototypic neurons present in the GPe.

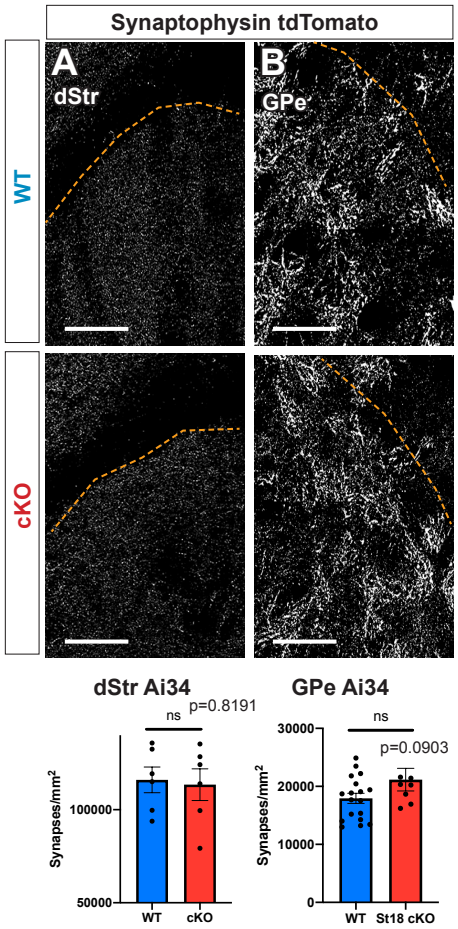

5.1.3 St18 cKO does not affect fate-mapped synapses for non-prototypic cells in the GPe or dStr

A) Quantification of Ai34 synaptic puncta density in the dStr (*Unpaired t test*). N= 6 WT and 6 St18 cKO.
B) Quantification of Ai34 synaptic puncta density in the GPe (*Unpaired t test*). N= 18 WT and 8 St18 cKO.

5.2 Loss of STN innervation is correlated with loss of GPe PV+ prototypic neurons

Having established that St18 loss of function leads to a loss of both PV+ prototypic neurons in the GPe and the proportional loss of prototypic innervation in the STN, I next sought to directly test whether the loss of PV+ GPe cells is correlated with the loss of Nkx2-1 lineage fate-mapped synapses in the STN. To do this, I examined the PV+ prototypic neuron counts in WT and St18 cKO GPe that were also fate-mapped with syn-tdT so that I could correlate the density of GPe PV+ neurons with the density of STN syn-tdT fate-mapped synaptic puncta within individual animals. This approach would allow me to confirm that the loss of PV+ neurons is causally linked to the loss of fate-mapped innervation in the STN. I confirmed that St18 cKO leads to both a reduction in GPe PV+ neuron density and in STN syn-tdT synaptic puncta density (Figure

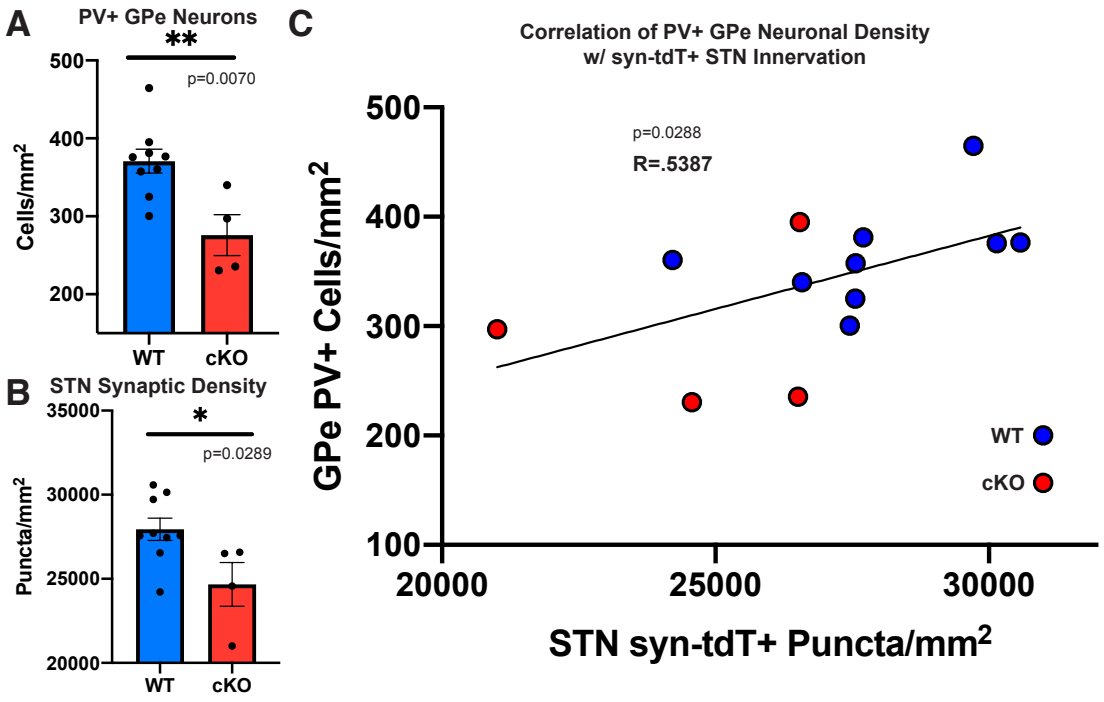

5.2.1 Loss of GPe PV+ neurons in St18 cKO is correlated with loss of STN fate-mapped synaptic innervation

A) Quantification of GPe PV+ neruons in WT and St18 cKO brains used for correlation experiment (*Unpaired t test*).

B) Quantification of STN syn-tdT+ synaptic innervation in WT and St18 brains used for correlation experiment (*Unpaired t test*).

C) Correlation analysis comparing GPe PV+ neuron density and STN syn-tdT+ synaptic innervation within the same brains (*Pearson's correlation coefficient*). Dataset shows the comparison of N= 13 total brains for correlation. N= 9 WT and 4 St18 cKO.

5.2.1 A,B). I also found that, when these values were correlated within the same animals, that these values are significantly positively correlated (Figure 5.2.1 C). This means that the observed loss of MGE lineage PV+ GPe neurons in St18 cKO is causally linked to the decrease in prototypic innervation on the STN also observed in St18 cKO.

5.3 Stereotaxic GPe injections show loss of prototypic projections in St18 cKO

Having established that St18 cKO leads to a decrease in the prototypic projection from PV+ GPe neurons to the STN, I next sought to further characterize the changes in basal ganglia connectivity upon St18 cKO. To do this, I sought to examine the canonical projections from the GPe in higher resolution by using AAV-GFP viral injections into the GPe in WT and St18 cKO. Briefly, I injected a GFP expressing adenovirus for anterograde labelling (AAV-CAGS-GFP) into the GPe by using established stereotaxic coordinates (Allen Brain Institute) to trace the projections from the GPe (Figure 5.3.1). This approach would allow me to visualize the changes in

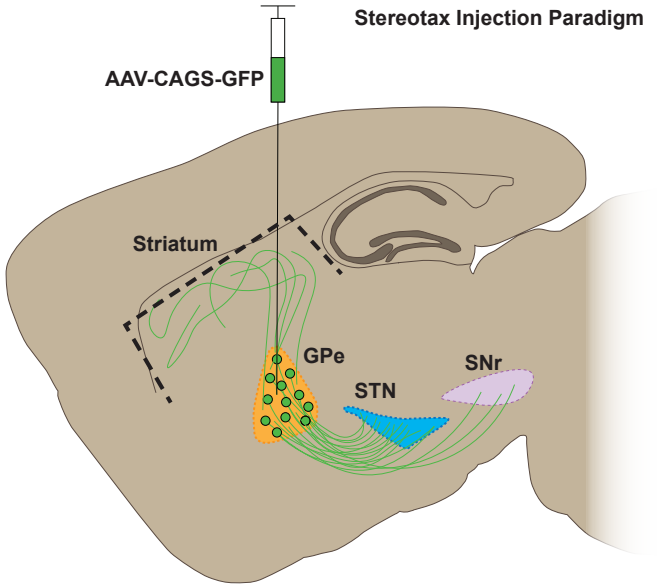

5.3.1 Stereotax injection experimental design

Schematic of the experimental design for the GFP stereotax injection experiments. Briefly, AAV-CAGS-GFP was injected in the GPe of WT and St18 cKO brains. The virus causes injected cells to express high levels of GFP, and this GFP expression virus fills the whole cell with GFP, allowing for subsequent assay of the GFP labelled projections in each genotype.

neural connectivity specifically in the basal ganglia indirect pathway as a result of St18 loss of function in the absence of fate mapping, making it easier to determine that the change in connectivity is related to St18 cKO. This would also allow me to assay if there is any compensatory change in neural circuitry to account for the loss of PV+ prototypic neurons.

To determine the effect of St18 cKO on indirect pathway architecture, I assayed the amount of GFP signal in three primary regions targeted by GPe neurons. For prototypic neurons, I measured GFP innervation in the STN and SNr, and for arkypallidal neurons, I measured GFP innervation in the striatum (Hernandez et al., 2015). In order to calculate the degree of target innervation in each injected animal, I normalized the measured GFP innervation with the total number of GFP labeled prototypic (PV+) or arkypallidal (Npas1+) neurons in injected brains. This would allow me to get a scaled approximation of the relative innervation of these principal cell types in WT and St18 cKO.

First, I counted the number of GFP+ prototypic and arkypallidal neurons in injected brains to both establish the baseline for my calculation of innervation as well as to determine the efficacy and consistency of my injections. I found that there were many GFP labeled PV+ prototypic cells in injected brains and that the levels of GFP expression were consistent across geno-

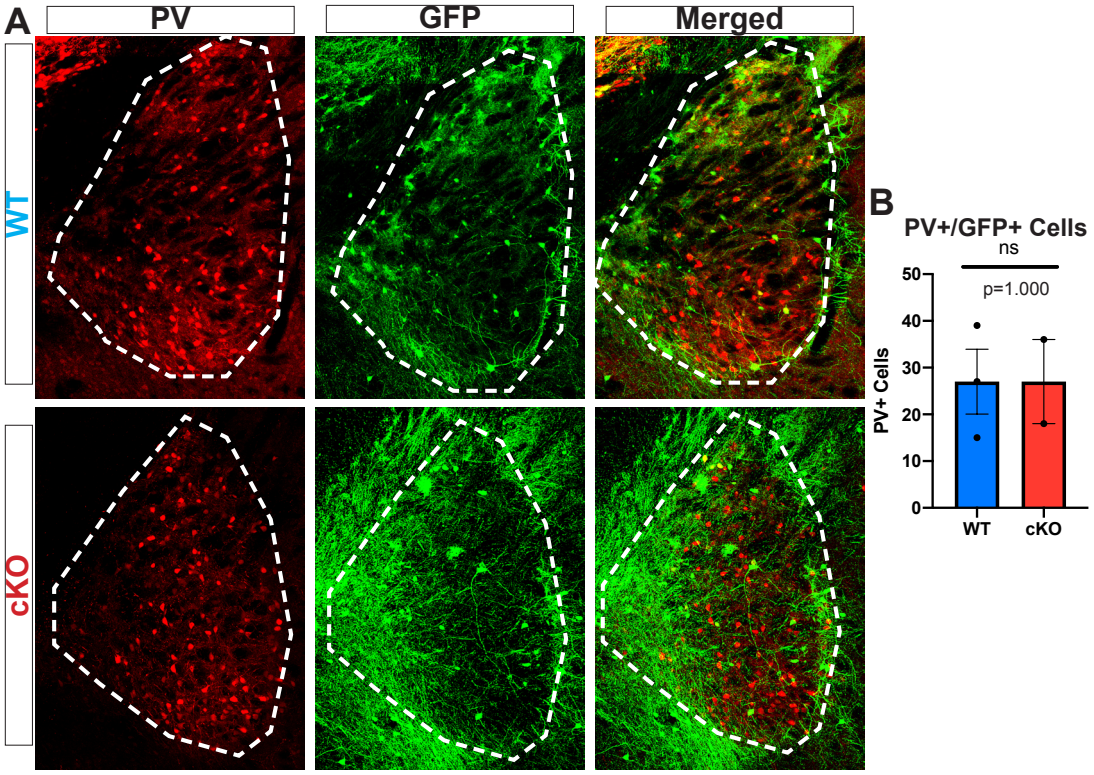

5.3.2 Viral injections produce consistent GFP labelling of PV+ GPe neurons in WT and St18 cKO

A) Representative images of WT and St18 cKO GPe labelled with PV, GFP, and merged.
B) Quantification of total PV+/GFP+ neurons in injected brains in WT and St18 cKO brains (*Unpaired t test*). N= 3 WT and 2 St18 cKO.

type and injection (Figure 5.3.2). I also found that the same was true for GPF labelled Npas1+ arkypallidal cells in injected brains (Figure 5.3.3). These results allow me to subsequently conclude that any changes in target innervation observed in St18 cKO would be due to changes in circuit architecture, not due to artifacts related to the injections themselves.

Having established that my GFP labelling strategy works effectively, I next assayed the GFP+ innervation relative to the numbers of virally labelled GPe cells in WT and St18 cKO animals. The first area I investigated was the STN, the primary synaptic partner of PV+ GPe prototypic neurons. I found a significant decrease in GFP+ innervation of the STN relative to the number of PV+ neurons in the GPe (Figure 5.3.4). I also see an increase in GFP+ axons that approach, but do not innervate the STN in St18 cKO (Figure 5.3.4 A). I next investigated the other primary synaptic target of PV+ prototypic neurons, the SNr. I saw the same decrease in GFP+ innervation in the SNr relative to the number of PV+ neurons in the GPe as I observed in the STN (Figure 5.3.5). Interestingly, I also note a similar pattern of GFP+ neuronal processes either

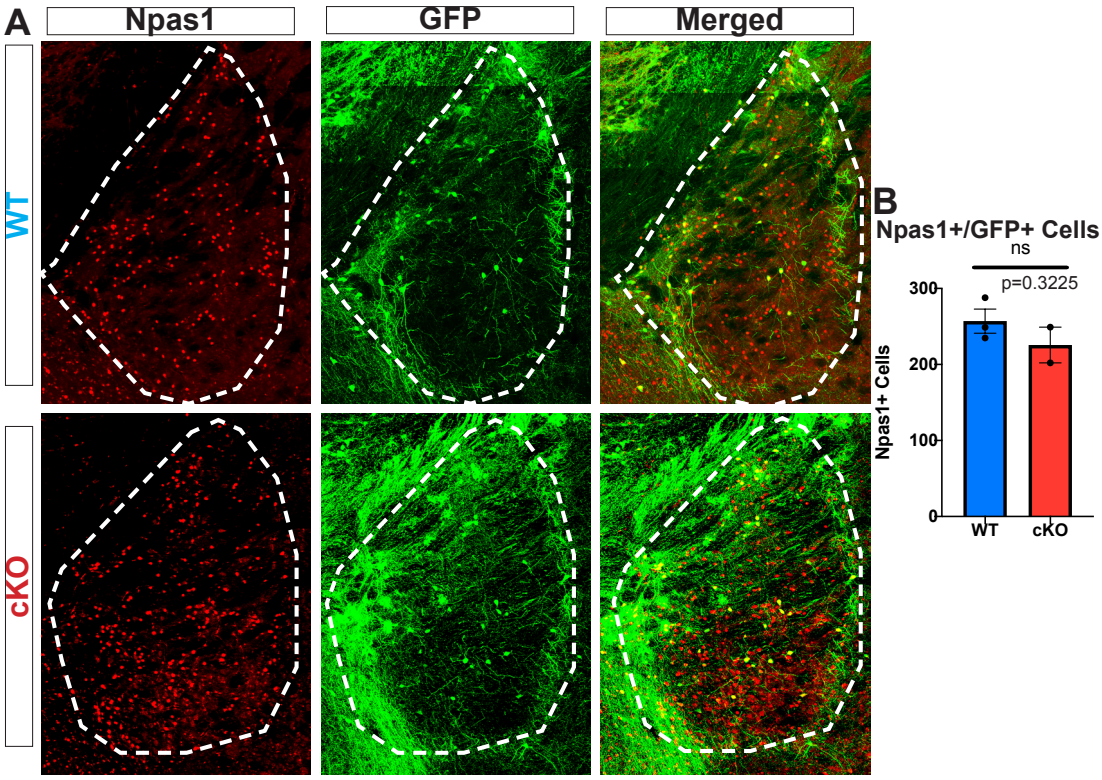

5.3.3 Viral injections produce consistent GFP labelling of Npas1+ GPe neurons in WT and St18 cKO

A) Representative images of WT and St18 cKO GPe labelled with Npas1, GFP, and merged.
B) Quantification of total Npas1+/GFP+ neurons in injected brains in WT and St18 cKO brains (*Unpaired t test*). N= 3 WT and 2 St18 cKO.

passing or failing to enter the St18 cKO SNr as was seen in the St18 cKO STN (Figure 5.3.5 A). Together, the decrease in prototypic innervation on the STN and SNr together with the apparent mistargeting of St18 cKO GFP+ neural processes raises the intriguing possibility that St18 cKO leads not only to a loss of many PV+ prototypic neurons, but also to a significant rewiring of other virally labelled GPe neurons.

To determine whether other GPe neurons are, in fact, re-wired in response to the loss of PV+ GPe prototypic neurons caused by St18 cKO, I investigated the population of Npas1+ arky-pallidal cells and their primary synaptic target in the striatum. I found that there is a significant increase in GFP+ striatum innervation relative to Npas1+ neuron numbers in the GPe (Figure 5.3.6). Taken together with the observed decrease in prototypic innervation on the STN and SNr, it is an intriguing possibility that akrypallidal cells produce an increase in inhibitory projections to the striatum as a homeostatic re-wiring of the basal ganglia indirect pathway. Together, I conclude that St18 cKO produces significant changes in the indirect pathway, characterized by

an increase in arkypallidal innervation of the striatum and a decrease in prototypic innervation of the STN and SNr.

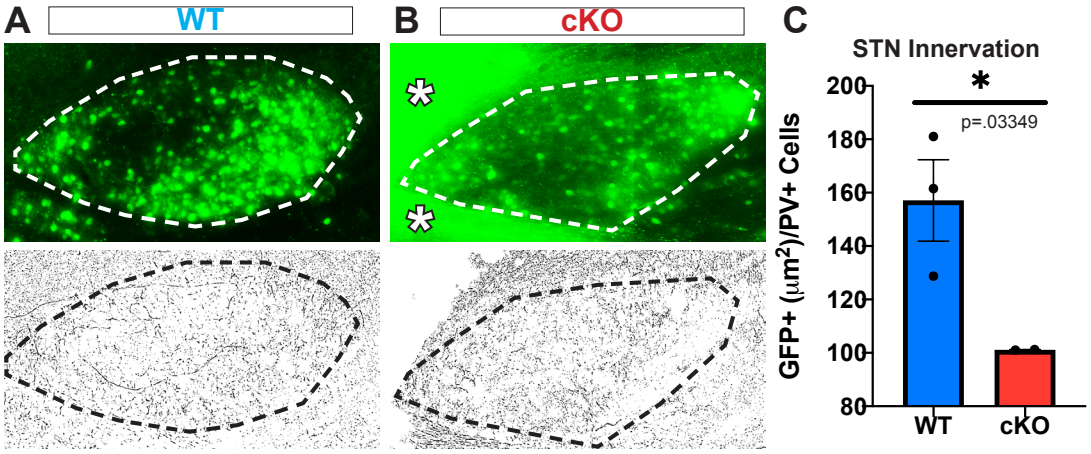

5.3.4 St18 cKO leads to a decrease in virally labelled GPe neuronal processes in the STN

A) Representative image of WT STN (outlined in white) with virally labelled GFP+ neuronal processes (top). Below is a processed mask of the same image that is used for quantification of GFP+ processes.

B) Representative image of St18 cKO STN (outlined in white) with virally labelled GFP+ neuronal processes (top). Asterisks indicate areas with erroneous GFP+ signal in relation to the STN. Below is a processed mask of the same image that is used for quantification of GFP+ processes.

C) Quantification of GFP+ STN innervation relative to the total number of virally labelled PV+ neurons in the WT and St18 cKO GPe (*Unpaired t test*). N= 3 WT and 2 St18 cKO.

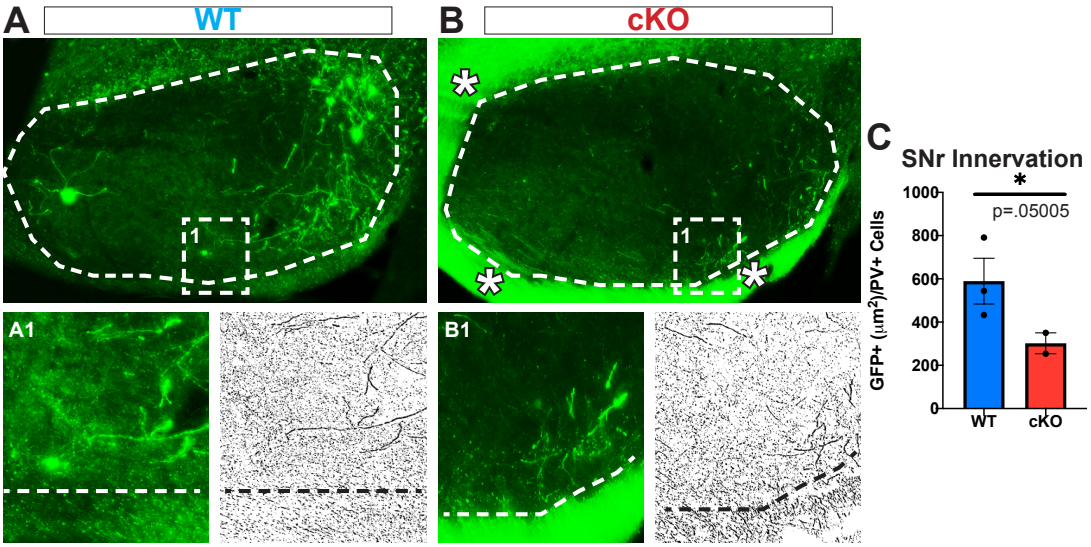

5.3.5 St18 cKO leads to a decrease in virally labelled GPe neuronal processes in the SNr

A) Representative image of WT SNr (outlined in white) with virally labelled GFP+ neuronal processes. Insets show a higher power image of the SNr (left) next to a processed mask of the same image that is used for quantification of GFP+ processes (right).

B) Representative image of St18 cKO SNr (outlined in white) with virally labelled GFP+ neuronal processes. Asterisks indicate areas with erroneous GFP+ signal in relation to the SNr. Insets show a higher power image of the SNr (left) next to a processed mask of the same image that is used for quantification of GFP+ processes (right).

C) Quantification of GFP+ SNr innervation relative to the total number of virally labelled PV+ neurons in the WT and St18 cKO GPe (*Unpaired t test*). N= 3 WT and 2 St18 cKO.

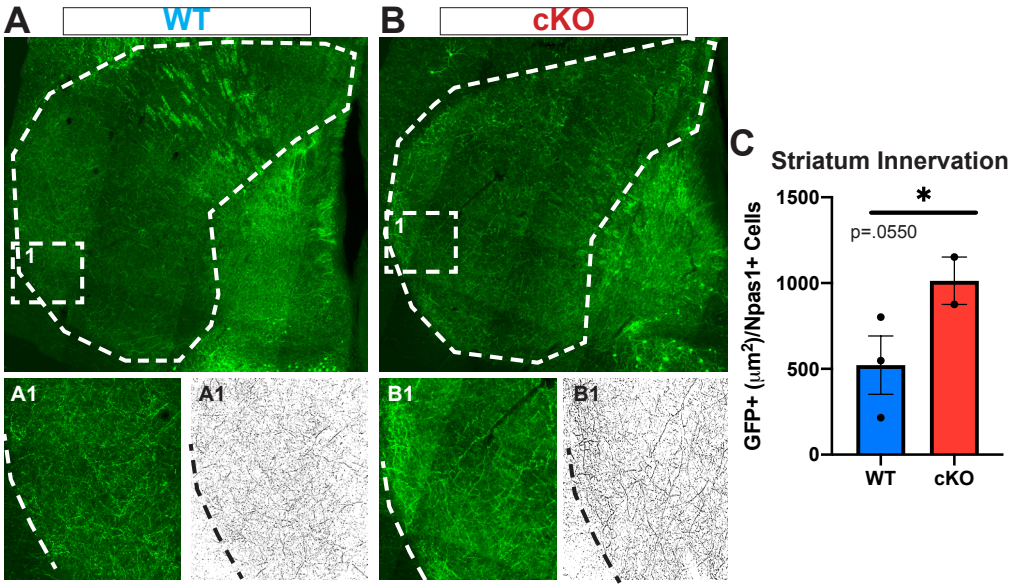

5.3.6 St18 cKO leads to an increase in virally labelled GPe neuronal processes in the striatum

A) Representative image of WT striatum (outlined in white) with virally labelled GFP+ neuronal processes. Insets show a higher power image of the striatum (left) next to a processed mask of the same image that is used for quantification of GFP+ processes (right).

B) Representative image of St18 cKO striatum (outlined in white) with virally labelled GFP+ neuronal processes. Insets show a higher power image of the straitum (left) next to a processed mask of the same image that is used for quantification of GFP+ processes (right).

C) Quantification of GFP+ striatum innervation relative to the total number of virally labelled Npas1+ neurons in the WT and St18 cKO GPe (*Unpaired t test*). N= 3 WT and 2 St18 cKO.

Chapter 6: St18 loss of function causes a disruption in mouse locomotor gait

Having now established that St18 loss of function produces a loss of GPe PV+ prototypic neurons that is causally linked to a disruption and potential re-wiring of the basal ganglia indirect pathway, I next sought to determine the effect of this observed St18 cKO phenotype on mouse behavior. To do this, I put WT and St18 cKO animals through a battery of motor and developmental related behavioral tests and found that St18 cKO leads to a disruption of mouse locomotor gait characterized by freezing of walk cycles. Therefore, St18 cKO causes a locomotor gait phenotype that is related to the loss of GPe PV+ prototypic neurons.

6.1 St18 cKO does not cause gross developmental phenotype

Given that I observe a loss of MGE lineage PV+ GPe projection neurons that leads to a decreased prototypic projection from the GPe to the STN and SNr, I next wondered if this change in the indirect pathway would produce a motor behavior phenotype, as the indirect pathway is involved in initiating and controlling voluntary movement (Freeze et al., 2010). First, in order to rule out any early developmental phenotype related to St18 cKO, I ran a battery of early developmental motor tests. The tests I ran were developmental weight, pup righting reflex, 45 degree geotaxis, and vertical screen tests, as these would cover both gross developmental progression as well as any early motor behaviors throughout development. Briefly, for pup righting reflex, I measured the amount of time the animals took to right themselves. For 45 degree geotaxis, I measured the amount of time the animals took to reverse direction at a 45 degree incline. For the vertical screen test, I measured the amount of time pups could maintain their grip before falling. All of these tests assay basic motor reflexes and how they develop. I found that St18 cKO does not lead to any developmental deficits, with St18 cKO animals weighing the same as and performing the same in motor tests as WT animals (Figure 6.1.1). This result is not surprising, as I have shown previously that St18 (-/-) embryos show no early deficits in cell proliferation, cell-death, or MGE lineage progenitor patterning.

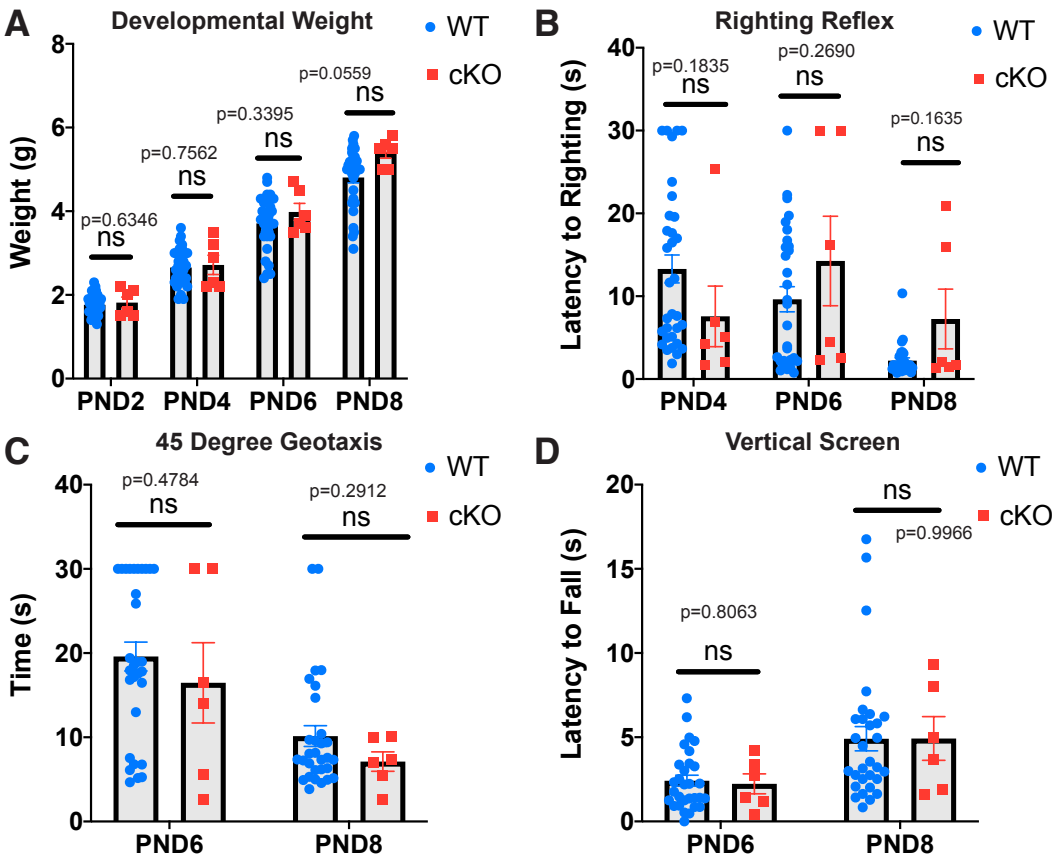

6.1.1 St18 cKO does not produce any gross developmental growth or motor deficits

A) Quantification of developmental weight over the first 8 post natal days (PND) of pup life (*Multiple t tests*). N= 32 WT and 6 St18 cKO.

B) Quantification of latency to pup righting reflex from PND 4 to PND 8 of pup life (*Multiple t tests*). N= 32 WT and 6 St18 cKO.

C) Quantification of latency to pup 45 degree geotaxis reflex from PND 6 to PND 8 of pup life (*Multiple t tests*). N= 30 WT and 6 St18 cKO.

D) Quantification of latency to fall in a vertical screen test from PND 6 to PND 8 of pup life (*Multiple t tests*). N= 30 WT and 6 St18 cKO.

6.2 St18 cKO does not cause a change in gross locomotion or coordination

Having established that St18 cKO does not produce any early developmental or motor phenotypes, I next assayed whether St18 produces any gross locomotor or coordination phenotypes. In order to do this, I first tested St18 cKO animals in an open field paradigm, a behavioral test that assays locomotor behavior over one hour to determine if St18 cKO animals walk the same distance at the same velocity as WT animals. I found that St18 cKO does not alter gross locomotion as assessed by ambulatory distance and velocity (Figure 6.2.1). Next, I tested whether St18 cKO has any effect on motor coordination, as determined by the Rotarod test, which assays motor coordination and balance by exhibiting experimental animals to graded speed increases on a small treadmill. I found that St18 cKO does not alter motor coordination and balance, as there

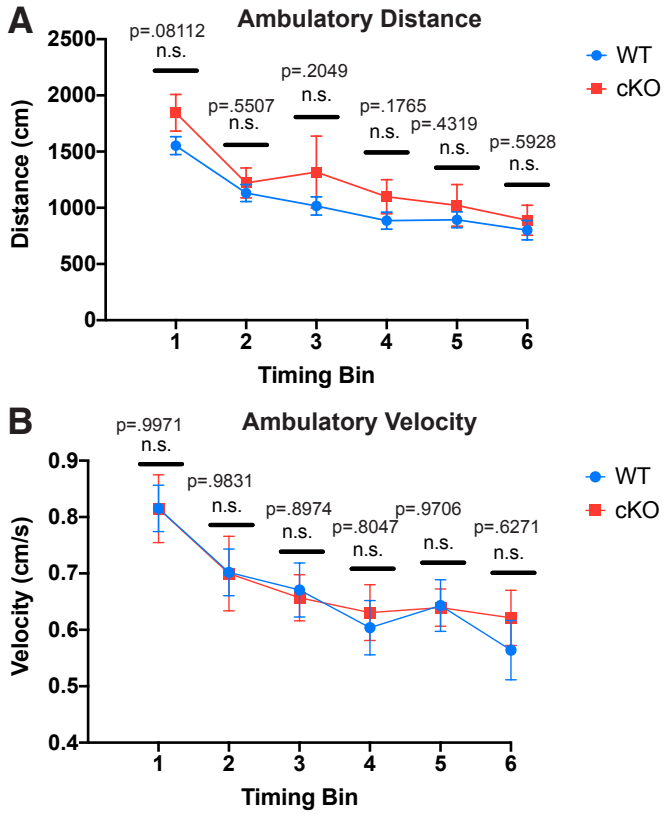

6.2.1 St18 cKO does not alter gross locomotion in an open field assay

A) Quantification of WT and St18 cKO ambulatory distance covered over a one hour open field experiment. The data are split into 10 minute bins to reflect relative decreases in locomotor behavior during the experimental paradigm (*Multiple t tests*). N= 23 WT and 5 St18 cKO.

B) Quantification of WT and St18 cKO ambulatory velocity over a one hour open field experiment. The data are binned as in (A) (*Multiple t tests*). N= 23 WT and 5 St18 cKO.

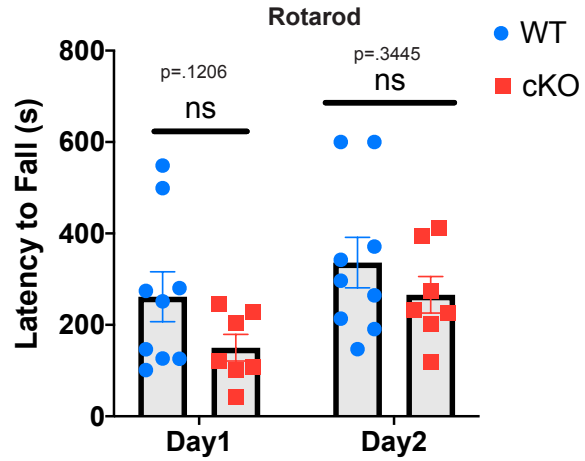

6.2.2 St18 cKO does not alter motor coordination and balance in a Rotarod test

Quantification of WT and St18 cKO performance in the Rotarod test over two testing days, measuring the latency to fall during the experiment (*Multiple t tests*). Briefly, each experimental day, an individual animal is tested three separate times, and those times are averaged to reflect the animals performance on any given day. N= 9 WT and 7 St18 cKO.

was no difference between WT and St18 cKO performance in the Rotarod (Figure 6.2.2). These results are not surprising because, while involved in the initiation and regulation of voluntary

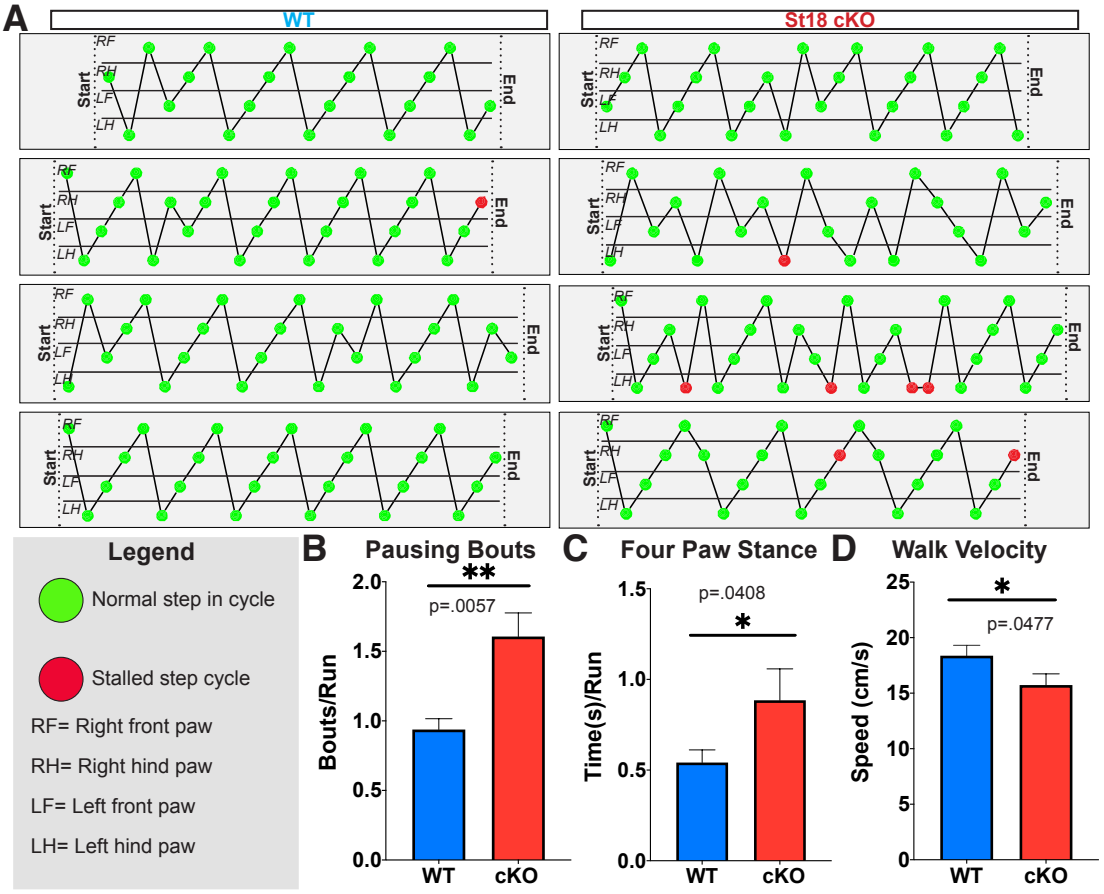

6.3.1 St18 cKO causes mouse walk cycles to stall during locomotion

A) Schematic representations of WT and St18 cKO walk cycles during data acquisition of catwalk experiment. Briefly, these schemes illustrate, during one traverse of the catwalk, the mouse's paw position and movement during the data acquisition phase of the experiment. Green circles indicate that the walk cycles were produced uninterrupted by stalling following that paw's placement. Red circles indicate that a paw placement was followed by a walk cycle stalling. The cycle record begins again once the mouse begins to locomote following the pausing bout. Data acquisition starts and ends during the trial based on software decisions based on relative location of the head and the tail of animal. The legend below the walk cycle schematics explains nomenclature further.

B) Quantification of pausing bouts for WT and St18 cKO animals during catwalk experiment (*Chi square test*). N= 41 WT and 18 St18 cKO.

C) Quantification of four-paw stance for WT and St18 cKO animals during catwalk experiment (*Unpaired t test*). N= 41 WT and 18 St18 cKO.

D) Quantification of average walk velocity for WT and St18 cKO animals during catwalk experiment (*Unpaired t test*). N= 41 WT and 18 St18 cKO.

movements and gait (Freeze et al., 2010), as these movements are controlled mostly by the spinal cord and cerebellum (Shiotsuki et al., 2010).

6.3 St18 cKO causes mouse walk cycles to sporadically stall

Given that St18 cKO produces a decrease in prototypic innervation of the STN and SNr that tracks with a decrease in PV+ GPe neurons also seen in St18 loss of function animals and that there appears to be no gross developmental or locomotor deficit associated with St18 loss of function, I next decided to investigate motor behaviors in a higher resolution manner. To do

this, I performed a catwalk experiment to measure mouse gait and walk cycle parameters in WT and St18 cKO animals (Hetze et al., 2012; Batka et al., 2014). Briefly, this experiment involves an experimental mouse being recorded while walking in a narrow runway that allows for only walking behaviors. While the animal walks, its gait is recorded at a high resolution, and software tracks the animal's paw placement among many other gait parameters. This experiment allows me to examine if there are any fine locomotor deficits associated with St18 loss of function.
I found that St18 cKO produces sporadically disrupted walk cycles, with St18 cKO animals suddenly halting while walking compared to WT animals, which produce rhythmic walk cycles relatively uninterrupted (Figure 6.3.1 A). This disruption in walk cycle production seen in St18 cKO animals compared to WT animals is quantified by an increase in both the amount of time spent per run in a four-paw stance as well as the number of pausing bouts (Figure 6.3.1 B,C).
I also find that there is a significant decrease in average run speed in St18 cKO animals, which tracks with the increased time per run spent in a fixed position (Figure 6.3.1 D).

Interestingly, and consistent with previous results that show that St18 cKO does not produce any gross locomotor deficit, I found that this increase in sporadic walk cycle stalling is not due to a general loss of motor coordination because the distribution of canonical mouse walk cycles is unchanged between WT and St18 cKO (Figure 6.3.2). Mice produce 6 canonical walk cycles characterized by paw placement during locomotion. I do note that one step sequence, alternate-alternate (AA), is significantly different between WT and St18 cKO, I note that, similar to previous reports, this walk cycle is relatively unused and therefore unimportant by comparison to the alternate-bilateral walk cycle, which accounts for nearly 70% of all step cycles (Hetze et al., 2012; Batka et al., 2014; Baldwin et al., 2017). In the absence of other changes aside from the change noted in AA step cycles, I conclude that this distribution is not different between WT and St18 cKO animals. Taken together, then, St18 cKO produces a specific disruption in gait production that produces sporadic stalling episodes that tracks with the loss of PV+ prototypic GPe neurons in the basal ganglia's indirect pathway. Importantly, this phenotype is specific to this behavior and not reflective of a gross locomotor deficit.

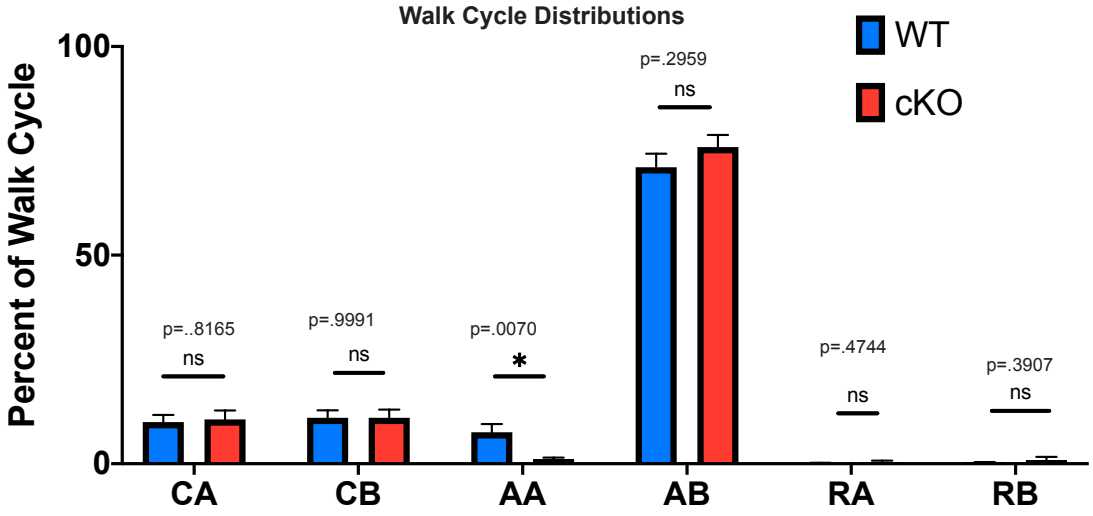

6.3.2 St18 cKO does not meaningfully alter the distribution of mouse walk cycles

Quantification of mouse walk cycles as a percentage of the total mouse walk cycle production for WT and St18 cKO animals (*Multiple t tests*). N= 41 WT and 18 St18 cKO. CA= Cruciate alternate. CB= Cruciate bilateral. AA= Alternate alternate. AB= Alternate bilateral. RA= Rotate alternate. RB= Rotate bilateral.

Discussion

Summary of results

In this study, I have demonstrated the role of a transcription factor, St18, that is expressed in the MGE in specifying projection neuron fate both *in vitro* and *in vivo*. By using an experimental system that allowed me to specify MGE lineage GABAergic neuronal lineages with St18 *in vitro*, I showed that St18 expression produces neurons that are strikingly different than typical MGE lineages, typically characterized as interneurons. Indeed, I find that St18 expression induces projection neuron identity in MGE lineage neurons. I mark the distinction between MGE lineage neurons specified with St18 versus generic MGE lineage neurons by highlighting the salient differences between projection neurons and interneurons. First, MGE lineage projection neurons migrate short distances to populate sub-cortical regions while MGE lineage interneurons migrate long distances tangentially into the cortex (Hu et al., 2017; Bupesh et al., 2011; Dodson et al., 2015; Nobrega-Pereira et al., 2010; Puelles et al., 2000; Xu et al., 2008; Wichterle et al., 2001). MGE lineage neurons specified with St18 demonstrate this difference, migrating short distances compared to generic MGE lineage controls. Second, projection neurons have polarized projection patterns characterized by specific, long-range targeting of distal synaptic partners while interneurons are characterized by short-range, multipolar synaptic targeting (Ofer et al., 2020; Kepecs and Fishell, 2014; O'Leary and Koester, 1993). MGE lineage neurons specified with St18 also demonstrate this difference, producing longer, less complex morphologies compared to their generic MGE lineage interneuron controls.

Having established that St18 gain of function in MGE lineage progenitors produces projection neurons, I next showed what genes St18 is regulating to produce this effect. By RNA sequencing, I showed that a number of genes relevant to neuronal differentiation and progenitor specification are upregulated downstream of St18 expression. I further showed that, from among this list of genes is a factor, Cbx7, that mediates St18 induced projection neuron migration *in vitro*. Indeed, upon inhibition of Cbx7, MGE lineage neurons specified by St18 no longer exhibited projection neuron migratory behavior, instead migrating to the same extent as generic MGE

lineage interneurons. Interestingly, I also noted that Cbx7 does not appear to be responsible for St18 mediate projection neuron morphology, as inhibition of Cbx7 does not revert neurons specified with St18 into interneuron-like morphologies.

Having established that St18 is involved in the transcriptional specification of MGE lineage projection neurons *in vitro*, I next showed that St18 is involved in the specification of MGE lineage projection neurons *in vivo*. In both whole animal St18 knockout and St18 conditional knockout within the MGE, I showed that there is a specific loss of MGE lineage PV+ GPe projection neurons (Nobrega Pereira et al., 2010; Abdi et al., 2015). I further showed by single cell RNA sequencing that this specific loss of a neuronal population of the GPe tracks with the reduction in a specific cluster of transcriptionally distinct early MGE lineage neurons. Together, these results suggest that St18 is involved in the specification of a discrete neuronal population within the MGE, namely GPe PV+ prototypic neurons.

I next showed that this loss of MGE lineage GPe prototypic neurons is causally linked to a decrease in innervation on the primary synaptic targets of PV+ prototypic neurons, the STN and SNr (Hernandez et al., 2016). Indeed, using a combination of synaptic fate-mapping and viral labelling of GPe projection neurons, I showed that prototypic projections onto the STN and the SNr are reduced following St18 loss of function. I also noted that there appears to be a degree of mistargeting of virally labelled GPe projections in the STN and SNr along with an increase in putative arkypallidal projections in the striatum. Taken together, I have shown that St18 loss of function is responsible for a disruption in the basal ganglia's indirect pathway, specifically in the prototypic projection from the GPe to the STN.

I next showed the functional consequences of this decrease in prototypic neuron projections by examining St18 loss of function animal development and motor skills. While I observed no gross developmental or motor related phenotype, I did observe a deficit in mouse walk cycle production that produces sporadic stalling episodes during locomotion. This behavioral phenotype tracks with the observed loss of GPe PV+ prototypic neurons, as the indirect pathway is involved in the initiation and inhibition of voluntary movements (Freeze et al., 2010).

St18, then, is responsible for specifying MGE lineage projection neurons of the GPe by controlling a projection-neuron-specific transcriptional cascade, and these GPe neurons are involved in mediating mouse locomotor gait via their activity in the basal ganglia's indirect pathway.

Discussion.1 MGE diversification is guided by spatio-temporal transcription factor expression

The transcriptional specification of MGE neuronal progenitors into bona fide mature neuronal cell types occurs via the spatial and temporal control of sequentially expressed transcription factors throughout neurogenesis. MGE specification begins early during development at E9.5 with the regionally restricted expression of the transcription factor Nkx2-1 (Butt et al., 2008; Sandberg et al., 2016; Sussel et al., 1999). Loss of Nkx2-1 during this stage of development causes MGE lineage progenitors to transform into progenitors that resemble the LGE and POA, meaning that Nkx2-1 expression is required for the repression of neighboring progenitor domain fates early during development (Flandin et al., 2010; Sandberg et al., 2016).

Having established MGE identity, neuronal progenitors in the MGE next are further specified via temporal and spatial control of gene expression that underlies the diversification of the lineage. For example, MGE progenitors are specified along the rostral-caudal axis by, in part, secreted factor signaling. The regional preference for the generation of PV+ and SST+ interneurons along the rostral-caudal axis, respectively, is informed by a Wnt signaling gradient that originates caudal to the MGE that is controlled by the non-canonical Wnt receptor Ryk (McKenzie et al., 2019). The MGE is also organized along the dorsal-ventral axis by the regionally restricted expression of the transcription factor Otx2 (Hoch et al., 2015). Indeed, loss of Otx2 leads to the ventral MGE taking on properties of the nearby POA progenitor domain, generally located ventral and caudal to the MGE and responsible for the generation of cholinergic neurons of the hypothalamus (Hoch et al., 2015). Furthermore, the regionally restricted expression of transcription factors also establishes the generation of either SST+ or PV+ cortical interneurons. The regionally restricted expression of CoupTF2 in a narrow band of the MGE establishes the

preferential generation of SST+ interneurons over PV+ neurons in a spatially dependent manner by driving Sox6 expression (Hu et al., 2017(1)).

Temporal factors also play a role in the specification of various MGE neuronal cell types. Subpallial lineages are specified along with MGE lineage cortical interneurons with precise timing. Indeed, Nkx2-1 expression, while it establishes ventricular progenitors as MGE, must be inhibited downstream of Dlx2 expression for MGE lineage cortical interneurons to migrate to the cortex, otherwise they become subpallial lineages of the striatum (McKinsey et al., 2013; Nobrega Pereira et al., 2008; van den Berghe et al., 2013). Another example of temporal control of MGE diversification is Lhx6 and Lhx8, which are involved in regulating and maintaining sonic hedgehog (Shh) expression in SVZ MGE progenitors, promoting their survival and thereby allowing for the establishment of late born MGE lineages (Flandin et al., 2011). The GPe is also specified with precise timing, arising early during MGE development in the ventral MGE in an Nkx2-1, Lhx6/8, Shh dependent manner (Flandin et al., 2010; Hu et al., 2017).

Given that the diversification of MGE neuronal lineages happens with the precise control of transcription factor expression in a spatial and temporal manner, my findings that St18, a transcription factor that is expressed in a tightly regulated spatial and temporal pattern (Matsushita et al., 2014), is involved in the specification of a specific MGE neuronal lineage is of particular interest. Recall that I have shown that St18 loss of function *in vivo* produces a loss of a significant portion of MGE lineage GPe PV+ projection neurons, a finding that tracks with my scRNAseq data that also shows a loss of a specific neuron cluster as a result of St18 loss of function. I importantly note that the loss of PV+ GPe neurons is not complete. Together, these findings suggest that St18 expression, which I have shown is restricted to the ventral MGE and embryonic GPe, further refines the generation of GPe neuronal lineages born in the MGE which are known to be controlled by Nkx2-1, Shh, and Lhx6/8 (Flandin et al., 2010; Hu et al., 2017; Nobrega Pereira et al., 2010). Indeed, St18 expression overlaps both temporally and spatially with the generation of the GPe (Flandin et al., 2010; Hu et al., 2017; Matsushita et al., 2014), but how St18 fits into the existing scheme of GPe development within the MGE is still relatively unknown.

Indeed, one of the most salient remaining questions from this study is how St18 expression is controlled in this temporally and spatially restricted manner to play a role in GPe development. To further parse the regulation of St18 expression, I would recapitulate St18 conditional loss of function experiments using Cre drivers that are involved in the specification and timing of GPe development. I would use the Lhx8-Cre driver to test if St18 is involved in post-mitotic maturation of GPe neurons given that Lhx8-Cre fate-maps nearly 100% of PV+ GPe neurons (Mayer et al., 2018) and because Lhx8 is expressed downstream of both Nkx2-1 and Shh. I would also use the Shh-Cre driver to test if St18 expression is influential early in the Nkx2-1 lineage downstream of Nkx2-1 expression or if it is influential after the GPe is established along the dorsal-ventral axis by Shh expression in the ventral MGE (Flandin et al., 2010). These experiments would begin to further reveal the transcriptional control of St18 expression and resolve its role in GPe development.

Discussion.2 St18 and Myt transcription factors are involved in neural differentiation

St18 (also known as Myt3 and NZF3) is a transcription factor in the Myt superfamily of transcription factors, characterized by zinc finger DNA binding motifs in highly conserved C-terminals across the entire family, which includes Myt1, Myt1L, and St18 (Matsushita et al., 2014; Kameyama et al., 2011). Specifically, these transcription factors are characterized by CCH-HC-type zing finger motifs as DNA-binding domains and are expressed most vigorously in the developing nervous system (Matsushita et al., 2014). Generally, Myt family transcription factors act as gene regulators by recruiting the transcriptional co-repressor Sin3B along with histone deacetylases (Nielsen et al., 2004; Romm et al., 2005). Myt family transcription factors, including St18, are induced in early post-mitotic neural progenitors and is involved in neural differentiation (Matsushita et al., 2014).

Myt1 promotes neurogenesis primarily via the inhibition of Notch signaling, promoting cell cycle exit in cycling neural progenitors (Vasconcelos et al., 2016). Interestingly, Myt1 mutants also have a significant neuronal phenotype, with decreased vagal nerve innervation of the diaphragm that leads to early post-natal lethality of Myt1 whole animal loss of function (Wang

et al., 2007). Myt1L is also very heavily implicated in neuronal differentiation. Myt1L is used as one of the trio of transcription factors required to produce induced neurons from fibroblasts *in vitro* (Vierbuchen et al., 2010). It was also shown that this effect of Myt1L expression in inducing neuronal fate is caused by Myt1L's ability to act as a broad repressor of non-neuronal differentiation in an all-but-one manner (Mall et al., 2017).

St18 has also been previously implicated in neuronal differentiation *in vitro*. Indeed, St18, when expressed in undifferentiated P19 cells in conjunction with Neurog1, significantly increased the rate of neuronal differentiation compared to Neurog1 expression alone (Kameyama et al., 2011). Beyond neuronal differentiation, St18 is thought to behave as a broad transcriptional repressor due to its high affinity DNA binding domain (Yee and Yu, 1998). St18 has a documented role in cancer genetics as well, acting either as a tumor suppressor or an oncogene depending on the cellular context. In breast cancer, St18 mRNA is downregulated in primary breast tumors, showing that there is tumor-specific downregulation of St18 (Jandrig et al., 2004). In liver cancer tumorigenesis, St18 expression is induced by tumor associated macrophages in a way that contributes to tumor growth, thereby making it an oncogene (Rava et al., 2017). St18 is also involved in various other cellular processes in the pancreas. Indeed, St18 induces pancreatic beta-cell apoptosis and curtails beta-cell replication, all of which impacts diabetes pathology (Henry et al., 2014). Furthermore, St18 is involved in the laminin-integrin dependent migration of pancreatic islet cell cells via regulation of Tgfbi signaling (Tennant et al., 2015). This documented role of St18 in migration is of particular interest, as I have shown that St18 induces a projection-neuron like migratory pattern *in vitro*.

Given that I have documented a novel role of St18 in the specification of MGE lineage projection neurons *in vitro* as well as in the specification of a population of GPe PV+ projection neurons, I have characterized for the first time the specific role of St18 in neuronal differentiation and in the development of neural migration and morphology. I have also characterized, using RNA sequencing, the genes associated with St18's role in driving projection neuron development in MGE progenitors. While Myt transcription factors have been implicated in the differentia-

tion of neurons among other tissues throughout the mammalian body, these findings illustrate for the first time the role of a Myt transcription factor in the differentiation of a specific neuronal lineage. One of the most intriguing outstanding questions from this work is whether St18 is involved in the development of other neuronal cohorts born outside the MGE given that it is expressed in the cortical plate as well as in the LGE and POA. It would be interesting to more closely assay the cellular phenotype of non-MGE lineages in St18 (-/-) animals to determine if St18 is involved in the specification of neuronal lineages in these other progenitor domains.

Another interesting question that remains to be answered would be what the St18 protein binds to on the genome to induce projection neuron differentiation in MGE progenitors. I have identified the effector gene Cbx7, which is involved in projection neuron migration, using the list of differentially expressed genes between N/D and N/D/S differentiated neurons. While this approach is useful in finding testable downstream effectors of St18, the general mechanism by which St18 controls this differential expression is still unknown. To answer this question, I would perform ChIP-Seq on N/D/S differentiated neurons to assay the chromatin signature of St18 gain of function *in vitro*. Fortunately, this experiment would be easily possible, as the St18 gain of function transgene used in the experiments presented earlier in chapters 1 and 2 has a V5 tag, thus facilitating the ChIP-seq experiment. This could show, like was shown in the case of Myt1L (Mall et al., 2017), that St18 induces projection neuron fate in an all-but-one repression manner.

Another outstanding question from my project regarding Myt family transcription factors is whether there is any redundant functionality of other Myt transcription factors following St18 loss of function. Recall that I have shown that, while St18 loss of function does produce a reduction in a specific neuronal lineage, that loss is not complete. This could suggest that the loss of St18 is offset by compensatory expression of either Myt1 or Myt1L in MGE progenitors. Indeed, when Myt1 is knocked out in pancreatic progenitors, the Myt1 loss of function phenotype can be compensated for by the activation of Myt1 paralogs St18 and Myt1L (Wang et al., 2007). To rule this possibility out, I would need to characterize St18 loss of function phenotypes in conjunction

with Myt1 and Myt1L conditional loss of function in the MGE.

Discussion.3 MGE neuronal migration is controlled in a cell-type specific manner

The cellular mechanisms that control neuronal migration for the heterogeneous cohort of neurons born in the MGE have been fairly well elucidated. Of note, however, is that the migratory mechanisms for MGE born projection neuron lineages are less well studied than the migratory mechanisms for various cortical and striatal interneuron cohorts are. Indeed, the long-range migration of MGE born interneurons and the migratory cellular morphology are some of the defining characteristics of the lineage (Marin 2013; Marin et al., 2006). Interneurons migrate via leading processes that follow various guidance cues that are differentially followed based on cell-type specific expression of cell-surface receptors (Martini et al., 2009; Yanagida et al., 2012; Nobrega-Pereira and Marin, 2009). In fact, new-born neurons in the MGE are initially polarized by the ventricular zone expression of Slit1 and Ephrina5, which moves cells from the ventricular zone to the MGE SVZ and mantle (Marillat et al., 2002; Zimmer et al., 2008). Then, migration from the MGE is stimulated by secreted brain-derived neurotrophic factor (BDNF) and neurotrophin-4 (NT4) (Polleux et al., 2002). As interneurons migrate tangentially away from the MGE, they next encounter the basal ganglia and striatum, wherein medium spiny neurons born in the LGE secrete Sema3A and Sema3F (Marin et al., 2001). These chemo-repulsive cues are sensed by neuropilin receptors expressed on interneurons migrating to the cortex, receptor expression that is induced by Nkx2-1 repression, which allows migrating neurons to pass the striatum en route to the cortex (Nobrega Pereira et al., 2008). Interneurons that do not repress Nkx2-1 fail to express neuropilin receptors and therefore do not sense the Sema3A and Sema3F present in the striatum, promoting their invasion of the striatum to become the MGE born complement of striatal interneurons (Nobrega Pereira et al., 2008). Cortical interneurons that have successfully passed the striatum are then guided to the pallium and cortex by chemo-attractive cues Nrg1 and sensed by cortical interneuron specific expression of the receptor Erbb4 (Flames et al., 2004).

While the mechanisms that guide MGE lineage cortical and striatal interneurons to their target regions are fairly well established, the mechanisms that guide MGE lineage GPe projec-

tion neurons are relatively poorly understood. Indeed, the only feature of MGE lineage GPe projection neuron migration that is established is the retention of Nkx2-1 expression in GPe neurons, which is believed to be involved in the sub-cortical migration of GPe neurons as these cells are insensitive to striatal and basal ganglia secreted Sema3A and Sema3F expression (Nobrega Pereira et al., 2010). Other than this, the only other established, salient feature of MGE lineage GPe neuronal migration is that they migrate short distances compared to other MGE lineages. Indeed, the embryonic GPe is very close to the MGE, which means that neurons only have to migrate short distances from the MGE into the GPe (Flandin et al., 2010).

I have shown in this work that St18 is involved in the specification of MGE lineage GPe PV+ projection neurons *in vivo*. I have also shown that St18 gain of function in an *in vitro* model of MGE development produces neurons that migrate significantly less than MGE lineage neurons not specified by St18, which migrate greater distances and morphologically resemble migratory interneurons. I have also shown that Cbx7, a transcriptional repressor that acts via involvement in the polycomb repressor complex 1 (PRC1), mediates St18 induced short range migration in MGE lineage neurons. Indeed, inhibition of Cbx7 causes N/D/S neurons specified by St18 to migrate at the same rate as MGE lineage controls, thereby resembling interneurons. Therefore, Cbx7 mediated PRC1 transcriptional repression downstream of St18 produces projection neuron short-range migration. St18 and its effector gene Cbx7, then, constitute, to my knowledge, the first MGE factors that lead to projection neuron lineage specific migration.

Importantly, the *in vitro* migration assay used characterize migration patterns of differentiated neurons has no guidance cues, so it is likely that St18 and Cbx7 restrict long-range migration cell autonomously. One potential mechanism that can explain this cell-intrinsic short-range migration of N/D/S neurons and MGE lineage GPe neurons is that these neurons do not undergo tangential migration but instead only migrate radially from the MGE a short distance into the nearby nascent GPe. Recall that, when observed by single cell RNA sequencing, St18 (-/-) MGE shows the loss of a specific neuron cluster, cluster 4 and that this specific loss of a neuron cluster tracks with the specific loss of MGE lineage GPe PV+ neurons seen in St18 loss of function. In

cluster 4, I also noted that one of the genes that is upregulated is the factor Rnd2, a gene that is involved in radial migration of cortical neurons born in the dorsal pallium (Heng et al., 2008). This suggests that MGE lineage GPe neurons have an intrinsically limited migratory ability, which changes MGE neuron migration from long to short range radial migration.

While I have uncovered an effector gene that mediates this St18 induced migratory phenotype, there is much to learn about GPe neuron migration from the MGE. Specifically, there are likely guidance cues present in the embryonic GPe and complementary receptors expressed in new-born GPe neurons in the MGE that can help to explain this cell-type specific migration of GPe neurons. This is likely true because, as is the case with other MGE neuronal lineages of the striatum and cortex, these cells likely express cell-type specific receptors to guide each lineage to its target brain structure. One way to elucidate this would be to investigate the expression and function of genes known presently to be regulated by Cbx7 and the PRC1. Cbx7 is known to be involved in early neuro-epithelium differentiation (Morey et al., 2013) as well as post-mitotic dorsal root ganglia neurite extension (Duan et al., 2018), both of which show that Cbx7 and the PRC1 are involved neural differentiation. Cbx7 also has a well characterized role in cancer biology. Loss of function mutations in Cbx7 are correlated with increased glioblastoma multiforme tumor invasiveness (Li et al., 2013; Wu et al., 2017). Restriction of migration is thought to be mediated by Cbx7 interaction with Wnt/b-catenin (Bao et al., 2017) and the YAP-TAZ pathway (Nawaz et al., 2016). Elevated levels of Cbx7 result in decreased cancer cell migration, a finding that is consistent with my findings that N/D/S neurons express high levels of Cbx7 and migrate shorter distances. Characterizing the molecular mechanisms by which Cbx7 mediates N/D/S projection neuron migration would further elucidate the mechanisms of projection neuron migration.

I have shown that Cbx7 is responsible for St18 mediated projection neuron differentiation and migration *in vitro*, but St18's role in specifying GPe neurons *in vivo* remains to be resolved. The first experiment I would do is to recapitulate MS351 treatment on *in vivo* embryonic MGE tissue to see if Cbx7 is regulating projection neuron migration. Briefly, I would use an MGE explant embedded in Matrigel with fate-mapped MGE neurons (Nkx2-1-Cre) in WT embryos with

either vehicle or MS351 treatment to assay *in vivo* migration into and around the embryonic GPe. If MS351 has a similar effect on *in vivo* neurons as is observed in *in vitro* projection neurons specified by St18, then MS351 treatment would produce an impoverished GPe.

Discussion.4 Specification of projection neuron morphology by St18

Very little is known about the molecular regulation of morphogenesis in neurons throughout the nervous system. However, one of the salient features of neuronal subtypes is that their morphologies are suited for specific cellular functions. Indeed, throughout the nervous system, neuronal morphologies have dendritic and axonal arbors that provide the form to the functionality of the nervous system. This morphogenic specificity that is fit to nervous system function is underwritten by cell type specific gene expression patterns. The genes responsible for this crucial developmental feature, however, remain poorly understood.

There is some understanding of the genetic control of distinct axonal projection patters in excitatory cortical neurons. Excitatory projection neurons of the cortex are born in the ventricular zone (VZ) of the dorsal aspect of the pallium (McConnell 1991). As individual cells are born in the VZ, they exit the cell cycle and begin to form the discrete layers of the cortex in a temporally sequential fashion (Leone et al., 2008; McConnell and Kaznowski, 1991). As these layers are sequentially produced, deep layer cortical neurons born early have a broader ability to produce all subsequent layers while later born neurons are restricted to only layers born after they have been established (Desai and McConnell, 2000). This establishes a cellular architecture defined by specific gene expression patterns that underlies the function of the cortex's discrete layers (Leone et al., 2008). Deep layer cortical neurons project to subcortical targets via the cortico spinal tract in layer 5 and to the thalamus in layer 6 (Leone et al., 2008). The specification of these neurons and their projection patterns is determined by Sox5 expression (Lai et al., 2008). In the absence of Sox5, layers 5 and 6 fail to form altogether (Lai et al., 2008). Upper layer cortical neurons express Cux1/2 and Brn1/2, which are essential for the production of layers 2, 3, and 4 in the cortex by promoting cell-cycle exit in the VZ (Sugitani et al., 2002; Zimmer et al., 2004). Among these upper layer cortical neurons are callosal projection neurons, which extent axons across the

corpus callosum to the opposite cerebral cortex hemisphere (Leone et al., 2008). This discrete class of upper layer cortical projection neurons is specified by the expression of Satb2, and in the absence of Satb2, upper layer cortical projection neurons project along the cortico spinal tract to subcortical synaptic targets (Britanova et al., 2008; Alcamo et al., 2008). These examples from the cohort of cortical projection neurons suggests that within specific subpopulations in a defined neuronal lineage, specific gene expression patterns underlie projection neuron morphogenesis during development and establishes neuron function in the mature brain.

The transcriptional establishment of cell-type specific neuronal morphology is also seen within the MGE neuronal lineage. Indeed, among the cardinal classes of cortical interneurons from the MGE, PV and SST, there are early transcriptional determinants that underlie early differentiation between PV and SST cell types (Kepecs and Fishell, 2014). Indeed, expression of Sp8/9 controls the post-mitotic tangential migration of PV+ interneurons in the cortex (Tao et al., 2019) while the differentiation and maturation of STT+ cortical interneurons is regulated by Satb1 (Close et al., 2012). Briefly, PV+ cortical interneurons tend to be either soma-targeting basket cells or axon-initial-segment targeting chandelier cells and SST+ cortical interneurons are dendritic targeting Martinotti cells (Kepecs and Fishell, 2014).

These differences in synaptic targeting and, therefore, morphology are essential for interneuron and cortical function. However, the transcriptional regulation of morphological maturation of these cardinal neuronal classes is relatively unknown. For example, PV+ chandelier cells are born late in the MGE, between E15-E18 from a late-born population of Nkx2-1+ progenitors, but how this temporal specification informs the unique axon targeting morphology of chandelier cells is a mystery (Taniguchi et al., 2013; Inan et al., 2012). Indeed, one of the only cell autonomous transcriptional mechanisms known to influence cortical interneuron morphology is characterized in SST+ Martinotti cells (Lim et al., 2018(1)). Upon the conditional deletion of Mafb, Martinotti cells fail to produce proper targeting of layer 1 dendrites in a cell autonomous manner (Lim et al., 2018(1)). While the intrinsic development of MGE lineage cortical interneuron morphology is poorly understood, it is possible that MGE lineage projection neuron lineages have

unique morphological determinants that differentiate them from the rest of the lineage transcriptionally as is seen in other projection neuron populations in the nervous system.

Recall that I have shown that N/D/S neurons specified by expression of St18 in an *in vitro* model of MGE development have morphologies that resemble projection neurons. Specifically, I have shown that N/D/S neurons have polarized morphologies with a prominent, long process among several shorter, non-branched processes compared to N/D neurons, that have multi-polar, highly branched morphologies that resemble cortical interneurons. St18, then, represents the first MGE expressed factor that cell-autonomously specifies projection neuron morphology. The remaining question, then, is how St18 is regulating this morphological characteristic. To answer this, I would utilize a similar approach used in characterizing Cbx7 as a downstream effector of St18 that is responsible for projection neuron migration. By examining the RNA sequencing data that highlighted the differential expression between N/D/S and N/D neurons, I would test genes known to be involved in morphogenesis and cytoskeletal processes in the 2D morphology assay I described earlier. This would further elucidate the mechanisms by which St18 cell-autonomously promotes the adoption of projection neuron identity during MGE neurogenesis.

Discussion.5 St18 KO related loss of GPe PV+ neurons is incomplete

One of the salient questions that arises from my study is the question of why, in St18 loss of function conditions, there is an approximately 40% decrease in PV+ GPe prototypic neurons while there is a far more significant decrease in neuron cluster four in my single cell RNA sequencing analysis of St18 (-/-) MGE. I hypothesize that this observation can be explained at least in part by the homeostatic normalization of cell numbers postnatally. Indeed, within the MGE lineage, there is ample evidence of the postnatal regulation of selective neuron survival and apoptosis that establishes the proper number of neurons in a given structure.

As MGE lineage cortical interneurons arrive in the cortex following tangential migration, the proper balance of inhibitory and excitatory neurons, and this balance is regulated by an endogenous period of programmed cell death that establishes proper cell numbers after interneuron invasion of the cortex (Rossignol, 2011). Programmed cell death of MGE derived cortical

interneurons is regulated by a number of different cellular mechanisms, but interneurons die at about the rate of 40% during cortical maturation to establish proper cell numbers (Southwell et al., 2012). This ratio of cell survival to cell death among MGE derived interneurons is an intrinsic feature of interneuron development (Southwell et al., 2012). This process of programmed cell death to establish proper cell numbers is regulated in part by cortical interneuron expression of clustered gamma protocadherin (Pcdhg) isoforms (Mancia Leon et al., 2020). The expression of particular isoforms of Pcdhg's differentially, cell autonomously regulates the selective survival of certain interneurons as proper cell numbers are being established after migration during programmed cell death (Mancia Leon et al., 2020). While some neurons have an intrinsically greater ability to survive, many cells rely on neural activity-related mechanisms to regulate survival (Priya et al., 2018). Indeed, MGE derived interneurons express a calcium-dependent phosphatase, Calcineurin, that sequentially links Ca2+ transients related to neuronal activity to maturation-related transcriptional programs (Priya et al., 2018). Inactivation of Calcineurin causes cortical interneurons to fail to mature properly, which is accompanied by an increase in apoptosis (Priya et al., 2018). Cortical pyramidal cells also regulate MGE lineage interneuron in an activity dependent manner (Wong et al., 2018). Cortical pyramidal cell activity negatively regulates PTEN signaling, thereby negatively regulating interneuron cell death during the time of programmed cell death in an activity dependent manner (Wong et al., 2018; Keniry and Parsons, 2008).

These intrinsic and non-cell autonomous mechanisms of cortical interneuron survival and cell death are plastic during nervous system development to provide homeostatic control for the proper establishment of cortical circuits (Rossignol, 2011). Given that GPe neurons are also MGE derived (Nobrega Pereira et al., 2010), it is possible that GPe neuronal numbers are similarly self-correcting during development. In St18 loss of function conditions, I see a significant but incomplete loss of PV+ GPe MGE lineage neurons. It is possible that, because of the homeostatic regulation of cell survival that allows neural populations to be robust to changes and deficits during development, in the case of St18 loss of function, these same mechanisms are homeostatically adjusting for the loss of GPe projection neurons during development as a result

of St18 loss of function. In order to account for this possibility, I would track GPe cell numbers during various times during early post-natal development. I would expect to see a decrease in GPe cell numbers early during development with a corresponding decrease in apoptosis in the GPe, which would show that the GPe is homeostatically allowing for more cell survival.

Discussion.6 PV+ GPe neurons are not a monolithic neuron class

The GPe is comprised of a heterogeneous cohort of neurons born either in the LGE or the MGE. The LGE born cohort of GPe neurons are mostly Npas1+ and FoxP2+ arkypallidal neurons that project primarily to the dorsal striatum and cortex (Abdi et al., 2015; Hernandez et al., 2015; Abecassis et al., 2020). The MGE born cohort of GPe neurons consists of three primary molecularly defined classes: PV+, ChAT+, and PV- (Abecassis et al., 2020). Among these primary classes of MGE derived GPe neuronal cohorts, the most heterogeneous is the PV+ population of GPe neurons. PV+ GPe neurons are divided into four classes based on molecular marker expression and physiological properties: Lhx6+, Dbx1+, Sox6+, and Nkx2-1+ (Abecassis et al., 2020). Other evidence suggests that a majority of PV+ GPe neurons also express Er81 (Abdi et al., 2015). The degree to which these subtypes overlap is relatively unknown, but each molecularly defined class of GPe PV+ neuron could represent either a non-overlapping neuronal population or a subset of another, larger class of MGE derived GPe neuron.

Recall that I have shown that, upon St18 whole animal and MGE specific knockout of St18, I see a loss of these PV+ GPe neurons of about 40% compared to WT. I also note a decrease in Er81+ and Nkx2-1+ neurons in St18 loss of function conditions that is relatively small compared to the loss of PV+ neurons. I also found a similarly small but significant decrease in tdT+ fate-mapped GPe neurons in St18 loss of function animals. These results show that St18 specifies MGE lineage GPe neurons. This raises a question in interpreting this observed cellular phenotype of St18 loss of function in the GPe: why is the decrease in PV+ neurons more severe than the loss of Er81+, Nkx2-1+, and tdT+ neurons in St18 loss of function conditions?

One potential explanation for this observation is that the subset of MGE lineage PV+ GPe neurons specified by St18 expression *in vivo* represents a particular subset of PV+ neurons.

Nearly 80-90% of Nkx2-1+ GPe neurons are PV+ (Abecassis et al., 2020). However, only about 60% of PV+ GPe neurons are Nkx2-1+ (Abecassis et al., 2020). This suggests that there is a fairly large cohort of MGE derived PV+ GPe neurons that do not express Nkx2-1. Indeed, upon St18 loss of function, I observe a significant loss of PV+ neurons, with the cohort of Nkx2-1+ neurons being apparently less susceptible to St18 loss of function. This finding tracks with the finding that Nkx2-1 lineage fate-mapped tdT+ neurons and Er81+ neurons decrease at the same rate as do Nkx2-1+ neurons in the GPe upon St18 loss of function, as all of these markers constitute general markers of MGE lineage GPe neuron identity compared with PV (Nobrega Pereira et al., 2010; Abdi et al., 2015; Abecassis et al., 2020). This suggests that the more severe loss of PV+ neurons in St18 loss of function is due to the fact that St18 specifies a subset of MGE lineage PV+ neurons, and only some of these express Nkx2-1 into adulthood. In order to better characterize the population of GPe neurons St18 is responsible for specifying, I would perform a fate-mapping experiment using either an St18-Cre or St18-Flp paired with a histological characterization of the fate-mapped GPe neurons. This would elucidate what GPe neuronal lineage St18 specifies beyond it being involved in the broad category of MGE derived GPe neurons.

Discussion.7 Principal GPe neuron classes are heterogeneous

One of the common misconceptions about the classifications of neuronal types is that these classes are homogenous once characterized. However, as is observed in large scale scRNA-seq experiments, principal cell types often have heterogeneous gene expression patterns. The MGE cohort of cortical interneurons, often characterized as either SST+ or PV+, actually express a diverse cohort of genes that define functional and anatomically distinct classes of each type of neuron (Tasic et al., 2018). Indeed, there are dozens of sub-divisions of these principal classes of cortical interneuron that are not trivial, but instead reflect real biological changes in both cell position and cell function. For example, one cluster of SST+ neurons identified corresponds to Nos1+ long-range projecting interneurons while another cluster corresponds to SST+ Calb2+ Martinotti cells (He et al., 2016; Paul et al., 2017; Tasic et al., 2018).

This potential for molecular sub-specification of neuronal subtypes is also exemplified in

the GPe's cohort of prototypic neurons, typically defined by PV and Nkx2-1 expression (Nobrega-Pereira et al., 2010; Abdi et al., 2015). Beyond the observed specification of GABAergic, MGE lineage projection neurons in the GPe by Nkx2-1, Lhx6, and Sox6 (Flandin et al., 2010; Du et al., 2008; Batistra-Brito et al., 2009; Jaglin et al., 2012), the specification of different cells types, defined by combinatorial expression of different transcription factors, is relatively poorly understood (Abecassis et al., 2020). Further, the anatomical and functional consequences of this differential expression is unknown. Indeed, within the GPe prototypic neuron class, which represents approximately 50% of the GPe, there is further heterogenous expression of the factors Dbx1, Lhx6, Sox6, and Nkx2-1 (Xu et al., 2008; Abecassis et al., 2020).

Given that I have found that the loss of St18 produces a significant, but not complete, loss of Nkx2-1+ PV+ projection neurons in the GPe, I hypothesize that St18 could be an MGE expressed transcription factor that defines some of this heterogeneity within the MGE cohort of GPe projection neurons. Given that I also find decreased prototypic innervation in the STN and in the SNr following St18 loss of function, I also hypothesize that St18 is responsible for the canonical PV+ prototypic neuron projection (Hernandez et al., 2015; Hegeman et al., 2016). I believe that a closer examination of the remaining PV+ neurons in St18 (-/-) and St18 cKO GPe would reveal that those neurons are of classes less well defined by a canonical prototypic characteristics, including but not limited to Nkx2-1 expression and projection anatomy. Furthermore, I believe that St18+ GPe lineages correspond to Nkx2-1+ and Dbx1+ cohorts, as Dbx1+ neurons are typically PV+ prototypic neurons (Abecassis et al., 2020). To prove this claim, I would recapitulate St18 conditional loss of function in Dbx1-Cre animals. This will determine to what extent Dbx1+ PV+ GPe neurons are specified by St18.

Discussion.8 PV+ neurons are a difficult MGE lineage to access early

One of the most prominent challenges to studying the MGE lineage cohort of PV+ neurons is that there are few presently identified early transcriptional antecedents of PV+ neurons. This is because, throughout the nervous system, PV expression is induced following sustained neuronal activity and Ca2+ currents (Filice et al., 2016; Hermanowicz-Sobeiraj and Robak, 2017;

del Rio et al., 1994). Therefore, there is a need to identify the early transcriptional antecedents to PV expression in order to make these neuronal populations accessible to researchers.

Indeed, the early specification of MGE lineage PV+ interneurons in the cortex has begun to be understood using single cell RNA sequencing. One study investigating the progression of ventral telencephalon progenitors identified potential early markers for cardinal cell identities of MGE lineage neurons (Mayer et al., 2018). Among the early transcriptional markers of cardinal MGE cell type identified was Mef2c, which, when deleted, causes a loss of PV+ cortical interneurons (Mayer et al., 2018). Another study that investigated the early emergence of mature MGE lineage neuronal subtypes during development and related embryonic gene expression with the gene expression of known adult MGE lineage neuronal subtypes (Mi et al., 2018). This approach identified a number of putative embryonic PV populations based on gene expression correlations with known adult cortical interneuron clusters (Tasic et al., 2018; Mi et al., 2018). This group verified the biological relevance of their predictions by showing that Maf is an early marker of SST+ cortical interneurons, as Maf was one of the differentially expressed genes that constituted a putative early SST+ population (Mi et al., 2018). This means that they have potentially identified a number of embryonically expressed genes implicated in the early specification of PV+ cortical interneurons (Mi et al., 2018).

This study, however, only uses the adult neocortex as a reference point for their correlational analysis of established MGE lineage neuronal cohorts and the embryonically identified clusters of neurons they have identified. This means that their analysis does not take into account sub-cortical interneuron or projection neuron lineages. Recall that I have shown that St18 loss of function leads to a significant decrease in the number of PV+ neurons in the GPe. This finding suggests that St18 is an embryonically expressed transcription factor that delineates PV+ fate early during neurogenesis. Furthermore, this finding would constitute the first early expressed gene that specifies a specific GPe PV+ projection neuron lineage. This means that the genes regulated by St18 and thereby affected by St18 loss of function could lend insight into the early adoption of PV+ neuronal fate. It would be possible to investigate this using the single cell RNA

sequencing data I presented earlier. Recall that I showed a specific loss of neuron cluster 4 following St18 loss of function. This cluster expresses a unique cohort of genes that I hypothesize constitute the putative early markers of PV+ GPe neuronal fate. Utilizing this dataset to elucidate the mechanisms by which GPe PV+ neurons adopt PV fate could be informative to the pursuit of understanding the adoption of PV+ neuronal fates in other MGE lineages.

Discussion.9 Projection neurons have specific transcriptomic signatures based on neuron function and anatomy

A defining characteristic of projection neurons is their highly specific targeting of distal synaptic targets. This key anatomic feature of projection neurons is seen throughout the brain from the neocortex to the spinal cord and is underwritten by specific gene expression patterns that mediate specific projection morphologies. In the spinal cord, different classes of sensory and motor projection neurons are specified along the dorsal, ventral axis in response to graded sonic hedgehog (Shh) signaling (Jessell, 2000). Shh controls the expression of a series of transcription factors that, due to cross repression and other post-translational mechanisms, produce a variety of different classes of projections neurons that all target specific functional regions (Jessell, 2000). For example, dorsally generated cerebellar projections in the spinal cord express the post-mitotic factors Bm3a, BarH1, and Lhx9 while ventrally generated primary motor neurons that project to muscle express the post-mitotic factors Hb9 and Isl1/2 (Alaynick et al., 2011). In the cortex, corticospinal motor neurons (CSMNs) are one class of many glutamatergic projection neurons born in temporally controlled fashion to populate the cortex's six layers (Bayer and Altman, 1991). CSMNs occupy layer V of the cortex and project to the spinal cord while other cortical projection neurons project either between layers of the cortex or between hemispheres (Bayer and Altman, 1991). It has been shown that CSMNs express a unique cohort of genes, including Diap3, Igfbp4, and Crim1, that distinguish these neurons from other layer V projection neurons (Arlotta et al., 2005). Indeed, this transcriptional specification can even further divide defined classes of projection neurons. In cortical layer V, there are two different types of pyramidal tract (PT) neurons that project to either the thalamus and express Npsr1 and Hpgd or express Slco2a1

and project to the medulla (Ecomomo et al., 2018). These two distinct classes of PT neurons are closely related and are often clonally related during development; however they express a few distinct genes that completely segregate these neurons both anatomically and functionally (Economo et al., 2018).

Given that projection neurons are defined by both their highly specific anatomical targeting of synaptic targets as well as by their tailor-made transcriptional profile that clearly defines projection function and anatomy, it is possible that the projection neurons of the GPe are specified in the same way. Given that the physiological function of the GPe in behavior is relatively poorly understood (Freeze et al., 2010) and that the heterogeneity of the GPe is only starting to be properly parsed (Abecassis et al., 2020), it is possible that examining the GPe projection neuron cohort in higher resolution will shed light both on the projection patterns of different prototypic and arkypallidal neurons in the GPe as well as to parse the distinction of the GPe's sub-classes. Given that I have shown that St18 specifies projection neurons *in vitro* and that the loss of St18 produces a loss of MGE lineage prototypic neurons in the GPe that leads to both an anatomical change in the basal ganglia circuitry as well as a pronounced locomotor deficit in St18 cKO animals, it is probable that St18 specifies a specific class of projection neuron within the MGE projection neuron cohort. Indeed, if St18 specifies a specific population of MGE lineage projection neuron in the GPe, other MGE lineage projection neurons, either in the GPe or otherwise, could be specified by other factors like St18. It is also possible that, given the majority of cells born in the MGE are interneurons, that this mechanism could be unique to MGE lineage projection neurons. Indeed, the transcriptional signatures of the principal cell types of MGE lineage cortical interneurons are shared across anatomical divides and synaptic targets (Tasic et al., 2018). The discovery and characterization of St18, then, could illustrate a methodology to both characterize otherwise genetically inaccessible neuronal populations as well as further understand both MGE diversification and neural specification in general.

Discussion.10 Interneuron versus projection neuron fate choice in a single progenitor pool

Neuronal progenitor cells throughout the nervous system have a multipotent ability to

produce either long range projection neurons or short-range interneurons. This ability has been well documented within the MGE neuronal lineage, with a large cohort of cortical interneurons being made in the same neurogenic zone as projection neurons of the GPe and MeA (Wichterle et al., 2001; Xu et al., 2008). In the developing spinal cord, p0 spinal cord progenitors give rise either to locally projecting V0 interneurons and commiserate long-range projection V0c projection neurons (Moran-Rivard et al., 2001; Peirani et al., 2001; Lanuza et al., 2004; Lu et al., 2015). In the cerebellum, Purkinje cells, the primary projection neuron projecting to the deep cerebellar nuclei, and the various types of locally projecting interneurons of the cerebellar circuit are born in the same Ptf1a+ VZ progenitor zone (Hoshino et al., 2005; Hoshino, 2006; Hibi and Shimizu, 2012).

While the ability of neuronal progenitors to diversify into a variety of different cell types is well established throughout the nervous system, the ability of discrete neuronal progenitors to become either a projection neuron or an interneuron is relatively poorly understood. Indeed, there is clear evidence that individual MGE progenitors are able to develop into either projection neurons of the GPe or into cortical interneurons based on viral lineage tracing of progenitor clones (Mayer et al., 2015). However, the transcriptional mechanisms responsible for this ability of MGE progenitors to become these two very different neuronal subtypes are unknown.

I have identified, to my knowledge, the first transcription factor that delineates between projection neuron and interneuron fate within a single neuronal progenitor lineage. I have shown that, *in vitro*, St18 expression is sufficient to produce projection neuron migration and morphology in a model of MGE lineage specification that generally makes only interneurons. *In vivo*, I have shown that St18 expression is also necessary for the development of a specific population of MGE lineage GPe projection neurons. Together, this finding highlights, for the first time, a transcriptional mechanism by which projection neurons are specified from interneurons. In order to better characterize this fundamental fate choice during neurogenesis, I would examine St18 chromatin binding by ChIP-seq *in vitro* using N/D/S differentiated neurons. This would help to determine the means by St18 exerts transcriptional control to lead to projection neuron specifi-

cation. This would also allow for future tests in other progenitor zones to determine the extent to which the fate switch between projection neuron and interneuron is a generalized developmental mechanism or if St18 shows an MGE specific mechanism.

Discussion.11 St18 is involved in neuron maturation, not progenitor survival

Neural progenitors are patterned and specified early during development as a result of both intrinsic and extrinsic factors that begin to define mature neuronal identity. For example, in the spinal cord, early progenitors are patterned by a morphogen gradient of sonic hedgehog (Shh) that induces the differential expression of various transcription factors that, early during development, are informative for post-mitotic neuronal identity (Jessell, 2000). After this early patterning and transcriptional specification, other aspects of neuronal identity are established post-mitotically as cells mature in neural circuits (Shirasaki and Pfaff, 2002). Indeed, neural migration, axonal morphology, soma placement, and neurotransmitter identity are frequently specified after neurons exit the cell cycle (Cheng et al., 2004).

This same sequential specification of early neuronal progenitors and post-mitotic, mature neuronal classes also happens among the cohort of MGE derived neurons (Fragkouli et al., 2009). MGE progenitors are specified as Nkx2-1+ progenitors, apart from neighboring LGE and CGE progenitor domains, because of a Shh morphogen gradient from the ventral portion of the developing telencephalon (Wilson and Rubenstein, 2000). After the MGE progenitor domain is specified by Shh and downstream induced Nkx2-1 expression, the post-mitotic specification of its various different lineages happens because of the differential control of transcription factor expression (Kepecs and Fishell, 2014; Hu et al., 2017; Marin, 2013). For example, as migrating interneurons leave the MGE and encounter the striatum, they can either repress Nkx2-1 and continue migrating to the cortex via chemo-repulsive guidance cue receptor expression or retain Nkx2-1 expression and migrate into the striatum (Nobrega Pereira et al., 2008). As MGE lineage interneurons enter the striatum, they are further specified as either GABAergic or cholinergic based on the combinatorial expression Lhx6, Lhx8, ane Isl1 (Fragkouli et al., 2009). Indeed, post-mitotic expression of Lhx6 is involved in GABAergic differentiation while post-mitotic

expression of Lhx8 and Isl1 is involved in cholinergic differentiation (Fragkouli et al., 2009).

The specification of MGE lineage GPe neurons presumably undergoes a similar process of transcriptional specification, with post-mitotic transcription factor expression leading to mature neuronal differentiation. Recall that I have shown that St18 loss of function leads to a significant reduction in GPe PV+ neurons. This suggests that St18 is a transcription factor responsible for specification of this neuronal population downstream of Nkx2-1 expression. One of the remaining questions regarding this phenotype is why there is no apparent early loss of GPe neurons in the embryonic stages of development in St18 (-/-) embryos. Recall that, despite the adult GPe being impoverished with fewer MGE lineage PV+ neurons, the embryonic GPe is unaffected by St18 loss of function. One potential explanation for this is that St18 acts in GPe neuronal lineages as Lhx6, Lhx8, and Isl1 do in striatal lineages (Fragkouli et al., 2009). Specifically, St18 could be specifying GPe neurons post-mitotically, effectively working to mature developing GPe neurons instead of specifying them early during mitotic progenitor development. I have some evidence to support this hypothesis. Recall, from my single cell RNA sequencing analysis of St18 (-/-) MGE, that St18 loss of function significantly effected the proportions of neuronal clusters but not progenitor clusters. This bolsters the claim that St18 expression in MGE progenitors leads to an effect in post-mitotic MGE neurons and not in progenitor cells, leading to the proper migration and maturation of PV+ GPe neurons.

Discussion.12 St18 specifies a non-interneuron PV+ lineage in the MGE

Recall that I have shown that St18 gain of function *in vitro* programs MGE lineage progenitors as projection neurons, an exception to a lineage that produces mostly locally projecting interneurons. I have also shown that St18 loss of function *in vitro* leads to the loss of a specific neuronal cohort in the GPe, determined histologically, as well as the loss of a specific cluster of post-mitotic neurons within the MGE lineage, determined by single cell RNA sequencing (scRNAseq). Further, I note that the specificity of the scRNAseq phenotype mirrors the specific loss of GPe prototypic neurons in St18 loss of function animals; I note the loss of cluster 4 neurons and the loss of GPe PV+ neurons. Along this line, it is appealing to speculate that the

identity of neuron cluster 4, which is strongly diminished in St18 (-/-) MGE, are nascent GPe prototypic neurons during development.

In support of this idea, I find that that cluster 4 neurons are enriched in expression for Nkx2-1. Recall that Nkx2-1 expression is essential for subcortical migration of migrating MGE neurons post-mitotically, with sustained expression being essential for the migration of MGE lineage GABAergic and cholinergic interneurons into the striatum (Nobrega Pereira et al., 2008). Futhermore, Nkx2-1 expression is maintained in a vast majority of MGE lineage projection neurons in the GPe (Nobrega Pereira et al., 2010; Flandin et al., 2010; Abdi et al., 2015; Hernandez et al., 2015; Abecassis et al., 2020). I also detected higher levels of Rnd2 in cluster 4 neurons. Rnd2 expression is stimulated in newborn excitatory neurons in the cortex, stimulating radial migration and the formation of cortical layers throughout development (Heng et al., 2008; Heng et al., 2015; Gladwyn-Ng et al., 2015). Given the close proximity of the MGE progenitor domain to the final location of the GPe, it is likely that immature GPe neurons migrate via radial versus tangential migration, making Rnd2 expression an intriguing marker for cluster 4.

In contrast, neurons clusters 2 and 5, which are both expanded following St18 loss of function, exhibit gene expression profiles which resemble MGE lineage PV+ interneurons. For example, both clusters 2 and 5 exhibit higher levels of APC expression. APC is involved in modulating microtubule severing in MGE derived interneurons, facilitating long-range tangential migration (Eom et al., 2015). Beyond this, I find numerous other genes in clusters 2 and 5 that further demonstrate that these cells are putative nascent PV+ cortical interneurons. Clusters 2 and 5 express high levels of Mef2C, a gene that is upregulated downstream of Maf and Mafb specification of PV+ cortical interneurons (Pai et al., 2020). Ccdn2 is also upregulated in clusters 2 and 5. Ccdn2 promotes MGE SVZ amplification of neural progenitors to ensure for sufficient PV+ interneuron development late in MGE neurogenesis (Glickstein et al., 2007). Together, I find by scRNAseq that in St18 (-/-) MGE, I find selective alterations in three PV+ neuronal populations. I see a decrease in cluster 4 neurons, which represent putative nascent GPe neurons. Conversely, I see an expansion of the proportions of neuron clusters 2 and 5, which represent pu-

tative PV+ interneurons. I therefore hypothesize these 3 PV+ populations share a common lineal origin within the MGE that is demarcated by the presence or absence of St18 expression, which specifies PV+ GPe projection neurons as opposed to PV+ interneurons. To test this hypothesis, it would be necessary to further examine the diagnostic markers identified in these clusters as either necessary or sufficient to specify either MGE lineage PV+ interneurons or projection neurons.

Discussion.13 MGE lineage identity is unchanged in St18 loss of function

There is mounting evidence that the cardinal neuronal cell types in the MGE lineage are established early during development as progenitor cells begin to express cell-type specific cohorts of transcription factors and other genes (Mayer et al., 2018; Mi et al., 2018). Two recent studies examined the dynamics of this process during MGE neurogenesis by scRNAseq (Mayer et al., 2018; Mi et al., 2018). One study shows that MGE neuronal progenitors share similar gene expression profiles as they pass through similar cell states during mitosis and early neuronal differentiation (Mayer et al., 2018). The other study shows how, from this early stage of common lineal differentiation, MGE progenitors then rapidly diversify as they transition out of the cell cycle (Mi et al., 2018). Indeed, St18 was identified as a diagnostic marker gene for an MGE progenitor pool during this process of diversification within the MGE neuronal lineage (Mi et al., 2018). However, shortly after MGE neurons are specified, they migrate extensively throughout the brain, making it a difficult task to link developmental gene expression with mature neuronal identity. Therefore, the neuronal identity of clusters that express St18 in these datasets remain uncharacterized.

Recall that, in my single cell RNA sequencing analysis of St18 loss of function MGE, I identify one cluster, cluster 4, that is diminished while clusters 2 and 5 are increased. Further, recall that this shift in the neuronal output of the MGE is not matched by a preceding shift in the progenitor cell identities of MGE clusters. Therefore, I have concluded that St18 loss of function causes a shift in a specific subset of MGE lineage neuronal output that precedes transcriptionally the cellular phenotype I have observed. Indeed, I have also hypothesized that the cluster that is

diminished, cluster 4, in St18 loss of function represents putative nascent GPe projection neurons, the cohort of cells lost in St18 loss of function animals. St18, then, is the first identified transcription factor that appears to direct general MGE lineages to adopt GPe fates. Of note, when the identities of the neuronal and progenitor clusters I've identified in this study are compared between WT and St18 (-/-) conditions, there is no change in the identities of these clusters caused by St18 loss of function. The only change I've noted is in the relative proportions of these otherwise stable cluster identities. This is likely because, as I've discussed earlier, St18 specifies a subset of MGE lineage PV+ GPe neurons, meaning that St18 expression in progenitors already specified as nascent subcortical PV+ cells are then further specified during the progenitor stage into a specialized St18+ population of GPe neurons. In order to better determine the identities of the neuronal clusters identified in my sequencing analysis, I would perform diagnostic correlation analysis to compare the clusters I've identified with the clusters identified in other studies (Mi et al., 2018). This could help determine to what extent I have recapitulated the clusters identified in this other study as well as determine how stable MGE lineage identity is at the embryonic stage.

Discussion.14 Movement is controlled by many circuits outside the basal ganglia

Locomotor gait is an essential behavior for nearly all other behaviors necessary for animal survival. It stands to reason, then, that the neural circuits responsible for controlling this fundamental behavior are rigorously established during development. I have shown that one of the components of motor control circuitry, the GPe, is required for the maintenance of locomotor gait following a loss of approximately 40% of the GPe PV+ prototypic neurons that project onto the STN. This is interesting because, having produced this phenotype by embryonic loss of function of St18, this is one of the first manipulations of GPe neurons during development that produces a significant locomotor phenotype.

The production of rhythmic, locomotor movement, like ambulatory gait, is mediated by coupled communication between neuronal populations in the brain and the spinal cord (Lemon, 2008; Lanciego et al., 2012; Kiehn, 2016). In the spinal cord, central pattern generators, circuits

of motoneurons and variously connected interneurons, control the rhythmicity of locomotion (Bellardita and Keihn, 2015). These central pattern generators in the spinal cord that control the muscle activity during locomotion receive essential top-down inputs from the brain, all of which are responsible for integrating and controlling rhythmic locomotor movements in the context of behavior (Drew and Marigold, 2015; Takakusaki, 2013). Indeed, the descending inputs to spinal cord central pattern generators in the cortex, basal ganglia, and cerebellum are simultaneously extensively studied and poorly understood; relatively little is known about what these structures contribute to locomotor gait beyond anatomy (Economo et al., 2018).

Current evidence suggests that motoneurons in the spinal cord are coordinated by descending inputs from the cortex and basal ganglia during locomotion (MacKay-Lyons, 2002). Dysfunction in specific components of this top-down motor production circuity, like the basal ganglia, can result in a range of pathologies involving gross motor impairment, including Parkinson's and Huntington's diseases (Kravitz et al., 2010; Bateup et al., 2010; McConnell et al., 2016). One of the crucial components of the descending inputs to the spinal cord is the GPe, which is responsible for modulating inhibition of directed and motor behaviors (Kravitz et al., 2010). The GPe's prototypic projection to the STN specifically is a crucial part of the motor control circuitry (Freeze et al., 2013; Neumann et al., 2018). This is known because, in Parkinson's disease, the GPe to STN prototypic projection produces an unusual, synchronized firing pattern caused by the loss of dopaminergic input to the striatum that is thought to contribute to the gross locomotor phenotypes observed in the disease pathology (Holgado et al., 2010; Sani et al., 2009). Indeed, the GPe to STN prototypic projection is an emerging therapeutic target patients with Parkinson's disease, suggesting that this connection in the motor control circuitry plays a significant role in both healthy and diseased locomotion (Kumar et al., 2000).

I have shown that St18 loss of function produces a loss of GPe PV+ prototypic neurons that tracks with a loss of innervation onto the STN. Given that the GPe prototypic projection to the STN has a well established role in healthy and pathological locomotor movement, one salient question that needs to be addressed is why there is not gross locomotor phenotype in St18 con-

ditional loss of function animals. Recall that I show no gross developmental or gross locomotor phenotype associated with St18 loss of function. I do show, however, a loss of fine gait coordination characterized by sporadic pausing in mouse walk cycles. One explanation for why there is no gross locomotor deficit despite the critical role that this circuit plays in regulating movement is that the St18 loss of function manipulation is relatively minor compared to typical scenarios where this circuit is observed. In fact, to my knowledge, this study represents the first manipulation that only partially reduces prototypic projections onto the STN. This means that it is likely that my behavioral findings fit well into the existing schema of the role of the prototypic projection from the GPe to the STN. I believe that, if St18 loss of function were recapitulated in a background of a Parkinson's disease model, the loss of gait coordination phenotype would be more severe. This is because, in a background of pathological loss of dopaminergic input to the basal ganglia, there would be less ability for the circuit to homeostatically compensate for the partial loss of GPe PV+ prototypic neurons seen in St18 loss of function. Recall that, when I observe arkypallidal projections to the striatum in virally labeled GPe of St18 loss of function animals I observe an increase in arkypallidal innervation. This suggests that the circuit is homeostatically adjusting to the loss of prototypic neurons in the GPe.

Discussion.15 Prototypic neurons' role in freezing of gait

One of the most devastating symptoms of Parkinson's disease (PD) is the occurrence of freezing of gait (FOG), a symptom that produces a majority of the clinical admissions in PD patients. (Anidi et al., 2018). FOG is characterized by sporadic stalling of locomotor gait, oftentimes producing sudden falls in PD patients. One of the salient features of FOG is that it is dopamine independent, meaning that patients experiencing FOG symptoms do so even after dopamine replacement therapies that are the current standard of care for PD patients (Anidi et al., 2018). This means that one of the pertinent and pressing questions facing neurologists and the neuroscientific field at large is what is the physiological source of FOG symptoms.

One of the primary causes for motor-related behavioral deficits in PD patients is the prevalence of dysregulated neuronal activity between the basal ganglia's various nuclei, all of which

are downstream of the primary locus of neuro-degradation in the substantia nigra pars compacta in PD pathology (Wang et al., 2018). In particular, the synaptic connection between the GPe and the STN is a particularly interesting locus not just in PD pathology, but also as a potential therapeutic target in PD (Pina-Fuentes et al., 2019; Wang et al., 2018). This is because, in human PD patients being measured by local field potential (LFP) while being treated with experimental deep brain stimulation (DBS) paradigms (Pina-Fuentes et al., 2019; Wang et al., 2018), an increase in beta-oscillations is detected in both the STN and GPe (Pina-Fuentes et al., 2019; Wang et al., 2018). These increases in beta-oscillations are correlated with an overall decrease in high frequency synchrony between the GPe and STN, thereby being causally linked with the pathology of PD movement symptoms (Pina-Fuentes et al., 2019; Wang et al., 2018). This makes these brain regions in particular a potential therapeutic target to reverse PD pathology. Indeed, in both the STN and the GPe, an increase in high frequency synchronous firing induced by DBS recuses both the beta-oscillations believed to cause PD movement related symptoms as well as the symptoms themselves (Pina-Fuentes et al., 2019; Wang et al., 2018).

This feature of PD pathology, specifically that there is an increase in beta-oscillations that is correlated with PD motor symptoms is also true in the case of FOG symptoms (Anidi et al., 2018). Indeed, in patients with FOG, and increase in beta-oscillation power in the STN was temporally correlated with gait freezing epochs during locomotion (Anidi et al., 2018). Furthermore, when high frequency synchronous stimulation was applied to the STN, the FOG symptoms were rescued (Anidi et al., 2018). This implicates the GPe to STN circuit in the regulation of locomotor gait, and it further implicates this circuit in locomotor gait that is sporadically interrupted in dysfunctional circumstances.

Recall, now, that I have shown that, upon St18 loss of function induced loss of GPe PV+ prototypic projection neurons onto the STN and a correlated loss of STN prototypic innervation, St18 loss of function animals exhibit sporadic gait stalling episodes. This phenotype is remarkably similar to human FOG patients, as mice locomote normally except for during these gait freezing episodes. This leads me to hypothesize that the PV+ GPe prototypic projection onto the

STN is a circuit component that is critical for the maintenance of locomotor walk cycles. One question that remains to be answered is what electrophysiological signature does the loss of PV+ GPe neurons have on St18 loss of function animals. To test this, I would perform LFP recordings in St18 loss of function GPe and STN during locomotor behavior. This would allow me to see if a similar change in beta-oscillations in prototypic projections is linked to freezing behavior as is seen in human patients. This would show, in a dopamine in-tact animal, the physiological role of prototypic GPe neurons in locomotion, a finding that would be significant because most of what has been learned about these neurons in behavior is in PD patients and manipulations modelling PD.

Conclusions

St18 is, to my knowledge, the first transcription factor expressed in the MGE that specifies projection neurons both *in vtiro* and *in vivo*. St18 expression in MGE lineage neural progenitors is sufficient to produce MGE lineage projection neurons, as judged by neuron migration and morphology. St18 expression in MGE lineage progenitors is also necessary for the development of a proportion of MGE lineage GPe PV+ prototypic neurons. These neurons specified by St18 during development are also necessary for the maintenance of locomotor gait, as the loss of this population of GPe PV+ neurons causes mice to sporadically freeze during walk cycles. The identification of the embryonic transcriptional antecedent to a specific neuronal population such as this provides ample opportunity to study in greater detail how, transcriptionally, cell fate decisions are made during the diversification of a particular neuronal lineage. Using the single cell RNA sequencing data from St18 loss of function animals, it will be possible to learn more about the specification of the projection neuron lineages of the MGE along with the transcriptional role of St18 in this fundamental fate choice. Furthermore, it is my belief that the identification of the early antecedents of neuronal diversity can prove useful in identifying neuronal populations susceptible to disease pathology while also highlighting new therapeutic targets.

In conclusion, St18's role in specifying PV+ GPe projection neurons within the MGE is one piece of a larger tapestry of neuronal diversity that is yet to be completed. I believe it is essential that neuroscience as a field not forget that the study of the brain must first begin with the study of its constitutive parts, its diverse set of neurons.

References

Abdi, A., Mallet, N., Mohamed, F. Y., Sharott, A., Dodson, P. D., Nakamura, K. C., . . . Magill, P. J. (2015). Prototypic and arkypallidal neurons in the dopamine-intact external globus pallidus. J Neurosci, 35(17), 6667-6688. doi:10.1523/JNEUROSCI.4662-14.2015

Abecassis, Z. A., Berceau, B. L., Win, P. H., Garcia, D., Xenias, H. S., Cui, Q., . . . Chan, C. S. (2020). Npas1(+)-Nkx2.1(+) Neurons Are an Integral Part of the Cortico-pallido-cortical Loop. J Neurosci, 40(4), 743-768. doi:10.1523/JNEUROSCI.1199-19.2019

Alaynick, W. A., Jessell, T. M., & Pfaff, S. L. (2011). SnapShot: spinal cord development. *Cell, 146*(1), 178-178 e171. doi:10.1016/j.cell.2011.06.038

Alcamo, E. A., Chirivella, L., Dautzenberg, M., Dobreva, G., Farinas, I., Grosschedl, R., & McConnell, S. K. (2008). Satb2 regulates callosal projection neuron identity in the developing cerebral cortex. *Neuron, 57*(3), 364-377. doi:10.1016/j.neuron.2007.12.012

Al-Khalaf, H. H., & Aboussekhra, A. (2013). p16(INK4A) positively regulates p21(WAF1) expression by suppressing AUF1-dependent mRNA decay. PLoS One, 8(7), e70133. doi:10.1371/journal.pone.0070133

Ambrozkiewicz, M. C., Schwark, M., Kishimoto-Suga, M., Borisova, E., Hori, K., Salazar-Lazaro, A., . . . Kawabe, H. (2018). Polarity Acquisition in Cortical Neurons Is Driven by Synergistic Action of Sox9-Regulated Wwp1 and Wwp2 E3 Ubiquitin Ligases and Intronic miR-140. *Neuron, 100*(5), 1097-1115 e1015. doi:10.1016/j.neuron.2018.10.008

Anderson, S., Mione, M., Yun, K., & Rubenstein, J. L. (1999). Differential origins of neocortical projection and local circuit neurons: role of Dlx genes in neocortical interneuronogenesis. Cereb Cortex, 9(6), 646-654. doi:10.1093/cercor/9.6.646

Anderson, S. A., Eisenstat, D. D., Shi, L., & Rubenstein, J. L. (1997). Interneuron migration from basal forebrain to neocortex: dependence on Dlx genes. Science, 278(5337), 474-476. doi:10.1126/science.278.5337.474

Anidi, C., O'Day, J. J., Anderson, R. W., Afzal, M. F., Syrkin-Nikolau, J., Velisar, A., & Bronte-Stewart, H. M. (2018). Neuromodulation targets pathological not physiological beta bursts during gait in Parkinson's disease. *Neurobiol Dis, 120*, 107-117. doi:10.1016/j.nbd.2018.09.004

Arlotta, P., Molyneaux, B. J., Chen, J., Inoue, J., Kominami, R., & Macklis, J. D. (2005). Neuronal subtype-specific genes that control corticospinal motor neuron development in vivo. *Neuron, 45*(2), 207-221. doi:10.1016/j.neuron.2004.12.036

Au, E., Ahmed, T., Karayannis, T., Biswas, S., Gan, L., & Fishell, G. (2013). A modular gain-of-function approach to generate cortical interneuron subtypes from ES cells. Neuron, 80(5), 1145-1158. doi:10.1016/j.neuron.2013.09.022

Baldwin, H. A., Koivula, P. P., Necarsulmer, J. C., Whitaker, K. W., & Harvey, B. K. (2017). Step Sequence Is a Critical Gait Parameter of Unilateral 6-OHDA Parkinson's Rat Models. *Cell Transplant, 26*(4), 659-667. doi:10.3727/096368916X693059

Bateup, H. S., Santini, E., Shen, W., Birnbaum, S., Valjent, E., Surmeier, D. J., . . . Greengard, P. (2010). Distinct subclasses of medium spiny neurons differentially regulate striatal motor behaviors. *Proc Natl Acad Sci U S A, 107*(33), 14845-14850. doi:10.1073/pnas.1009874107

Batista-Brito, R., Rossignol, E., Hjerling-Leffler, J., Denaxa, M., Wegner, M., Lefebvre, V., . . . Fishell, G. (2009). The cell-intrinsic requirement of Sox6 for cortical interneuron development. *Neuron, 63*(4), 466-481. doi:10.1016/j.neuron.2009.08.005

Batka, R. J., Brown, T. J., McMillan, K. P., Meadows, R. M., Jones, K. J., & Haulcomb, M. M. (2014). The need for speed in rodent locomotion analyses. *Anat Rec (Hoboken), 297*(10), 1839-1864. doi:10.1002/ar.22955

Bao, Z., Xu, X., Liu, Y., Chao, H., Lin, C., Li, Z., . . . Ji, J. (2017). CBX7 negatively regulates migration and invasion in glioma via Wnt/beta-catenin pathway inactivation. Oncotarget, 8(24), 39048-39063. doi:10.18632/oncotarget.16587

Bellardita, C., & Kiehn, O. (2015). Phenotypic characterization of speed-associated gait changes in mice reveals modular organization of locomotor networks. *Curr Biol, 25*(11), 1426-1436. doi:10.1016/j.cub.2015.04.005

Bernard, D., Martinez-Leal, J. F., Rizzo, S., Martinez, D., Hudson, D., Visakorpi, T., . . . Gil, J. (2005). CBX7 controls the growth of normal and tumor-derived prostate cells by repressing the Ink4a/Arf locus. Oncogene, 24(36), 5543-5551. doi:10.1038/sj.onc.1208735

Blanchet, P., Bebin, M., Bruet, S., Cooper, G. M., Thompson, M. L., Duban-Bedu, B., . . . McNeill, A. (2017). MYT1L mutations cause intellectual disability and variable obesity by dysregulating gene expression and development of the neuroendocrine hypothalamus. PLoS Genet, 13(8), e1006957. doi:10.1371/journal.pgen.1006957

Britanova, O., de Juan Romero, C., Cheung, A., Kwan, K. Y., Schwark, M., Gyorgy, A., . . . Tarabykin, V. (2008). Satb2 is a postmitotic determinant for upper-layer neuron specification in the neocortex. *Neuron, 57*(3), 378-392. doi:10.1016/j.neuron.2007.12.028

Bupesh, M., Abellan, A., & Medina, L. (2011). Genetic and experimental evidence supports the continuum of the central extended amygdala and a mutiple embryonic origin of its principal neurons. J Comp Neurol, 519(17), 3507-3531. doi:10.1002/cne.22719

Butt, S. J., Sousa, V. H., Fuccillo, M. V., Hjerling-Leffler, J., Miyoshi, G., Kimura, S., & Fishell, G. (2008). The requirement of Nkx2-1 in the temporal specification of cortical interneuron subtypes. Neuron, 59(5), 722-732. doi:10.1016/j.neuron.2008.07.031

Carney, R. S., Mangin, J. M., Hayes, L., Mansfield, K., Sousa, V. H., Fishell, G., . . . Corbin, J. G. (2010). Sonic hedgehog expressing and responding cells generate neuronal diversity in the medial amygdala. Neural Dev, 5, 14. doi:10.1186/1749-8104-5-14

Carpenter, M. B., Fraser, R. A., & Shriver, J. E. (1968). The organization of pallidosubthalamic fibers in the monkey. Brain Res, 11(3), 522-559. doi:10.1016/0006-8993(68)90145-5

Carter, D. A., & Fibiger, H. C. (1978). The projections of the entopeduncular nucleus and globus pallidus in rat as demonstrated by autoradiography and horseradish peroxidase histochemistry. J Comp Neurol, 177(1), 113-123. doi:10.1002/cne.901770108

Close, J., Xu, H., De Marco Garcia, N., Batista-Brito, R., Rossignol, E., Rudy, B., & Fishell, G. (2012). Satb1 is an activity-modulated transcription factor required for the terminal differentiation and connectivity of medial ganglionic eminence-derived cortical interneurons. J Neurosci, 32(49), 17690-17705. doi:10.1523/JNEUROSCI.3583-12.2012

Cucca, A., Biagioni, M. C., Fleisher, J. E., Agarwal, S., Son, A., Kumar, P., . . . Di Rocco, A. (2016). Freezing of gait in Parkinson's disease: from pathophysiology to emerging therapies. Neurodegener Dis Manag, 6(5), 431-446. doi:10.2217/nmt-2016-0018

del Rio, J. A., de Lecea, L., Ferrer, I., & Soriano, E. (1994). The development of parvalbumin-immunoreactivity in the neocortex of the mouse. *Brain Res Dev Brain Res, 81*(2), 247-259. doi:10.1016/0165-3806(94)90311-5

Desai, A. R., & McConnell, S. K. (2000). Progressive restriction in fate potential by neural progenitors during cerebral cortical development. *Development, 127*(13), 2863-2872.

Dodson, P. D., Larvin, J. T., Duffell, J. M., Garas, F. N., Doig, N. M., Kessaris, N., . . . Magill, P. J. (2015). Distinct developmental origins manifest in the specialized encoding of movement by adult neurons of the external globus pallidus. Neuron, 86(2), 501-513. doi:10.1016/j.neuron.2015.03.007

Drew, T., & Marigold, D. S. (2015). Taking the next step: cortical contributions to the control of locomotion. *Curr Opin Neurobiol, 33*, 25-33. doi:10.1016/j.conb.2015.01.011

Du, T., Xu, Q., Ocbina, P. J., & Anderson, S. A. (2008). NKX2.1 specifies cortical interneuron fate by activating Lhx6. Development, 135(8), 1559-1567. doi:10.1242/dev.015123

Duan, R. S., Tang, G. B., Du, H. Z., Hu, Y. W., Liu, P. P., Xu, Y. J., . . . Liu, C. M. (2018). Polycomb protein family member CBX7 regulates intrinsic axon growth and regeneration. Cell Death Differ, 25(9), 1598-1611. doi:10.1038/s41418-018-0064-0

Dubach, J. M., Kim, E., Yang, K., Cuccarese, M., Giedt, R. J., Meimetis, L. G., . . . Weissleder, R. (2017). Quantitating drug-target engagement in single cells in vitro and in vivo. Nat Chem Biol, 13(2), 168-173. doi:10.1038/nchembio.2248

Economo, M. N., Viswanathan, S., Tasic, B., Bas, E., Winnubst, J., Menon, V., . . . Svoboda, K. (2018). Distinct descending motor cortex pathways and their roles in movement. *Nature, 563*(7729), 79-84. doi:10.1038/s41586-018-0642-9

Eom, T. Y., Stanco, A., Guo, J., Wilkins, G., Deslauriers, D., Yan, J., . . . Anton, E. S. (2014). Differential regulation of microtubule severing by APC underlies distinct patterns of projection neuron and interneuron migration. *Dev Cell, 31*(6), 677-689. doi:10.1016/j.devcel.2014.11.022

Evans, R. C., Twedell, E. L., Zhu, M., Ascencio, J., Zhang, R., & Khaliq, Z. M. (2020). Functional Dissection of Basal Ganglia Inhibitory Inputs onto Substantia Nigra Dopaminergic Neurons. Cell Rep, 32(11), 108156. doi:10.1016/j.celrep.2020.108156

Ferreira, T., Ou, Y., Li, S., Giniger, E., & van Meyel, D. J. (2014). Dendrite architecture organized by transcriptional control of the F-actin nucleator Spire. Development, 141(3), 650-660. doi:10.1242/dev.099655

Filice, F., Vorckel, K. J., Sungur, A. O., Wohr, M., & Schwaller, B. (2016). Reduction in parvalbumin expression not loss of the parvalbumin-expressing GABA interneuron subpopulation in genetic parvalbumin and shank mouse models of autism. *Mol Brain, 9*, 10. doi:10.1186/s13041-016-0192-8

Flames, N., Long, J. E., Garratt, A. N., Fischer, T. M., Gassmann, M., Birchmeier, C., . . . Marin, O. (2004). Short- and long-range attraction of cortical GABAergic interneurons by neuregulin-1. Neuron, 44(2), 251-261. doi:10.1016/j.neuron.2004.09.028

Flandin, P., Kimura, S., & Rubenstein, J. L. (2010). The progenitor zone of the ventral medial ganglionic eminence requires Nkx2-1 to generate most of the globus pallidus but few neocortical interneurons. J Neurosci, 30(8), 2812-2823. doi:10.1523/JNEUROSCI.4228-09.2010

Flandin, P., Zhao, Y., Vogt, D., Jeong, J., Long, J., Potter, G., . . . Rubenstein, J. L. (2011). Lhx6 and Lhx8 coordinately induce neuronal expression of Shh that controls the generation of interneuron progenitors. *Neuron, 70*(5), 939-950. doi:10.1016/j.neuron.2011.04.020

Fogarty, M., Grist, M., Gelman, D., Marin, O., Pachnis, V., & Kessaris, N. (2007). Spatial genetic patterning of the embryonic neuroepithelium generates GABAergic interneuron diversity in the adult cortex. J Neurosci, 27(41), 10935-10946. doi:10.1523/JNEUROSCI.1629-07.2007

Fragkouli, A., van Wijk, N. V., Lopes, R., Kessaris, N., & Pachnis, V. (2009). LIM homeodomain transcription factor-dependent specification of bipotential MGE progenitors into cholinergic and GABAergic striatal interneurons. *Development, 136*(22), 3841-3851. doi:10.1242/dev.038083

Freeze, B. S., Kravitz, A. V., Hammack, N., Berke, J. D., & Kreitzer, A. C. (2013). Control of basal ganglia output by direct and indirect pathway projection neurons. J Neurosci, 33(47), 18531-18539. doi:10.1523/JNEUROSCI.1278-13.2013

Friedel, P., Kahle, K. T., Zhang, J., Hertz, N., Pisella, L. I., Buhler, E., . . . Medina, I. (2015). WNK1-regulated inhibitory phosphorylation of the KCC2 cotransporter maintains the depolarizing action of GABA in immature neurons. *Sci Signal, 8*(383), ra65. doi:10.1126/scisignal.aaa0354

Gladwyn-Ng, I. E., Li, S. S., Qu, Z., Davis, J. M., Ngo, L., Haas, M., . . . Heng, J. I. (2015). Bacurd2 is a novel interacting partner to Rnd2 which controls radial migration within the developing mammalian cerebral cortex. *Neural Dev, 10*, 9. doi:10.1186/s13064-015-0032-z

Glickstein, S. B., Moore, H., Slowinska, B., Racchumi, J., Suh, M., Chuhma, N., & Ross, M. E. (2007). Selective cortical interneuron and GABA deficits in cyclin D2-null mice. *Development, 134*(22), 4083-4093. doi:10.1242/dev.008524

He, M., Tucciarone, J., Lee, S., Nigro, M. J., Kim, Y., Levine, J. M., . . . Huang, Z. J. (2016). Strategies and Tools for Combinatorial Targeting of GABAergic Neurons in Mouse Cerebral Cortex. *Neuron, 92*(2), 555. doi:10.1016/j.neuron.2016.10.009

Hegeman, D. J., Hong, E. S., Hernandez, V. M., & Chan, C. S. (2016). The external globus pallidus: progress and perspectives. *Eur J Neurosci, 43*(10), 1239-1265. doi:10.1111/ejn.13196

Heng, J. I., Nguyen, L., Castro, D. S., Zimmer, C., Wildner, H., Armant, O., . . . Guillemot, F. (2008). Neurogenin 2 controls cortical neuron migration through regulation of Rnd2. *Nature, 455*(7209), 114-118. doi:10.1038/nature07198

Heng, J. I., Qu, Z., Ohtaka-Maruyama, C., Okado, H., Kasai, M., Castro, D., . . . Tan, S. S. (2015). The zinc finger transcription factor RP58 negatively regulates Rnd2 for the control of neuronal migration during cerebral cortical development. *Cereb Cortex, 25*(3), 806-816. doi:10.1093/cercor/bht277

Henry, C., Close, A. F., & Buteau, J. (2014). A critical role for the neural zinc factor ST18 in pancreatic beta-cell apoptosis. J Biol Chem, 289(12), 8413-8419. doi:10.1074/jbc.M114.554915

Hermanowicz-Sobieraj, B., & Robak, A. (2017). The ontogenetic development of neurons containing calcium-binding proteins in the septum of the guinea pig: Late onset of parvalbumin immunoreactivity versus calbindin and calretinin. *J Chem Neuroanat, 79*, 22-31. doi:10.1016/j.jchemneu.2016.10.001

Hernandez, V. M., Hegeman, D. J., Cui, Q., Kelver, D. A., Fiske, M. P., Glajch, K. E., . . . Chan, C. S. (2015). Parvalbumin+ Neurons and Npas1+ Neurons Are Distinct Neuron Classes in the Mouse External Globus Pallidus. J Neurosci, 35(34), 11830-11847. doi:10.1523/JNEUROSCI.4672-14.2015

Hetze, S., Romer, C., Teufelhart, C., Meisel, A., & Engel, O. (2012). Gait analysis as a method for assessing neurological outcome in a mouse model of stroke. *J Neurosci Methods, 206*(1), 7-14. doi:10.1016/j.jneumeth.2012.02.001

Hibi, M., & Shimizu, T. (2012). Development of the cerebellum and cerebellar neural circuits. *Dev Neurobiol, 72*(3), 282-301. doi:10.1002/dneu.20875

Hobert, O., & Kratsios, P. (2019). Neuronal identity control by terminal selectors in worms, flies, and chordates. Curr Opin Neurobiol, 56, 97-105. doi:10.1016/j.conb.2018.12.006

Hoch, R. V., Lindtner, S., Price, J. D., & Rubenstein, J. L. (2015). OTX2 Transcription Factor Controls Regional Patterning within the Medial Ganglionic Eminence and Regional Identity of the Septum. *Cell Rep, 12*(3), 482-494. doi:10.1016/j.celrep.2015.06.043

Holgado, A. J., Terry, J. R., & Bogacz, R. (2010). Conditions for the generation of beta oscillations in the subthalamic nucleus-globus pallidus network. J Neurosci, 30(37), 12340-12352. doi:10.1523/JNEUROSCI.0817-10.2010

Hoshino, M. (2006). Molecular machinery governing GABAergic neuron specification in the cerebellum. *Cerebellum, 5*(3), 193-198. doi:10.1080/14734220600589202

Hoshino, M., Nakamura, S., Mori, K., Kawauchi, T., Terao, M., Nishimura, Y. V., . . . Nabeshima, Y. (2005). Ptf1a, a bHLH transcriptional gene, defines GABAergic neuronal fates in cerebellum. *Neuron, 47*(2), 201-213. doi:10.1016/j.neuron.2005.06.007

Hu, J. S., Vogt, D., Lindtner, S., Sandberg, M., Silberberg, S. N., & Rubenstein, J. L. R. (2017). Coup-TF1 and Coup-TF2 control subtype and laminar identity of MGE-derived neocortical interneurons. *Development, 144*(15), 2837-2851. doi:10.1242/dev.150664 (1)

Hu, J. S., Vogt, D., Sandberg, M., & Rubenstein, J. L. (2017). Cortical interneuron development: a tale of time and space. Development, 144(21), 3867-3878. doi:10.1242/dev.132852

Hu, R., Walker, E., Huang, C., Xu, Y., Weng, C., Erickson, G. E., . . . Gu, G. (2020). Myt Transcription Factors Prevent Stress-Response Gene Overactivation to Enable Postnatal Pancreatic beta Cell Proliferation, Function, and Survival. Dev Cell, 53(6), 754. doi:10.1016/j.devcel.2020.06.007

Huang, C., Walker, E. M., Dadi, P. K., Hu, R., Xu, Y., Zhang, W., . . . Gu, G. (2018). Synaptotagmin 4 Regulates Pancreatic beta Cell Maturation by Modulating the Ca(2+) Sensitivity of Insulin Secretion Vesicles. Dev Cell, 45(3), 347-361 e345. doi:10.1016/j.devcel.2018.03.013

Inan, M., Welagen, J., & Anderson, S. A. (2012). Spatial and temporal bias in the mitotic origins of somatostatin- and parvalbumin-expressing interneuron subgroups and the chandelier subtype in the medial ganglionic eminence. Cereb Cortex, 22(4), 820-827. doi:10.1093/cercor/bhr148

Jaglin, X. H., Hjerling-Leffler, J., Fishell, G., & Batista-Brito, R. (2012). The origin of neocortical nitric oxide synthase-expressing inhibitory neurons. *Front Neural Circuits, 6*, 44. doi:10.3389/fncir.2012.00044

Jandrig, B., Seitz, S., Hinzmann, B., Arnold, W., Micheel, B., Koelble, K., . . . Rosenthal, A. (2004). ST18 is a breast cancer tumor suppressor gene at human chromosome 8q11.2. Oncogene, 23(57), 9295-9302. doi:10.1038/sj.onc.1208131

Jaudon, F., Raynaud, F., Wehrle, R., Bellanger, J. M., Doulazmi, M., Vodjdani, G., . . . Schmidt, S. (2015). The RhoGEF DOCK10 is essential for dendritic spine morphogenesis. *Mol Biol Cell, 26*(11), 2112-2127. doi:10.1091/mbc.E14-08-1310

Jessell, T. M. (2000). Neuronal specification in the spinal cord: inductive signals and transcriptional codes. *Nat Rev Genet, 1*(1), 20-29. doi:10.1038/35049541

Jiang, Y., Bai, X., Li, T. T., Al-Hawwas, M., Jin, Y., Zou, Y., . . . Xiong, L. L. (2020). COX5A over-expression protects cortical neurons from hypoxic ischemic injury in neonatal rats associated with TPI up-regulation. *BMC Neurosci, 21*(1), 18. doi:10.1186/s12868-020-00565-5

Joel, D., & Weiner, I. (1997). The connections of the primate subthalamic nucleus: indirect pathways and the open-interconnected scheme of basal ganglia-thalamocortical circuitry. Brain Res Brain Res Rev, 23(1-2), 62-78. doi:10.1016/s0165-0173(96)00018-5

Joyner, A.L (2000). Gene targeting: a practical approach, 2nd edn (Oxford ; New York: Oxford University Press).

Kameyama, T., Matsushita, F., Kadokawa, Y., & Marunouchi, T. (2011). Myt/NZF family transcription factors regulate neuronal differentiation of P19 cells. Neurosci Lett, 497(2), 74-79. doi:10.1016/j.neulet.2011.04.033

Kang, D. S., Yang, Y. R., Lee, C., Park, B., Park, K. I., Seo, J. K., . . . Suh, P. G. (2018). Netrin-1/DCC-mediated PLCgamma1 activation is required for axon guidance and brain structure development. *EMBO Rep, 19*(11). doi:10.15252/embr.201846250

Keniry, M., & Parsons, R. (2008). The role of PTEN signaling perturbations in cancer and in targeted therapy. *Oncogene, 27*(41), 5477-5485. doi:10.1038/onc.2008.248

Kennedy, L. M., & Grishok, A. (2014). Neuronal migration is regulated by endogenous RNAi and chromatin-binding factor ZFP-1/AF10 in Caenorhabditis elegans. *Genetics, 197*(1), 207-220. doi:10.1534/genetics.114.162917

Kepa, A., Martinez Medina, L., Erk, S., Srivastava, D. P., Fernandes, A., Toro, R., . . . Desrivieres, S. (2017). Associations of the Intellectual Disability Gene MYT1L with Helix-Loop-Helix Gene Expression, Hippocampus Volume and Hippocampus Activation During Memory Retrieval. Neuropsychopharmacology, 42(13), 2516-2526. doi:10.1038/npp.2017.91

Kepecs, A., & Fishell, G. (2014). Interneuron cell types are fit to function. Nature, 505(7483), 318-326. doi:10.1038/nature12983

Keshavarzi, S., Sullivan, R. K., Ianno, D. J., & Sah, P. (2014). Functional properties and projections of neurons in the medial amygdala. J Neurosci, 34(26), 8699-8715. doi:10.1523/JNEUROSCI.1176-14.2014

Kiehn, O. (2016). Decoding the organization of spinal circuits that control locomotion. *Nat Rev Neurosci, 17*(4), 224-238. doi:10.1038/nrn.2016.9

Kim, J. G., & Hudson, L. D. (1992). Novel member of the zinc finger superfamily: A C2-HC finger that recognizes a glia-specific gene. Mol Cell Biol, 12(12), 5632-5639. doi:10.1128/mcb.12.12.5632-5639.1992

Kohwi, M., & Doe, C. Q. (2013). Temporal fate specification and neural progenitor competence during development. Nat Rev Neurosci, 14(12), 823-838. doi:10.1038/nrn3618

Kravitz, A. V., Freeze, B. S., Parker, P. R., Kay, K., Thwin, M. T., Deisseroth, K., & Kreitzer, A. C. (2010). Regulation of parkinsonian motor behaviours by optogenetic control of basal ganglia circuitry. *Nature, 466*(7306), 622-626. doi:10.1038/nature09159

Kroepfl, T., Petek, E., Schwarzbraun, T., Kroisel, P. M., & Plecko, B. (2008). Mental retardation in a girl with a subtelomeric deletion on chromosome 20q and complete deletion of the myelin transcription factor 1 gene (MYT1). Clin Genet, 73(5), 492-495. doi:10.1111/j.1399-0004.2008.00982.x

Kumar, R., Lang, A. E., Rodriguez-Oroz, M. C., Lozano, A. M., Limousin, P., Pollak, P., . . . Obeso, J. A. (2000). Deep brain stimulation of the globus pallidus pars interna in advanced Parkinson's disease. *Neurology, 55*(12 Suppl 6), S34-39.

Lai, T., Jabaudon, D., Molyneaux, B. J., Azim, E., Arlotta, P., Menezes, J. R., & Macklis, J. D. (2008). SOX5 controls the sequential generation of distinct corticofugal neuron subtypes. *Neuron, 57*(2), 232-247. doi:10.1016/j.neuron.2007.12.023

Lam, B. Y., & Chawla, S. (2007). MEF2D expression increases during neuronal differentiation of neural progenitor cells and correlates with neurite length. *Neurosci Lett, 427*(3), 153-158. doi:10.1016/j.neulet.2007.09.030

Lanciego, J. L., Luquin, N., & Obeso, J. A. (2012). Functional neuroanatomy of the basal ganglia. *Cold Spring Harb Perspect Med, 2*(12), a009621. doi:10.1101/cshperspect.a009621

Lanuza, G. M., Gosgnach, S., Pierani, A., Jessell, T. M., & Goulding, M. (2004). Genetic identification of spinal interneurons that coordinate left-right locomotor activity necessary for walking movements. *Neuron, 42*(3), 375-386. doi:10.1016/s0896-6273(04)00249-1

Le, T. N., Zhou, Q. P., Cobos, I., Zhang, S., Zagozewski, J., Japoni, S., . . . Eisenstat, D. D. (2017). GABAergic Interneuron Differentiation in the Basal Forebrain Is Mediated through Direct Regulation of Glutamic Acid Decarboxylase Isoforms by Dlx Homeobox Transcription Factors. J Neurosci, 37(36), 8816-8829. doi:10.1523/JNEUROSCI.2125-16.2017

Lemon, R. N. (2008). Descending pathways in motor control. *Annu Rev Neurosci, 31*, 195-218. doi:10.1146/annurev.neuro.31.060407.125547

Leone, D. P., Srinivasan, K., Chen, B., Alcamo, E., & McConnell, S. K. (2008). The determination of projection neuron identity in the developing cerebral cortex. *Curr Opin Neurobiol, 18*(1), 28-35. doi:10.1016/j.conb.2008.05.006

Li, G., Warden, C., Zou, Z., Neman, J., Krueger, J. S., Jain, A., . . . Chen, M. (2013). Altered expression of polycomb group genes in glioblastoma multiforme. PLoS One, 8(11), e80970. doi:10.1371/journal.pone.0080970

Lim, L., Mi, D., Llorca, A., & Marin, O. (2018). Development and Functional Diversification of Cortical Interneurons. Neuron, 100(2), 294-313. doi:10.1016/j.neuron.2018.10.009

Lim, L., Pakan, J. M. P., Selten, M. M., Marques-Smith, A., Llorca, A., Bae, S. E., . . . Marin, O. (2018). Optimization of interneuron function by direct coupling of cell migration and axonal targeting. *Nat Neurosci, 21*(7), 920-931. doi:10.1038/s41593-018-0162-9 (1)

Lin, S., Liu, M., Mozgova, O. I., Yu, W., & Baas, P. W. (2012). Mitotic motors coregulate microtubule patterns in axons and dendrites. *J Neurosci, 32*(40), 14033-14049. doi:10.1523/JNEUROSCI.3070-12.2012

Lischinsky, J. E., Sokolowski, K., Li, P., Esumi, S., Kamal, Y., Goodrich, M., . . . Corbin, J. G. (2017). Embryonic transcription factor expression in mice predicts medial amygdala neuronal identity and sex-specific responses to innate behavioral cues. Elife, 6. doi:10.7554/eLife.21012

Loid, P., Makitie, R., Costantini, A., Viljakainen, H., Pekkinen, M., & Makitie, O. (2018). A novel MYT1L mutation in a patient with severe early-onset obesity and intellectual disability. Am J Med Genet A, 176(9), 1972-1975. doi:10.1002/ajmg.a.40370

Longair, M. H., Baker, D. A., & Armstrong, J. D. (2011). Simple Neurite Tracer: open source software for reconstruction, visualization and analysis of neuronal processes. Bioinformatics, 27(17), 2453-2454. doi:10.1093/bioinformatics/btr390

Lu, D. C., Niu, T., & Alaynick, W. A. (2015). Molecular and cellular development of spinal cord locomotor circuitry. *Front Mol Neurosci, 8*, 25. doi:10.3389/fnmol.2015.00025

Lu, Y. C., Nazarko, O. V., Sando, R., 3rd, Salzman, G. S., Li, N. S., Sudhof, T. C., & Arac, D. (2015). Structural Basis of Latrophilin-FLRT-UNC5 Interaction in Cell Adhesion. *Structure, 23*(9), 1678-1691. doi:10.1016/j.str.2015.06.024

Luigetti, M., Sauchelli, D., Primiano, G., Cuccagna, C., Bernardo, D., Lo Monaco, M., & Servidei, S. (2016). Mitochondrial neuropathy: considerations on pathogenesis. Eur J Neurol, 23(8), e55. doi:10.1111/ene.13049

Lundgren, S. E., Callahan, C. A., Thor, S., & Thomas, J. B. (1995). Control of neuronal pathway selection by the Drosophila LIM homeodomain gene apterous. Development, 121(6), 1769-1773.

MacKay-Lyons, M. (2002). Central pattern generation of locomotion: a review of the evidence. *Phys Ther, 82*(1), 69-83. doi:10.1093/ptj/82.1.69

Macosko, Evan Z., Basu, A., Satija, R., Nemesh, J., Shekhar, K., Goldman, M., Tirosh, I., Bialas, Allison R., Kamitaki, N., Martersteck, Emily M., et al. (2015). Highly Parallel Genome-wide Expression Profiling of Individual Cells Using Nanoliter Droplets. Cell 161, 1202-1214.

Malik, R., Pai, E. L., Rubin, A. N., Stafford, A. M., Angara, K., Minasi, P., . . . Vogt, D. (2019). Tsc1 represses parvalbumin expression and fast-spiking properties in somatostatin lineage cortical interneurons. Nat Commun, 10(1), 4994. doi:10.1038/s41467-019-12962-4

Mall, M., Kareta, M. S., Chanda, S., Ahlenius, H., Perotti, N., Zhou, B., . . . Wernig, M. (2017). Myt1l safeguards neuronal identity by actively repressing many non-neuronal fates. Nature, 544(7649), 245-249. doi:10.1038/nature21722

Mancia Leon, W. R., Spatazza, J., Rakela, B., Chatterjee, A., Pande, V., Maniatis, T., . . . Alvarez-Buylla, A. (2020). Clustered gamma-protocadherins regulate cortical interneuron programmed cell death. Elife, 9. doi:10.7554/eLife.55374

Manukyan, A., Kowalczyk, I., Melhuish, T. A., Lemiesz, A., & Wotton, D. (2018). Analysis of transcriptional activity by the Myt1 and Myt1l transcription factors. J Cell Biochem, 119(6), 4644-4655. doi:10.1002/jcb.26636

Marillat, V., Cases, O., Nguyen-Ba-Charvet, K. T., Tessier-Lavigne, M., Sotelo, C., & Chedotal, A. (2002). Spatiotemporal expression patterns of slit and robo genes in the rat brain. *J Comp Neurol, 442*(2), 130-155. doi:10.1002/cne.10068

Marin, O. (2013). Cellular and molecular mechanisms controlling the migration of neocortical interneurons. Eur J Neurosci, 38(1), 2019-2029. doi:10.1111/ejn.12225

Marin, O., Plump, A. S., Flames, N., Sanchez-Camacho, C., Tessier-Lavigne, M., & Rubenstein,

J. L. (2003). Directional guidance of interneuron migration to the cerebral cortex relies on subcortical Slit1/2-independent repulsion and cortical attraction. Development, 130(9), 1889-1901. doi:10.1242/dev.00417

Marin, O., Valdeolmillos, M., & Moya, F. (2006). Neurons in motion: same principles for different shapes? *Trends Neurosci, 29*(12), 655-661. doi:10.1016/j.tins.2006.10.001

Marin, O., Yaron, A., Bagri, A., Tessier-Lavigne, M., & Rubenstein, J. L. (2001). Sorting of striatal and cortical interneurons regulated by semaphorin-neuropilin interactions. Science, 293(5531), 872-875. doi:10.1126/science.1061891

Martini, F. J., Valiente, M., Lopez Bendito, G., Szabo, G., Moya, F., Valdeolmillos, M., & Marin, O. (2009). Biased selection of leading process branches mediates chemotaxis during tangential neuronal migration. *Development, 136*(1), 41-50. doi:10.1242/dev.025502

Matsushita, F., Kameyama, T., Kadokawa, Y., & Marunouchi, T. (2014). Spatiotemporal expression pattern of Myt/NZF family zinc finger transcription factors during mouse nervous system development. Dev Dyn, 243(4), 588-600. doi:10.1002/dvdy.24091

Matz, A., Lee, S. J., Schwedhelm-Domeyer, N., Zanini, D., Holubowska, A., Kannan, M., . . . Stegmuller, J. (2015). Regulation of neuronal survival and morphology by the E3 ubiquitin ligase RNF157. *Cell Death Differ, 22*(4), 626-642. doi:10.1038/cdd.2014.163

Mayer, C., Hafemeister, C., Bandler, R. C., Machold, R., Batista Brito, R., Jaglin, X., . . . Satija, R. (2018). Developmental diversification of cortical inhibitory interneurons. Nature, 555(7697), 457-462. doi:10.1038/nature25999

Mayer, C., Jaglin, X. H., Cobbs, L. V., Bandler, R. C., Streicher, C., Cepko, C. L., . . . Fishell, G. (2015). Clonally Related Forebrain Interneurons Disperse Broadly across Both Functional Areas and Structural Boundaries. *Neuron, 87*(5), 989-998. doi:10.1016/j.neuron.2015.07.011

McConnell, S. K. (1991). The generation of neuronal diversity in the central nervous system. *Annu Rev Neurosci, 14*, 269-300. doi:10.1146/annurev.ne.14.030191.001413

McConnell, S. K., & Kaznowski, C. E. (1991). Cell cycle dependence of laminar determination in developing neocortex. *Science, 254*(5029), 282-285. doi:10.1126/science.1925583

McConnell, G. C., So, R. Q., & Grill, W. M. (2016). Failure to suppress low-frequency neuronal oscillatory activity underlies the reduced effectiveness of random patterns of deep brain stimulation. *J Neurophysiol, 115*(6), 2791-2802. doi:10.1152/jn.00822.2015

McKenzie, M. G., Cobbs, L. V., Dummer, P. D., Petros, T. J., Halford, M. M., Stacker, S. A., . . . Au, E. (2019). Non-canonical Wnt Signaling through Ryk Regulates the Generation of Somatostatin- and Parvalbumin-Expressing Cortical Interneurons. Neuron, 103(5), 853-864 e854.

doi:10.1016/j.neuron.2019.06.003

McKinsey, G. L., Lindtner, S., Trzcinski, B., Visel, A., Pennacchio, L. A., Huylebroeck, D., . . . Rubenstein, J. L. (2013). Dlx1&2-dependent expression of Zfhx1b (Sip1, Zeb2) regulates the fate switch between cortical and striatal interneurons. Neuron, 77(1), 83-98. doi:10.1016/j.neuron.2012.11.035

McNeely, K. C., Cupp, T. D., Little, J. N., Janisch, K. M., Shrestha, A., & Dwyer, N. D. (2017). Mutation of Kinesin-6 Kif20b causes defects in cortical neuron polarization and morphogenesis. *Neural Dev, 12*(1), 5. doi:10.1186/s13064-017-0082-5

Meissner, A., Eminli, S., & Jaenisch, R. (2009). Derivation and manipulation of murine embryonic stem cells. Methods Mol Biol, 482, 3-19. doi:10.1007/978-1-59745-060-7_1

Mi, D., Li, Z., Lim, L., Li, M., Moissidis, M., Yang, Y., . . . Marin, O. (2018). Early emergence of cortical interneuron diversity in the mouse embryo. Science, 360(6384), 81-85. doi:10.1126/science.aar6821

Monory, K., Massa, F., Egertova, M., Eder, M., Blaudzun, H., Westenbroek, R., . . . Lutz, B. (2006). The endocannabinoid system controls key epileptogenic circuits in the hippocampus. Neuron, 51(4), 455-466. doi:10.1016/j.neuron.2006.07.006

Moran-Rivard, L., Kagawa, T., Saueressig, H., Gross, M. K., Burrill, J., & Goulding, M. (2001). Evx1 is a postmitotic determinant of v0 interneuron identity in the spinal cord. *Neuron, 29*(2), 385-399. doi:10.1016/s0896-6273(01)00213-6

Morey, L., Aloia, L., Cozzuto, L., Benitah, S. A., & Di Croce, L. (2013). RYBP and Cbx7 define specific biological functions of polycomb complexes in mouse embryonic stem cells. Cell Rep, 3(1), 60-69. doi:10.1016/j.celrep.2012.11.026

Nawaz, Z., Patil, V., Arora, A., Hegde, A. S., Arivazhagan, A., Santosh, V., & Somasundaram, K. (2016). Cbx7 is epigenetically silenced in glioblastoma and inhibits cell migration by targeting YAP/TAZ-dependent transcription. Sci Rep, 6, 27753. doi:10.1038/srep27753

Neumann, W. J., Schroll, H., de Almeida Marcelino, A. L., Horn, A., Ewert, S., Irmen, F., . . . Kuhn, A. A. (2018). Functional segregation of basal ganglia pathways in Parkinson's disease. Brain, 141(9), 2655-2669. doi:10.1093/brain/awy206

Ni, S., Wang, H., Zhu, X., Wan, C., Xu, J., Lu, C., . . . He, Z. (2017). CBX7 suppresses cell proliferation, migration, and invasion through the inhibition of PTEN/Akt signaling in pancreatic cancer. *Oncotarget, 8*(5), 8010-8021. doi:10.18632/oncotarget.14037

Nielsen, J. A., Berndt, J. A., Hudson, L. D., & Armstrong, R. C. (2004). Myelin transcription factor 1 (Myt1) modulates the proliferation and differentiation of oligodendrocyte lineage cells. *Mol Cell Neurosci, 25*(1), 111-123. doi:10.1016/j.mcn.2003.10.001

Nobrega-Pereira, S., Gelman, D., Bartolini, G., Pla, R., Pierani, A., & Marin, O. (2010). Origin and molecular specification of globus pallidus neurons. J Neurosci, 30(8), 2824-2834. doi:10.1523/JNEUROSCI.4023-09.2010

Nobrega-Pereira, S., Kessaris, N., Du, T., Kimura, S., Anderson, S. A., & Marin, O. (2008). Postmitotic Nkx2-1 controls the migration of telencephalic interneurons by direct repression of guidance receptors. Neuron, 59(5), 733-745. doi:10.1016/j.neuron.2008.07.024

Nobrega-Pereira, S., & Marin, O. (2009). Transcriptional control of neuronal migration in the developing mouse brain. *Cereb Cortex, 19 Suppl 1*, i107-113. doi:10.1093/cercor/bhp044

Ofer, N., Shefi, O., & Yaari, G. (2020). Axonal Tree Morphology and Signal Propagation Dynamics Improve Interneuron Classification. *Neuroinformatics, 18*(4), 581-590. doi:10.1007/s12021-020-09466-8

Ohnishi, T., Shirane, M., & Nakayama, K. I. (2017). SRRM4-dependent neuron-specific alternative splicing of protrudin transcripts regulates neurite outgrowth. *Sci Rep, 7*, 41130. doi:10.1038/srep41130

O'Leary, C., Cole, S. J., Langford, M., Hewage, J., White, A., & Cooper, H. M. (2013). RGMa regulates cortical interneuron migration and differentiation. PLoS One, 8(11), e81711. doi:10.1371/journal.pone.0081711

O'Leary, D. D., & Koester, S. E. (1993). Development of projection neuron types, axon pathways, and patterned connections of the mammalian cortex. *Neuron, 10*(6), 991-1006. doi:10.1016/0896-6273(93)90049-w

Pai, E. L., Chen, J., Fazel Darbandi, S., Cho, F. S., Chen, J., Lindtner, S., . . . Rubenstein, J. L. (2020). Maf and Mafb control mouse pallial interneuron fate and maturation through neuropsychiatric disease gene regulation. Elife, 9. doi:10.7554/eLife.54903

Pai, E. L., Vogt, D., Clemente-Perez, A., McKinsey, G. L., Cho, F. S., Hu, J. S., . . . Rubenstein, J. L. R. (2019). Mafb and c-Maf Have Prenatal Compensatory and Postnatal Antagonistic Roles in Cortical Interneuron Fate and Function. Cell Rep, 26(5), 1157-1173 e1155. doi:10.1016/j.celrep.2019.01.031

Pantakani, D. V., Czyzewska, M. M., Sikorska, A., Bodda, C., & Mannan, A. U. (2011). Oligomerization of ZFYVE27 (Protrudin) is necessary to promote neurite extension. *PLoS One, 6*(12), e29584. doi:10.1371/journal.pone.0029584

Patterson-Cross, R.B., Levine, A.J., and Menon, V. (2021). Selecting single cell clustering parameter values using subsampling-based robustness metrics. BMC Bioinformatics 22, 39.

Paul, A., Crow, M., Raudales, R., He, M., Gillis, J., & Huang, Z. J. (2017). Transcriptional Architecture of Synaptic Communication Delineates GABAergic Neuron Identity. *Cell, 171*(3), 522-539 e520. doi:10.1016/j.cell.2017.08.032

Pavlides, A., Hogan, S. J., & Bogacz, R. (2012). Improved conditions for the generation of beta oscillations in the subthalamic nucleus--globus pallidus network. Eur J Neurosci, 36(2), 2229-2239. doi:10.1111/j.1460-9568.2012.08105.x

Pierani, A., Moran-Rivard, L., Sunshine, M. J., Littman, D. R., Goulding, M., & Jessell, T. M. (2001). Control of interneuron fate in the developing spinal cord by the progenitor homeodomain protein Dbx1. *Neuron, 29*(2), 367-384. doi:10.1016/s0896-6273(01)00212-4

Pina-Fuentes, D., van Dijk, J. M. C., & M, B. (2019). Adaptive DBS in Parkinson's disease: Headlines, perspectives and challenges. *Brain Stimul, 12*(4), 1091-1092. doi:10.1016/j.brs.2019.04.014

Polleux, F., Whitford, K. L., Dijkhuizen, P. A., Vitalis, T., & Ghosh, A. (2002). Control of cortical interneuron migration by neurotrophins and PI3-kinase signaling. *Development, 129*(13), 3147-3160.

Priya, R., Paredes, M. F., Karayannis, T., Yusuf, N., Liu, X., Jaglin, X., . . . Fishell, G. (2018). Activity Regulates Cell Death within Cortical Interneurons through a Calcineurin-Dependent Mechanism. Cell Rep, 22(7), 1695-1709. doi:10.1016/j.celrep.2018.01.007

Puelles, L., Kuwana, E., Puelles, E., Bulfone, A., Shimamura, K., Keleher, J., . . . Rubenstein, J. L. (2000). Pallial and subpallial derivatives in the embryonic chick and mouse telencephalon, traced by the expression of the genes Dlx-2, Emx-1, Nkx-2.1, Pax-6, and Tbr-1. J Comp Neurol, 424(3), 409-438. doi:10.1002/1096-9861(20000828)424:3<409::aid-cne3>3.0.co;2-7

Raiborg, C., Wenzel, E. M., Pedersen, N. M., Olsvik, H., Schink, K. O., Schultz, S. W., . . . Stenmark, H. (2015). Repeated ER-endosome contacts promote endosome translocation and neurite outgrowth. *Nature, 520*(7546), 234-238. doi:10.1038/nature14359

Rava, M., D'Andrea, A., Doni, M., Kress, T. R., Ostuni, R., Bianchi, V., . . . Amati, B. (2017). Mutual epithelium-macrophage dependency in liver carcinogenesis mediated by ST18. Hepatology, 65(5), 1708-1719. doi:10.1002/hep.28942

Ren, C., Smith, S. G., Yap, K., Li, S., Li, J., Mezei, M., . . . Zhou, M. M. (2016). Structure-Guided Discovery of Selective Antagonists for the Chromodomain of Polycomb Repressive Protein CBX7. ACS Med Chem Lett, 7(6), 601-605. doi:10.1021/acsmedchemlett.6b00042

Romm, E., Nielsen, J. A., Kim, J. G., & Hudson, L. D. (2005). Myt1 family recruits histone deacetylase to regulate neural transcription. *J Neurochem, 93*(6), 1444-1453. doi:10.1111/j.1471-4159.2005.03131.x

Rossignol, E. (2011). Genetics and function of neocortical GABAergic interneurons in neurodevelopmental disorders. *Neural Plast, 2011*, 649325. doi:10.1155/2011/649325

Sanchez-Alcaniz, J. A., Haege, S., Mueller, W., Pla, R., Mackay, F., Schulz, S., . . . Marin, O. (2011). Cxcr7 controls neuronal migration by regulating chemokine responsiveness. Neuron, 69(1), 77-90. doi:10.1016/j.neuron.2010.12.006

Sandberg, M., Flandin, P., Silberberg, S., Su-Feher, L., Price, J. D., Hu, J. S., . . . Rubenstein, J. L. R. (2016). Transcriptional Networks Controlled by NKX2-1 in the Development of Forebrain GABAergic Neurons. Neuron, 91(6), 1260-1275. doi:10.1016/j.neuron.2016.08.020

Sani, S., Ostrem, J. L., Shimamoto, S., Levesque, N., & Starr, P. A. (2009). Single unit "pauser" characteristics of the globus pallidus pars externa distinguish primary dystonia from secondary dystonia and Parkinson's disease. Exp Neurol, 216(2), 295-299. doi:10.1016/j.expneurol.2008.12.006

Shiotsuki, H., Yoshimi, K., Shimo, Y., Funayama, M., Takamatsu, Y., Ikeda, K., . . . Hattori, N. (2010). A rotarod test for evaluation of motor skill learning. *J Neurosci Methods, 189*(2), 180-185. doi:10.1016/j.jneumeth.2010.03.026

Sousa, V. H., Miyoshi, G., Hjerling-Leffler, J., Karayannis, T., & Fishell, G. (2009). Characterization of Nkx6-2-derived neocortical interneuron lineages. Cereb Cortex, 19 Suppl 1, i1-10. doi:10.1093/cercor/bhp038

Southwell, D. G., Paredes, M. F., Galvao, R. P., Jones, D. L., Froemke, R. C., Sebe, J. Y., . . . Alvarez-Buylla, A. (2012). Intrinsically determined cell death of developing cortical interneurons. Nature, 491(7422), 109-113. doi:10.1038/nature11523

Stanco, A., Szekeres, C., Patel, N., Rao, S., Campbell, K., Kreidberg, J. A., . . . Anton, E. S. (2009). Netrin-1-alpha3beta1 integrin interactions regulate the migration of interneurons through the cortical marginal zone. Proc Natl Acad Sci U S A, 106(18), 7595-7600. doi:10.1073/pnas.0811343106

Steinecke, A., Gampe, C., Zimmer, G., Rudolph, J., & Bolz, J. (2014). EphA/ephrin A reverse signaling promotes the migration of cortical interneurons from the medial ganglionic eminence. Development, 141(2), 460-471. doi:10.1242/dev.101691

Sugitani, Y., Nakai, S., Minowa, O., Nishi, M., Jishage, K., Kawano, H., . . . Noda, T. (2002).

Brn-1 and Brn-2 share crucial roles in the production and positioning of mouse neocortical neurons. *Genes Dev, 16*(14), 1760-1765. doi:10.1101/gad.978002

Sun, X., Gao, L., Yu, R. K., & Zeng, G. (2006). Down-regulation of WNK1 protein kinase in neural progenitor cells suppresses cell proliferation and migration. *J Neurochem, 99*(4), 1114-1121. doi:10.1111/j.1471-4159.2006.04159.x

Sussel, L., Marin, O., Kimura, S., & Rubenstein, J. L. (1999). Loss of Nkx2.1 homeobox gene function results in a ventral to dorsal molecular respecification within the basal telencephalon: evidence for a transformation of the pallidum into the striatum. Development, 126(15), 3359-3370.

Takakusaki, K. (2013). Neurophysiology of gait: from the spinal cord to the frontal lobe. *Mov Disord, 28*(11), 1483-1491. doi:10.1002/mds.25669

Taniguchi, H., Lu, J., & Huang, Z. J. (2013). The spatial and temporal origin of chandelier cells in mouse neocortex. Science, 339(6115), 70-74. doi:10.1126/science.1227622

Tao, G., Li, Z., Wen, Y., Song, X., Wei, S., Du, H., . . . You, Y. (2019). Transcription Factors Sp8 and Sp9 Regulate Medial Ganglionic Eminence-Derived Cortical Interneuron Migration. Front Mol Neurosci, 12, 75. doi:10.3389/fnmol.2019.00075

Tasic, B., Yao, Z., Graybuck, L. T., Smith, K. A., Nguyen, T. N., Bertagnolli, D., . . . Zeng, H. (2018). Shared and distinct transcriptomic cell types across neocortical areas. *Nature, 563*(7729), 72-78. doi:10.1038/s41586-018-0654-5

Tennant, B. R., Chen, J., Shih, A. Z., Luciani, D. S., & Hoffman, B. G. (2015). Myt3 Mediates Laminin-V/Integrin-beta1-Induced Islet-Cell Migration via Tgfbi. Mol Endocrinol, 29(9), 1254-1268. doi:10.1210/ME.2014-1387

Tennant, B. R., Islam, R., Kramer, M. M., Merkulova, Y., Kiang, R. L., Whiting, C. J., & Hoffman, B. G. (2012). The transcription factor Myt3 acts as a pro-survival factor in beta-cells. PLoS One, 7(12), e51501. doi:10.1371/journal.pone.0051501

Thor, S., & Thomas, J. B. (1997). The Drosophila islet gene governs axon pathfinding and neurotransmitter identity. Neuron, 18(3), 397-409. doi:10.1016/s0896-6273(00)81241-6

Truett, G. E., Heeger, P., Mynatt, R. L., Truett, A. A., Walker, J. A., & Warman, M. L. (2000). Preparation of PCR-quality mouse genomic DNA with hot sodium hydroxide and tris (HotSHOT). Biotechniques, 29(1), 52, 54. doi:10.2144/00291bm09

van den Berghe, V., Stappers, E., Vandesande, B., Dimidschstein, J., Kroes, R., Francis, A., . . . Seuntjens, E. (2013). Directed migration of cortical interneurons depends on the cell-autonomous action of Sip1. Neuron, 77(1), 70-82. doi:10.1016/j.neuron.2012.11.009

Vandamme, J., Volkel, P., Rosnoblet, C., Le Faou, P., & Angrand, P. O. (2011). Interaction proteomics analysis of polycomb proteins defines distinct PRC1 complexes in mammalian cells. Mol Cell Proteomics, 10(4), M110 002642. doi:10.1074/mcp.M110.002642

Vasconcelos, F. F., Sessa, A., Laranjeira, C., Raposo, A., Teixeira, V., Hagey, D. W., . . . Castro, D. S. (2016). MyT1 Counteracts the Neural Progenitor Program to Promote Vertebrate Neurogenesis. Cell Rep, 17(2), 469-483. doi:10.1016/j.celrep.2016.09.024

Vierbuchen, T., Ostermeier, A., Pang, Z. P., Kokubu, Y., Sudhof, T. C., & Wernig, M. (2010). Direct conversion of fibroblasts to functional neurons by defined factors. Nature, 463(7284), 1035-1041. doi:10.1038/nature08797

Villar-Cervino, V., Kappeler, C., Nobrega-Pereira, S., Henkemeyer, M., Rago, L., Nieto, M. A., & Marin, O. (2015). Molecular mechanisms controlling the migration of striatal interneurons. J Neurosci, 35(23), 8718-8729. doi:10.1523/JNEUROSCI.4317-14.2015

Wang, D. D., de Hemptinne, C., Miocinovic, S., Ostrem, J. L., Galifianakis, N. B., San Luciano, M., & Starr, P. A. (2018). Pallidal Deep-Brain Stimulation Disrupts Pallidal Beta Oscillations and Coherence with Primary Motor Cortex in Parkinson's Disease. *J Neurosci, 38*(19), 4556-4568. doi:10.1523/JNEUROSCI.0431-18.2018

Wang, F., Flanagan, J., Su, N., Wang., L. C., Bui, S., Nielson, A., . . . Luo, Y. (2012) RNAscope: A novel in situ RNA analysis platform for formalin-fixed, paraffin-embedded tissues. J Mol Diagn, 14(1), 22-29. doi: 10.1016/j.jmoldx.2011.08.002

Wang, S., Zhang, J., Zhao, A., Hipkens, S., Magnuson, M. A., & Gu, G. (2007). Loss of Myt1 function partially compromises endocrine islet cell differentiation and pancreatic physiological function in the mouse. Mech Dev, 124(11-12), 898-910. doi:10.1016/j.mod.2007.08.004

Wang, Y., Li, G., Stanco, A., Long, J. E., Crawford, D., Potter, G. B., . . . Rubenstein, J. L. (2011). CXCR4 and CXCR7 have distinct functions in regulating interneuron migration. Neuron, 69(1), 61-76. doi:10.1016/j.neuron.2010.12.005

Watanabe, K., Kamiya, D., Nishiyama, A., Katayama, T., Nozaki, S., Kawasaki, H., . . . Sasai, Y. (2005). Directed differentiation of telencephalic precursors from embryonic stem cells. Nat Neurosci, 8(3), 288-296. doi:10.1038/nn1402

Way, J. C., & Chalfie, M. (1988). mec-3, a homeobox-containing gene that specifies differentiation of the touch receptor neurons in C. elegans. Cell, 54(1), 5-16. doi:10.1016/0092-8674(88)90174-2

Wichterle, H., Turnbull, D. H., Nery, S., Fishell, G., & Alvarez-Buylla, A. (2001). In utero fate mapping reveals distinct migratory pathways and fates of neurons born in the mammalian basal forebrain. Development, 128(19), 3759-3771.

Wilson, S. W., & Rubenstein, J. L. (2000). Induction and dorsoventral patterning of the telencephalon. *Neuron, 28*(3), 641-651. doi:10.1016/s0896-6273(00)00171-9

Windels, F., Carcenac, C., Poupard, A., & Savasta, M. (2005). Pallidal origin of GABA release within the substantia nigra pars reticulata during high-frequency stimulation of the subthalamic nucleus. J Neurosci, 25(20), 5079-5086. doi:10.1523/JNEUROSCI.0360-05.2005

Wong, F. K., Bercsenyi, K., Sreenivasan, V., Portales, A., Fernandez-Otero, M., & Marin, O. (2018). Pyramidal cell regulation of interneuron survival sculpts cortical networks. Nature, 557(7707), 668-673. doi:10.1038/s41586-018-0139-6

Wu, C., Niu, L., Yan, Z., Wang, C., Liu, N., Dai, Y., . . . Xu, R. (2015). Pcdh11x Negatively Regulates Dendritic Branching. *J Mol Neurosci, 56*(4), 822-828. doi:10.1007/s12031-015-0515-8

Wu, W., Zhou, X., Yu, T., Bao, Z., Zhi, T., Jiang, K., . . . You, Y. (2017). The malignancy of miR-18a in human glioblastoma via directly targeting CBX7. Am J Cancer Res, 7(1), 64-76.
Xu, Q., Tam, M., & Anderson, S. A. (2008). Fate mapping Nkx2.1-lineage cells in the mouse telencephalon. J Comp Neurol, 506(1), 16-29. doi:10.1002/cne.21529

Xu, Q., Tam, M., & Anderson, S. A. (2008). Fate mapping Nkx2.1-lineage cells in the mouse telencephalon. *J Comp Neurol, 506*(1), 16-29. doi:10.1002/cne.21529

Yamagishi, S., Bando, Y., & Sato, K. (2020). Involvement of Netrins and Their Receptors in Neuronal Migration in the Cerebral Cortex. Front Cell Dev Biol, 8, 590009. doi:10.3389/fcell.2020.590009

Yanagida, M., Miyoshi, R., Toyokuni, R., Zhu, Y., & Murakami, F. (2012). Dynamics of the leading process, nucleus, and Golgi apparatus of migrating cortical interneurons in living mouse embryos. *Proc Natl Acad Sci U S A, 109*(41), 16737-16742. doi:10.1073/pnas.1209166109

Yee, K. S., & Yu, V. C. (1998). Isolation and characterization of a novel member of the neural zinc finger factor/myelin transcription factor family with transcriptional repression activity. J Biol Chem, 273(9), 5366-5374. doi:10.1074/jbc.273.9.5366

Zhang, P., Wu, C., Liu, N., Niu, L., Yan, Z., Feng, Y., & Xu, R. (2014). Protocadherin 11 x regulates differentiation and proliferation of neural stem cell in vitro and in vivo. *J Mol Neurosci, 54*(2), 199-210. doi:10.1007/s12031-014-0275-x

Zimmer, C., Tiveron, M. C., Bodmer, R., & Cremer, H. (2004). Dynamics of Cux2 expression suggests that an early pool of SVZ precursors is fated to become upper cortical layer neurons. *Cereb Cortex, 14*(12), 1408-1420. doi:10.1093/cercor/bhh102

Zimmer, G., Rudolph, J., Landmann, J., Gerstmann, K., Steinecke, A., Gampe, C., & Bolz, J. (2011). Bidirectional ephrinB3/EphA4 signaling mediates the segregation of medial ganglionic eminence- and preoptic area-derived interneurons in the deep and superficial migratory stream. J Neurosci, 31(50), 18364-18380. doi:10.1523/JNEUROSCI.4690-11.2011

Zimmer, G., Garcez, P., Rudolph, J., Niehage, R., Weth, F., Lent, R., & Bolz, J. (2008). Ephrin-A5 acts as a repulsive cue for migrating cortical interneurons. *Eur J Neurosci, 28*(1), 62-73. doi:10.1111/j.1460-9568.2008.06320.x